

2

DTIC FILE COPY

NPS 68-89-006

NAVAL POSTGRADUATE SCHOOL

Monterey, California

AD-A219 591



THESIS

DTIC
ELECTE
MAR 26 1990
S E D

SALINE IMPACT ON THE CALIFORNIA CURRENT
SYSTEM

by

Christopher R. Gunderson

September 1989

Thesis Advisor

Mary L. Batteen

Approved for public release; distribution is unlimited.

Prepared for:
Office of Naval Research
800 N. Quincy Street
Arlington, VA 22217-5000

90 03 23 065

NAVAL POSTGRADUATE SCHOOL
Monterey, CA. 93943


Rear Admiral Ralph W. West, Jr.
Superintendent

Harrison Shull
Provost

This report was prepared in conjunction with research conducted for Chief of Naval Research and Funded by the Naval Postgraduate School.

Reproduction of this report is authorized.

Released By:

A handwritten signature in cursive script, appearing to read "G. E. Schacher".

GORDON E. SCHACHER
Dean of Science and Engineering

Unclassified

security classification of this page

REPORT DOCUMENTATION PAGE				
1a Report Security Classification Unclassified			1b Restrictive Markings	
2a Security Classification Authority			3 Distribution Availability of Report	
2b Declassification Downgrading Schedule			Approved for public release; distribution is unlimited.	
4 Performing Organization Report Number(s) NPS-68-89-006			5 Monitoring Organization Report Number(s)	
6a Name of Performing Organization Naval Postgraduate School		6b Office Symbol (if applicable) 68	7a Name of Monitoring Organization Office of Naval Research	
6c Address (city, state, and ZIP code) Monterey, CA 93943-5000			7b Address (city, state, and ZIP code) 800 N. Quincy St., Arlington, VA 22217-5000	
8a Name of Funding/Sponsoring Organization Naval Postgraduate School		8b Office Symbol (if applicable)	9 Procurement Instrument Identification Number O&MN, Direct Funding	
8c Address (city, state, and ZIP code) Monterey, CA. 93943			10 Source of Funding Numbers	
			Program Element No	Project No
			Task No	Work Unit Accession No
11 Title (include security classification) SALINE IMPACT ON THE CALIFORNIA CURRENT SYSTEM (Unclassified)				
12 Personal Author(s) Christopher R. Gunderson in conjunction with M.L. Batteen and C.S. Nelson				
13a Type of Report Master's Thesis		13b Time Covered From To	14 Date of Report (year, month, day) September 1989	15 Page Count 118
16 Supplementary Notation The views expressed in this thesis are those of the author and do not reflect the official policy or position of the Department of Defense or the U.S. Government.				
17 Cosati Codes		18 Subject Terms (continue on reverse if necessary and identify by block number)		
Field	Group	Subgroup	salinity, California Current, variance, density, anomaly, Thesis, sea water	
19 Abstract (continue on reverse if necessary and identify by block number) There are some indications that in large measure the density anomaly field of the California Current System (CCS) follows temperature, salinity playing a significantly lesser role. These indications have been used as justification for ignoring salinity variations in dynamic models. An extensive data base of simultaneous temperature-salinity observations taken in the CCS is used to calculate and assess the saline contribution to specific volume anomaly, dynamic height, and density variance. The results show that the distribution of salinity can be important in defining the large scale circulation of the CCS, and that the variability can be quite significant.				
20 Distribution/Availability of Abstract <input checked="" type="checkbox"/> unclassified unlimited <input type="checkbox"/> same as report <input type="checkbox"/> DTIC users			21 Abstract Security Classification Unclassified	
22a Name of Responsible Individual Mary L. Batteen			22b Telephone (include Area code) (408) 646-3265	22c Office Symbol 68Bv

DD FORM 1473,84 MAR

83 APR edition may be used until exhausted
All other editions are obsolete

security classification of this page

Unclassified

Approved for public release; distribution is unlimited.

Saline Impact on the California Current System

by

Christopher R. Gunderson
Lieutenant Commander, United States Navy
B.S., United States Naval Academy, 1977

Submitted in partial fulfillment of the
requirements for the degree of

MASTER OF SCIENCE IN METEOROLOGY AND OCEANOGRAPHY

from the

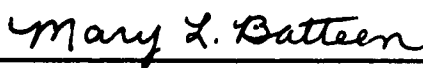
NAVAL POSTGRADUATE SCHOOL
September 1989

Author:



Christopher R. Gunderson

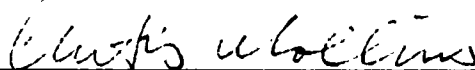
Approved by:



Mary L. Batteen, Thesis Advisor



Craig S. Nelson, Second Reader



Curtis A. Collins, Chairman,
Department of Oceanography



Gordon E. Schacher,
Dean of Science and Engineering

ABSTRACT

There are some indications that in large measure the density anomaly field of the California Current System (CCS) follows temperature, salinity playing a significantly lesser role. These indications have been used as justification for ignoring salinity variations in dynamic models. An extensive data base of simultaneous temperature-salinity observations taken in the CCS is used to calculate and assess the saline contribution to specific volume anomaly, dynamic height, and density variance. The results show that the distribution of salinity can be important in defining the large scale circulation of the CCS, and that the local variability can be quite significant.

Accession For	
NTIS GPA&I	<input checked="" type="checkbox"/>
DTIC TAB	<input type="checkbox"/>
Unannounced	<input type="checkbox"/>
Justification	
By	
Distribution/	
Availability Codes	
Dist	Avail and/or Special
A-1	



TABLE OF CONTENTS

I. INTRODUCTION: IMPORTANCE OF SALINITY	1
II. DATA DESCRIPTION	7
A. SOURCES AND TYPES OF DATA	7
B. DATA MANIPULATION	8
III. CHARACTERISTIC SALINITY OF THE CALIFORNIA CURRENT SYSTEM	9
A. GENERAL FEATURES	9
B. VARIABILITY	9
IV. EFFECT OF SALINITY	13
A. STRATEGY	13
B. SPECIFIC VOLUME ANOMALY	13
1. Method	13
2. Results	16
C. VARIANCE AND CORRELATION OF THE SPECIFIC VOLUME ANOMALY CONSTITUENTS	25
1. Method	25
2. Results	34
D. MEAN DIFFERENCES OF THE SPECIFIC VOLUME ANOMALY CONSTITUENTS	35
1. Method	35
2. Results	35
E. DYNAMIC HEIGHT	46
1. Method	46
2. Results	52
F. PROPAGATION OF T-S VARIANCE THROUGH THE EOS	58
1. Method	58
2. Results	65

V. SUMMARY AND CONCLUSIONS	86
A. STERIC ANOMALY.	86
B. DYNAMIC HEIGHT	87
C. VARIANCE IN THE DENSITY FIELD	87
VI. RECOMMENDATIONS	89
A. PROFILE	89
B. FINER RESOLUTION	89
C. MODELING CONSIDERATIONS	89
D. SOUND SPEED CALCULATIONS	91
APPENDIX A. NUMBER OF OBSERVATIONS	93
APPENDIX B. SMALL SCALE EFFECTS OF SALINITY ON DYNAMIC HEIGHT	102
LIST OF REFERENCES	103
INITIAL DISTRIBUTION LIST	106

LIST OF FIGURES

Figure 1.	Dynamic Height of the Tropical Ocean 0/400 m	2
Figure 2.	CalCOFI Line 60, July	5
Figure 3.	Temperature, Salinity, and Density Gradients	6
Figure 4.	Surface Salinity of the CCS	10
Figure 5.	Typical Salinity Profiles of the CCS	11
Figure 6.	Steric Anomaly, July, 10 m	18
Figure 7.	Steric Anomaly, July, 100 m	19
Figure 8.	Steric Anomaly, July, 500 m	20
Figure 9.	Specific Volume Anomaly (T-S), July, 10 m	21
Figure 10.	Specific Volume Anomaly (T), July, 10 m	22
Figure 11.	Specific Volume Anomaly (S), July, 10 m	23
Figure 12.	Specific Volume Anomaly (T-S), July, 500 m	24
Figure 13.	Specific Volume Anomaly (T), July, 500 m	26
Figure 14.	Specific Volume Anomaly (S), July, 500 m	27
Figure 15.	Specific Volume Anomaly (T), July, 100 m	28
Figure 16.	Specific Volume Anomaly (S), July, 100 m	29
Figure 17.	Specific Volume Anomaly (T), July, 200 m	30
Figure 18.	Specific Volume Anomaly (S), July, 200 m	31
Figure 19.	Specific Volume Anomaly (S), October, 200 m	32
Figure 20.	Specific Volume Coefficient of Determination (T), July, 10 m	36
Figure 21.	Specific Volume Coefficient of Determination (T), July, 100 m	37
Figure 22.	Specific Volume Coefficient of Determination (S), July, 10 m	38
Figure 23.	Specific Volume Coefficient of Determination (S), July, 100 m	39
Figure 24.	Specific Volume Coefficient of Determination (T), February, 10 m	40
Figure 25.	Specific Volume Coefficient of Determination (S), February, 10 m	41
Figure 26.	Specific Volume Coefficient of Determination (T), March, 10 m	42
Figure 27.	Specific Volume Coefficient of Determination (S), March, 10 m	43
Figure 28.	Specific Volume Coefficient of Determination (T), January, 10 m	44
Figure 29.	Variance in Steric Anomaly from Temperature, January, 10 m	45
Figure 30.	Specific Volume Anomaly RMSE (T), July, 10 m.	47
Figure 31.	Specific Volume Anomaly RMSE (T), July, 500 m.	48

Figure 32. Specific Volume Anomaly RMSE (‰), July, 10 m.	49
Figure 33. Specific Volume Anomaly RMSE (‰), July, 500 m.	50
Figure 34. Specific Volume Anomaly RMSE (‰), September, 10 m.	51
Figure 35. Dynamic Height, 0/500 m, January	54
Figure 36. Dynamic Height, 0/500 m, July	55
Figure 37. Dynamic Height Difference, 0/500 m, July	56
Figure 38. Dynamic Height (Salinity 35), 0/500 m, July	57
Figure 39. Dynamic Height, 100/500 m, July	59
Figure 40. Dynamic Height (Salinity 35), 100/500 m, July	60
Figure 41. Dynamic Height Difference, 100/500 m, July	61
Figure 42. Dynamic Height, 200/500 m, July	62
Figure 43. Dynamic Height (Salinity 35), 200/500 m, July	63
Figure 44. Dynamic Height Difference, 200/500 m, July	64
Figure 45. Total Density Variance, 10 m, Summer	67
Figure 46. Salinity Contribution to Total Density Variance, 10 m, Summer	68
Figure 47. Temperature Contribution to Total Density Variance, 10 m, Summer ..	69
Figure 48. Total Density Variance, 200 m, Summer	70
Figure 49. Salinity Contribution to Total Density Variance, 500 m, Summer	71
Figure 50. Total Density Variance, 500 m, Summer	72
Figure 51. Alongshore and Cross-Shore Density Variance Contribution	74
Figure 52. Alongshore Line 1, Contributions to Density Variance	75
Figure 53. Alongshore Line 2, Contributions to Density Variance	76
Figure 54. Cross-shore Line 46, Contributions to Density Variance	77
Figure 55. Cross-shore Line 26, Contributions to Density Variance	78
Figure 56. Cross-shore Line 28, Contributions to Density Variance	80
Figure 57. Alongshore Line 6, Contributions to Density Variance	81
Figure 58. Alongshore Line 3, Contributions to Density Variance	82
Figure 59. Alongshore Line 4, Contributions to Density Variance	83
Figure 60. Cross-shore Line 27, Contributions to Density Variance	84
Figure 61. Cross-shore Line 29, Contributions to Density Variance	85
Figure 62. Coefficient of Determination (T-S), Summer, 500 m	92
Figure 63. Number of Observations at 10 m, January.	94
Figure 64. Number of Observations at 10 m, April.	95
Figure 65. Number of Observations at 10 m, July.	96
Figure 66. Number of Observations at 10 m, October.	97

Figure 67. Number of Observations at 500 m, January.	98
Figure 68. Number of Observations at 500 m April.	99
Figure 69. Number of Observations at 500 m, July.	100
Figure 70. Number of Observations at 500 m, October.	101

ACKNOWLEDGEMENTS

I would like to acknowledge my advisor, Dr. Mary Batteen, for taking on this short-fused project. Thanks are due Cdr. Craig Nelson and Dynalysis of Princeton for providing a very clean data set. The patient assistance of Arlene Bird and Paul Jessen was very much appreciated. I am deeply grateful to those professors of oceanography and meteorology who are willing to discuss science, and especially mathematics, with students. I offer my special thanks to Bob, Roberta, and Kathy for their material and spiritual support.

I. INTRODUCTION: IMPORTANCE OF SALINITY

At a given pressure, the density of seawater depends on temperature and salinity. Except for high latitude regions and near sources and sinks of salt, temperature is usually considered to vary more than salinity in the upper ocean, and is generally considered to be the major source of density variations (Pickard and Emery, 1982). Recently Cooper (1988) has demonstrated the importance of salinity as a consideration in modeling motions in the tropics. This result is surprising because in the tropics the thermal expansion coefficient, which increases with temperature and salinity, is large, and the salinity contraction coefficient, which decreases as temperature and salinity increase, is relatively small, and temperature variation might reasonably be expected to dominate forcing of density differentials. Is it possible that salinity variability in the California Current System (CCS), which is geographically between the polar regions and the tropics, is also an important consideration for modeling dynamics? A close examination of the southern CCS area in Figure 1 suggests that salinity variation could have as important an effect in the CCS as in the tropics.

The CCS is in the eastern quadrant of the North Pacific anticyclonic gyre, and, according to Hickey (1979), is composed of four currents. The California Current (CC) is on the surface and extends as far as 1000 km from the coast. A surface poleward flow exists during the fall and winter north of Point Conception called the Davidson Current. South of Point Conception, and inshore of the Channel Islands is another surface flow called the Southern California Countercurrent. Finally, the California Undercurrent (CU) is a subsurface poleward flow that occurs over the continental slope. Typical mean velocities associated with the CC are on the order of 10 cm s^{-1} , but superimposed on the mean flow are small scale eddies and jets (Bernstein *et al.*, 1977; Mooers and Robinson, 1984; Rienecker *et al.*, 1985, 1988). The meanders can have wavelengths of several hundred kilometers, can intensify and separate from the mean flow and can exist as isolated cyclonic or anticyclonic eddies (Bernstein *et al.*, 1977). Baroclinic jets, typically $\sim 70 \text{ km}$ wide, with peak velocities near 80 cm s^{-1} are embedded in the eddy field (Mooers and Robinson, 1984; Rienecker *et al.*, 1985; Flament *et al.*, 1985; Kosro and Huyer, 1986). Mean surface temperatures in the CCS range roughly from 10 to 20° C while surface salinities increase from 32 psu in the north to 34 psu in the south.

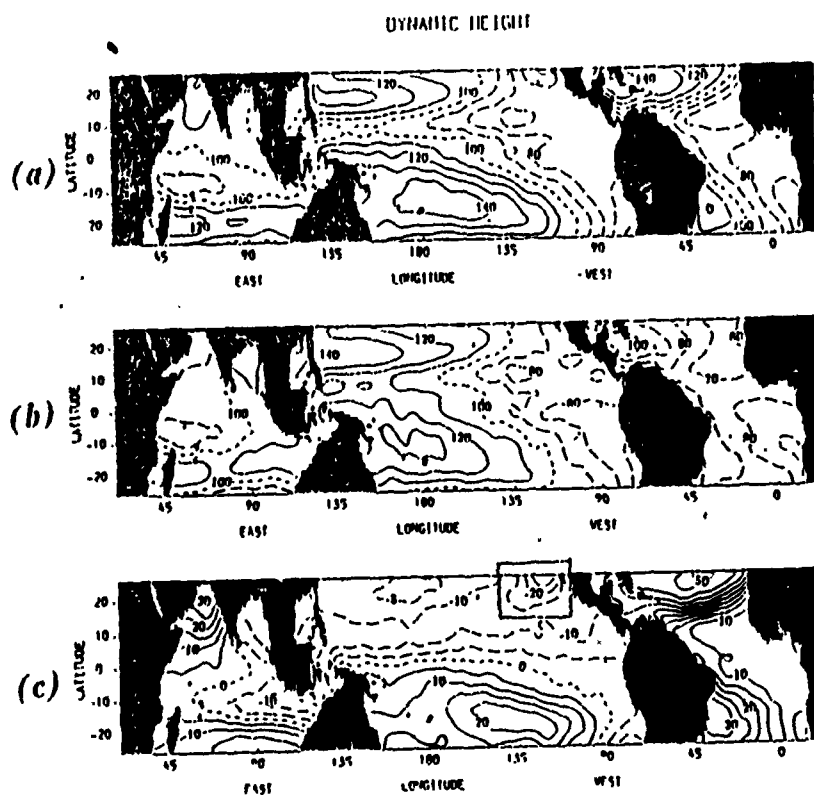


Figure 1. Dynamic Height of the Tropical Ocean 0/400 m: Calculated from Levitus (1982) data. (a) Salinity set to constant 35, (b) salinity varying as in Levitus data, and (c) difference between (a) and (b). Contour intervals are 10 *dyn cm* in (a) and (b), and 5 *dyn cm* in (c) (From Cooper, 1988).

A typical section across the CCS, from San Francisco Bay southwest to 33° N, 134° W (Figure 2), shows that isopycnals very closely follow isotherms, and intersect isohalines. The implication is that temperature variation is much more important than salinity variation in driving the density gradient. On the other hand, examination of Figure 3, which depicts the coastal area of the CCS just north of Point Arena (at ~39° N and near the shoreward end of Figure 2) shows that at a depth of 100 m, about a third of the cross-shore density gradient over a degree of longitude is due to salinity change. In the CCS, unlike all other eastern boundary currents, salinity increases with depth (Wooster and Reid, 1963). Therefore, if this cold, salty 100 m water were upwelled to the surface, the resulting horizontal density gradient would be one third greater than if the salinity profile were constant.

The approximate equation of state for seawater is:

$$\rho = \rho_0[1 - \alpha(T - T_0) + \beta(S - S_0)], \quad (1)$$

which can be rewritten as:

$$\Delta\rho = -\alpha\rho_0\Delta T + \beta\rho_0\Delta S, \quad (2)$$

where α and β are the expansion and contraction coefficients for temperature, T , and salinity, S , respectively, ρ is density, S_0 is the reference salinity (35 *psu*) and T_0 is the reference temperature (0° C).

This equation can be employed to get a rough idea of the large scale importance of salinity if typical CCS values for T and S are used. Entering the International Oceanographic Tables (UNESCO, 1987) for α and β with 15°C and 33 *psu*, and considering typical surface temperature and salinity ranges of 10° C and 2 *psu* for the CCS, computations of the contributions of temperature and salinity to the density anomaly are 10.5 and 7.5 kg m^{-3} , respectively. Annually, a mean temperature of 12° C plus or minus 3° C variation, associated with a mean salinity of 33 with .3 *psu* variation, is roughly characteristic of the central region of the CCS. Use of the 1987 tables here shows a 1.7 and 2.7 kg m^{-3} contribution to the annual density anomaly change for salinity and temperature, respectively, over the course of a year. Vertically a mean temperature at 500 m of about 5° C plus or minus 5° C surface to 1000 m, in conjunction with an approximate mean salinity of 34, plus or minus 0.5 *psu*, yields density anomaly changes of 7.2 kg m^{-3} from temperature and 3.8 kg m^{-3} from salinity.

These crude calculations seem to indicate that the importance of salinity variation should not be summarily dismissed when considering CCS density gradients in any dimension. Yet often dynamic models of the CCS (e.g., Batteen *et al.*, 1989) do not allow salinity contributions to density gradients. What is the price of this omission?

The objective of this thesis is to address that question by investigating the saline impact on the CCS. The data set used is described in Section II. A general description of the characteristic salinity of the CCS is provided in Section III. In Section IV several techniques are used to analyze the data. Mean values for each of the constituents of the thermosteric anomaly, δ_t , δ_s , and δ_{ts} , are computed at various depths and analyzed. Mean dynamic heights are computed from salinity and temperature observations and are compared to dynamic heights computed from temperature and constant salinity values. The equation of state for seawater is differentiated with respect to temperature and salinity, variances and covariances of temperature and salinity are computed, and the contributions of each to variance in the density field are determined. A summary of the results is presented in Section V and recommendations for future work are in Section VI.

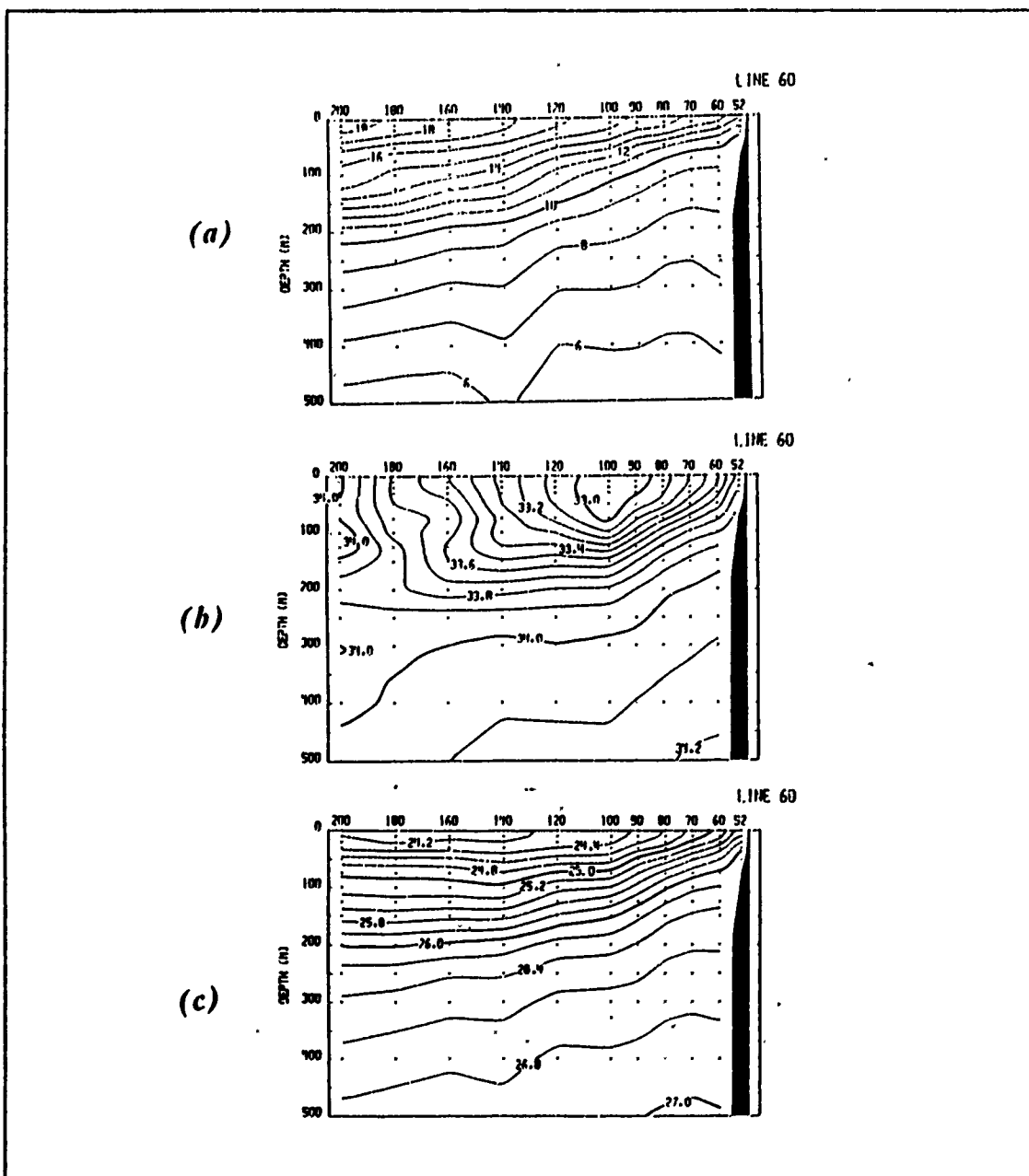


Figure 2. CalCOFI Line 60, July: 33° N, 134° W, to 37° N, 123° W: (a) Temperature (°C), (b) Salinity (ppt), (c) Density Anomaly (from Lynn *et al.*, 1982).

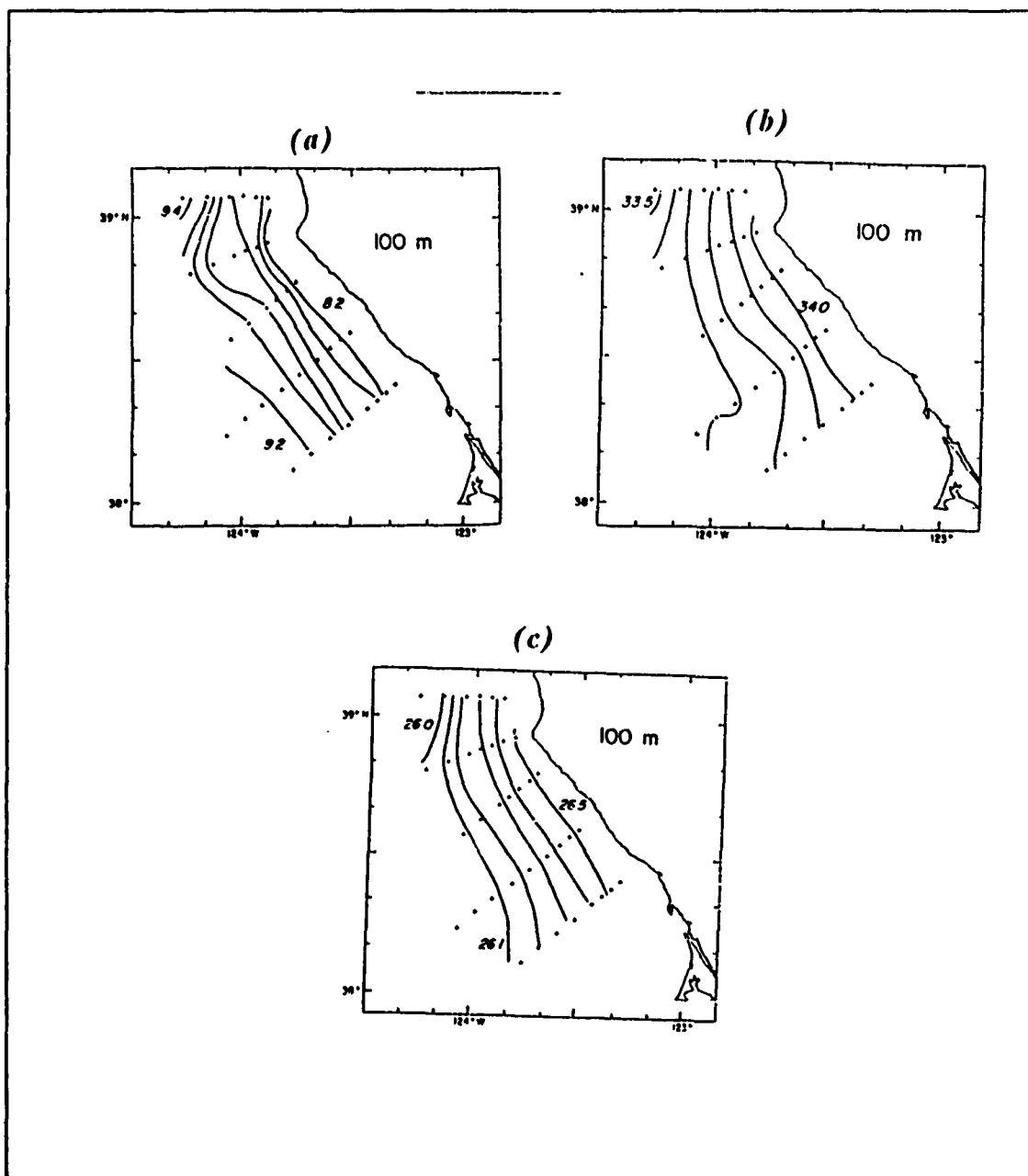


Figure 3. Temperature, Salinity, and Density Gradients: Near Pt. Arena (39° N), at 100 m depth: (a) Temperature (° C), (b) Salinity (ppt), (c) Density Anomaly (from Huyer and Kosro, 1987).

II. DATA DESCRIPTION

A. SOURCES AND TYPES OF DATA

The data base used for all calculations was compiled by Dynalysis of Princeton, and is described in detail in their final report to the U.S. Department of the Interior (Blumberg *et al.*, 1984). Coverage extends along the west coast of North America to 133 ° W, and from 20° to 50° N. Sources include the National Oceanographic Data Center (NODC) historical data archives, the Fleet Numerical Oceanography Center (FNOC) data files, California Cooperative Oceanic Fisheries Investigation (CalCOFI) surveys which have been made systematically since 1949, and the Coastal Ocean Dynamics Experiment (CODE). CODE data are the most current, dating from as recently as 1983, and cover the coastal area near Point Arena within a one degree square domain. The highest density of NODC data is the result of observations from Oregon State University standard surveys along the "Newport" line (~ 45° N) and University of Washington surveys of the Columbia River plume (46-47° N). Original files overlapped, but the data have been carefully screened by Dynalysis to eliminate duplicate observations. The combined data set consists of over 300,000 data points with observations at up to 33 standard levels to 4000 m. The more than 40,000 of these points which included any simultaneous temperature and salinity observations at 500 m or above, were considered here, while those including only temperature were not used. Original observations of salinity were reported in units of parts per thousand (ppt) rather than practical salinity units (*psu*). However, because the difference in units is very slight (Lewis and Perkin, 1981) and not significant at the scales discussed here, the currently preferred *psu* is used throughout this thesis. Most of the retained records are from CalCOFI surveys, which were collected at average intervals of 74 km along lines spaced 74 km apart covering from San Francisco to Baja California (Reid, 1988). As a result the CalCOFI collection defines for the most part the maximum resolution possible from the data set, exceptions being along the Oregon coast, and near Point Arena, where finer resolution may be possible. Generally the number of observations increases toward the coast, with greatest concentration along the coasts of California and Oregon. There are very few data more than 500 km off the coast or between 38° and 42° N. Discussion here is limited to the area bounded by the extent of this data.

B. DATA MANIPULATION

For this study, data were placed in bins identified by one degree squares centered at half degree latitude-longitude intersections, by month or season, and by depth level. Information so cataloged is referred to as a data block throughout this paper. Standard depth levels 0, 10, 20, 30, 50, 75, 100, 125, 150, 200, 250, 300, 400, and 500 m were considered. Choice of 500 m as the maximum depth level was made due to data availability and because the phenomenon of interest, the CCS, has been classically considered shoaler than that depth, at least within 300 km of shore (Hickey, 1979). Choice of one degree squares was made again due to data availability; the CalCOFI sampling grid does not support finer resolution.

Plots of the numbers of observations associated with each data block for the months January, April, July and October are in Appendix A. When mean values and variances were calculated, at least ten observations in a data block were required, except in the calculation of mean dynamic height, where five observations were used. Mean values generated from these numbers of observations were considered statistically significant and used unweighted in subsequent analyses. Weighting based on redundancy was not applied to avoid biasing results in favor of areas of frequent observation. The determination of ten observations as statistically significant was done subjectively after studying the data. Unfortunately specific years over which statistics for a given data block were not considered, and a bias toward a particular year, or years, may well exist. For mean dynamic height calculations, only casts which include temperature and salinity data at all standard depths from the surface to 500 m were used.

III. CHARACTERISTIC SALINITY OF THE CALIFORNIA CURRENT SYSTEM

A. GENERAL FEATURES

Along the west coast of the United States, sea surface salinity generally increases from about 32 *psu* near the Washington-Canadian border to about 34 *psu* near Baja California. At a given latitude salinity tends to be maximum at the coast, decrease off-shore, then increase again at the western limits of the CCS (Figure 4). That is, the isohalines describe a trough, the axis of which extends from the coast near the mouth of the Columbia River near 46° 15' N to a point about 500 km off the coast at Baja California. In the southwest corner of the CCS, approximately 700 km off the coast, the isohalines are oriented northwest-southeast with a relatively tight gradient, of the order 0.1 *psu* in 40 km.

As mentioned earlier, the stratification of the CCS, unlike that of other eastern boundary currents, has salinity generally increasing with depth. Profiles (Figure 5) are marked by permanent haloclines: sharp and shallow, 150 m (Huyer, 1983) in the north and less distinct and deeper, 200 m, to the south (Emery and Dewar, 1982). At 500 m the mean salinity increases from 34.1 *psu* near 50° N to 34.5 *psu* near 20° N.

B. VARIABILITY

The most dramatic seasonal change to the surface salinity in the CCS results from river discharge. During the summer the only important sources of fresh water runoff along the West Coast are the Fraser River, which discharges through the Straits of Georgia and Juan de Fuca at 48° 30' N, and the Columbia River at 46° 15' N. The Fraser's fresh water is mixed deep and its signature lost, but the direct effect of the Columbia is visible as far south as San Francisco (Huyer, 1983). During spring an area of tight isohaline spacing, roughly 0.1 *psu* in 30 km, exists within ~500 km radius of the Columbia's mouth. Through the course of a year the area of tight gradient (Figure 4) gradually decreases until by winter the strong gradient exists only in the immediate vicinity of the mouth of the river and northward along the coast of Washington.

Using CalCOFI data collected as far north as San Francisco through 1978, Lynn and Simpson (1987) have examined the physical characteristics of the CCS including salinity. The salinity minimum is at the surface off the coast of northern California and 50 to 100 m deep in the Baja California region. Near southern California there is

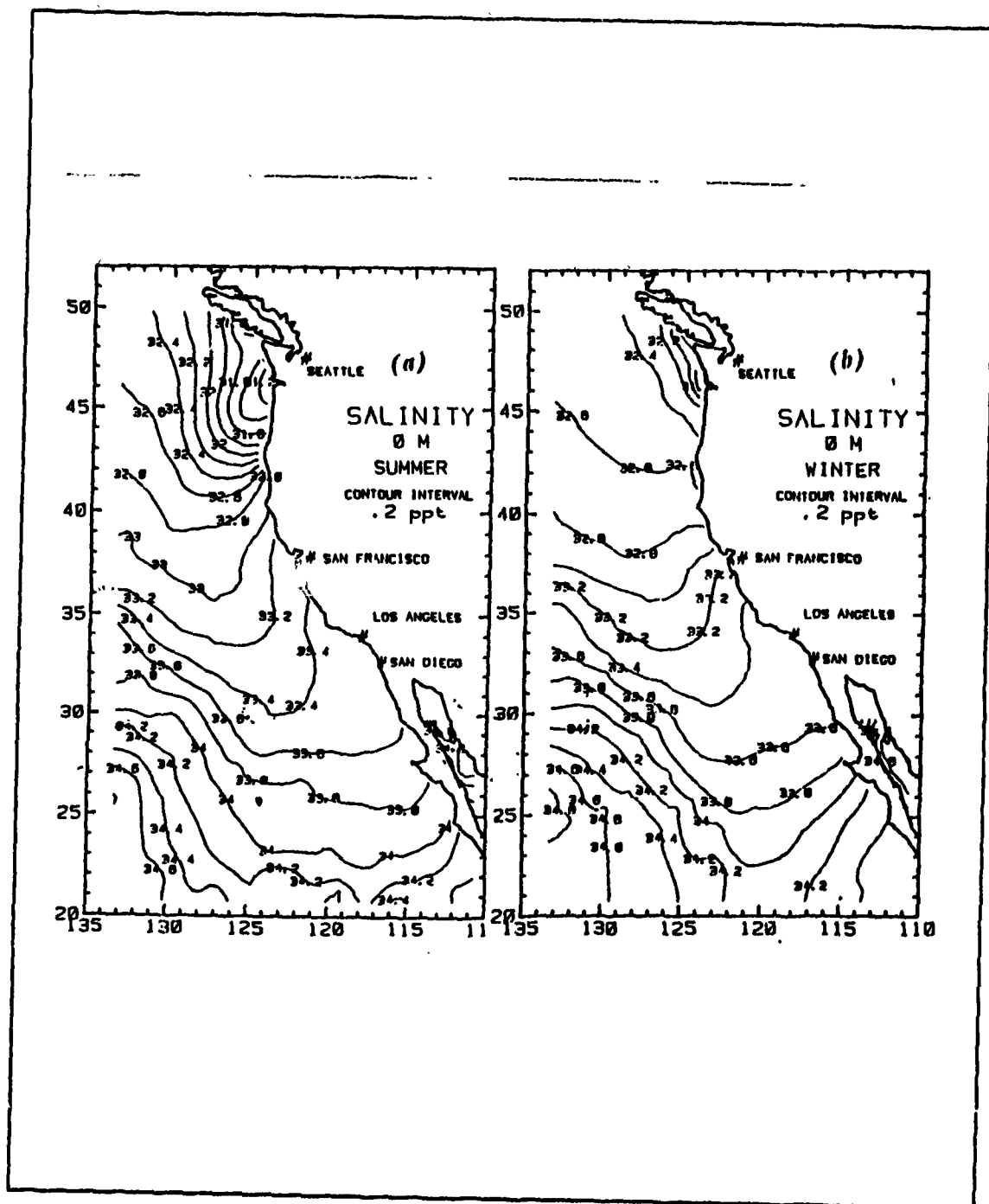


Figure 4. Surface Salinity of the CCS: Units are ppt. (a) Summer (b) Winter (from Blumberg *et al.*, 1984).

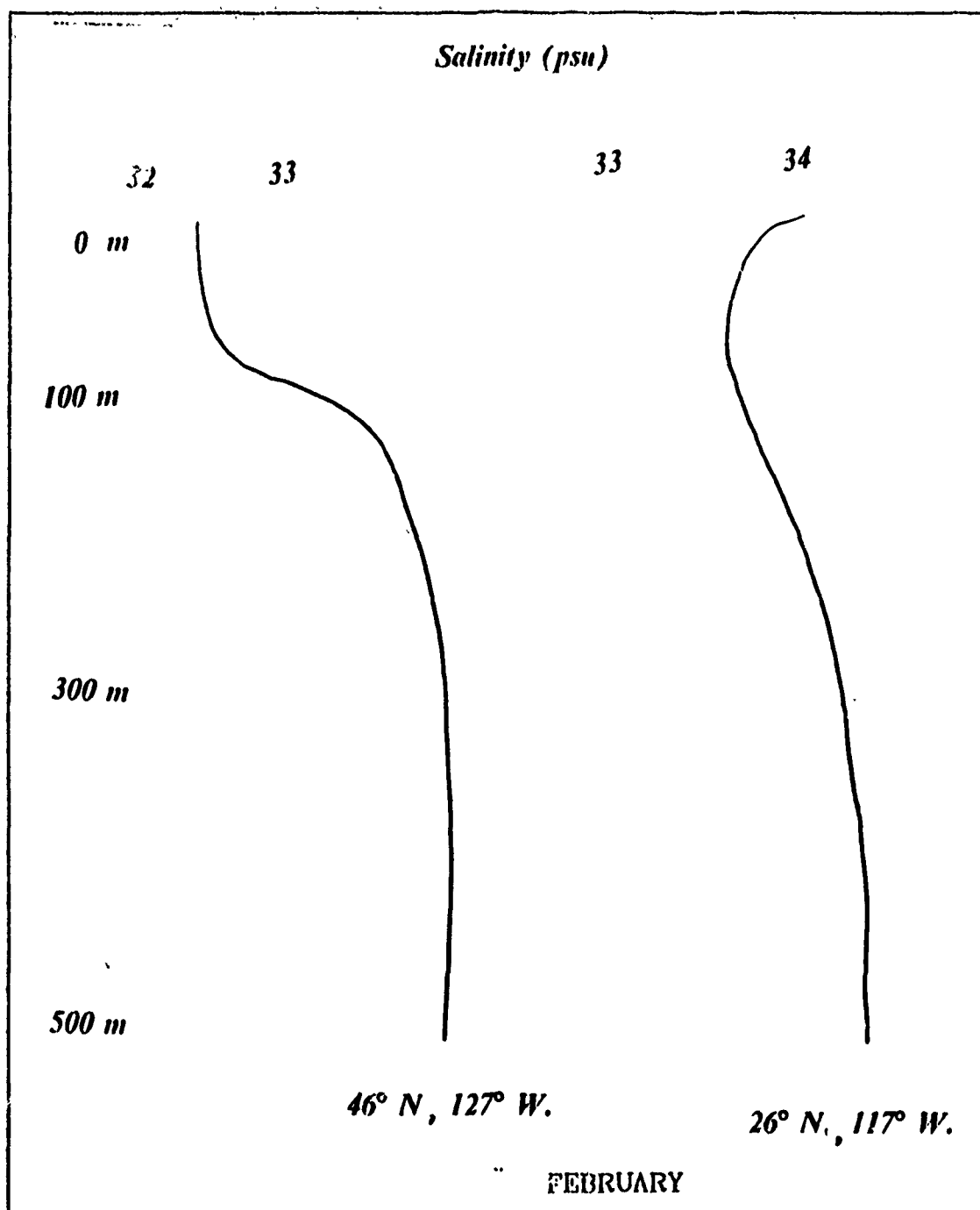


Figure 5. Typical Salinity Profiles of the CCS: These salinity (psu) profiles display mean values for February generated from the CCS data base used for this study.

generally a minimum at the surface, but in the autumn a subsurface minimum appears. Lynn and Simpson (1987) have noted significant correlations between the location of the salinity minimum and the behavior of the CC. In January, a strong inshore poleward current exists while the salinity minimum near Baja California is below the surface and offshore of the continental slope. As this minimum moves inshore and to the surface, the inshore flow becomes strongly equatorward. In October, the salinity distribution is similar to that of January, but the inshore flow is equatorward. Elsewhere in the CalCOFI region, the area of minimum salinity is consistently near, but seaward of, the maximum equatorward flow of 4 to 20 cm s^{-1} . Because of the high correlation of salinity minimum to velocity maximum to a depth of 100 m, Lynn and Simpson (1987) suggest that the low salinity core can describe the path of the CC.

IV. EFFECT OF SALINITY

A. STRATEGY

Several techniques were used to analyze the data and are described in the following sections: specific volume anomaly (Section IVB), variance and correlation of the specific volume anomaly constituents (Section IVC), mean differences of the specific volume anomaly constituents (Section IVD), dynamic height (Section IVE), and propagation of the temperature-salinity variance (Section IVF). Each method was applied at depths 10, 100, 200, and 500 m. Except in Section IVF, twelve mean months were examined. In Section IVF the statistical techniques invoked called for use of maximum number of observations, so the data were partitioned into three-month seasons; winter, for example, was defined as January-March. Graphics, except where otherwise noted, were generated for all four depths, each time period, and each technique. Practical limits on space prevent inclusion of all these plots in this thesis.¹ Only representative examples, which when contoured were hand contoured, are reproduced in the body of the text. In particular, the month of July is often chosen as the illustrative period because the coastal upwelling phenomenon is usually at its peak during that month.

B. SPECIFIC VOLUME ANOMALY

1. Method

Specific volume anomaly (defined: $V - V_{350}$, where V is specific volume, and subscripts in the second term indicate salinity 35 *psu*, temperature 0° C, and pressure in db) can be expressed as a sum of constituents related to the parameters that define the density of sea water:

$$\delta = (\delta_t + \delta_s + \delta_{st}) + \delta_{tp} + \delta_{sp} + \delta_{stp} \quad (3)$$

(1) (2) (3) (4) (5) (6)

Subscripts t, s, and p stand for temperature, salinity and pressure, respectively. In this linear construct, specific volume anomaly, also termed steric anomaly, is the sum of a part due to variation in temperature from 0° C, salinity other than 35 *psu*, their interaction, and the interaction of deviant temperature and salinity with pressure (Sverdrup

¹ Unpublished data are on file at the Department of Oceanography, Naval Postgraduate School, Monterey, CA.

et al., 1942:57-59). Since the term δ_{sp} is much smaller than the other terms, it is virtually always ignored, and is not considered in this thesis. The sum of terms in parenthesis represents the total combined contribution of temperature and salinity calculated at surface pressure, is called the thermosteric anomaly, Δ_{st} , and is by far the greatest contribution to the total specific volume anomaly. Sverdrup (1933) introduced the use of the thermosteric anomaly, which is easily determined in total from the measured or computed surface density, as a computational convenience. After the density anomaly calculated at zero pressure is converted to Δ_{st} , only the two values δ_{sp} and δ_{st} are necessary to determine specific volume anomaly.

Traditionally then, since Sverdrup (1933), only three tables (or calculations) are used to determine δ . However, it can sometimes be quite useful to know the individual contributions to Δ_{st} . For example, if δ_t is small or constant while δ_s is large and fluctuating, a dynamic modeler might simplify his model by keeping salinity constant. Similarly, if a feature can be defined by its salinity signature, an observationalist might identify the feature's boundary by a sharp gradient in δ_s .

The equation of state for seawater:

$$\rho_{stp} = \frac{\rho_{st0}}{(1 - P/k_{stp})}, \quad (4)$$

where k is the secant bulk modulus and P pressure, translates to an equation for thermosteric anomaly:

$$\Delta_{st} = \frac{1}{\rho_{st0}} - 9.7266204 \times 10^{-4} \quad (5)$$

or

$$\Delta_{st} = \frac{1}{(\rho_w = \sum_{n=0}^5 a_n t^n) + S(\sum_{n=0}^4 b_n t^n) + S^{3/2}(\sum_{n=0}^2 c_n t^n) + d_0 S^2} - 9.7266204 \times 10^{-4}, \quad (6)$$

where ρ_w is the density of reference pure water, a , b , and c are coefficients in power series on temperature, and d_0 is a coefficient on salinity (UNESCO, 1987). This inverted sum of terms in S and T , cannot readily be analytically sorted into parts due solely to temperature, salinity, and their interaction. Therefore, some other means of defining δ_{st} , δ_s , and δ_t is needed. In UNESCO (1987) equation (5) is modeled by:

$$d_{stp} = d_{s0} + (d_{35sp} - d_{350}) + (d_{s0p} - d_{s00}) \quad (7)$$

(1)
(2)
(3)
(4)
(5)

(a)
(b)
(c)

(Here d is used in lieu of δ to alleviate confusion that might otherwise result when comparing terms of equation (3) to terms of equation (7)). Clearly specific volume calculated for a given salinity and temperature at surface pressure, d_{s0} , is precisely the thermosteric anomaly. Term (b), the difference between d calculated at temperature and depth with salinity 35 *psu* and d calculated for the same temperature but at surface pressure, describes the interplay of temperature and pressure, δ_p . Similarly, term (c) represents δ_p . (Terms a, b, and c correspond to UNESCO, 1987, tables III, V, and VI.)

Now, consistent with the currently accepted equation of state for seawater (UNESCO, 1981), how does one model the individual constituents of the thermosteric anomaly? Term (3) in equation (7) is the value of δ that would result at zero pressure if salinity were a constant 35 *psu*. Therefore $(d_{sp} - d_{350})$ represents the part of δ due to salinity deviation from 35 *psu* and interaction of temperature with that deviation at a certain pressure p , or:

$$d_{sp} - d_{350} = (\delta_s + \delta_{st} + \delta_{tp} + \delta_{sp}). \quad (8)$$

Similarly:

$$d_{stp} - d_{s00} = (\delta_{st} + \delta_{tp} + \delta_{sp} + \delta_t). \quad (9)$$

Subtraction of equation (9) from equation (8) yields:

$$\delta_t - \delta_s = d_{350} - d_{s00}. \quad (10)$$

It would appear d_{350} and d_{s00} can serve as models for δ_t and δ_s . Using that assumption, equation (3) can be reconfigured from appropriate elements of equation (7):

$$\begin{aligned}
\delta_t &= d_{35t0} \\
\delta_s &= d_{s00} \\
\delta_{st} &= \Delta_{st} - \delta_t - \delta_s = d_{st0} - d_{35t0} - d_{s00} \\
\delta_{tp} &= d_{35tp} - d_{35t0} \\
\delta_{sp} &= d_{s0p} - d_{s00} \\
d_{stp} &= d_{35t0} + d_{s00} + (d_{st0} - d_{35t0} - d_{s00}) + (d_{35tp} - d_{35t0}) + (d_{s0p} - d_{s00}).
\end{aligned}
\tag{11}$$

(1)
(2)
(3)
(4)
(5)

Collection of terms shows equation (11) to be identical to equation (7) and therefore this model to be consistent with the UNESCO (1987) table formulation. Descriptively this formulation should also be acceptable: the temperature contribution is defined as the specific volume that would result from the observed temperature, if salinity were 35 *psu* and pressure 0 db; the salinity contribution at the same depth is similarly the specific volume anomaly that would result from actual salinity and 0° C; the combined term is simply the difference of the sum of those two terms and Δ_{st} or the amount by which their sum misrepresents Δ_{st} .

It follows that $(\delta_t + \delta_p)$ can be represented by d_{35tp} , and $(\delta_t + \delta_s)$ by d_{t0p} . It was decided to use this combined temperature and temperature-pressure term in order to compare total saline effect to temperature effect at a given pressure. As a notational convenience, throughout the remainder of this thesis " δ_T " and " δ_s " will be used in lieu of " $(\delta_t + \delta_p)$ " and " $(\delta_t + \delta_s)$ " and be considered synonymous with " d_{35tp} " and " d_{t0p} ." In this formulation, the term $\delta_{st} = \Delta_{st} - \delta_T - \delta_s$ will include pressure effects. Since units used to describe specific volume anomaly will in every case be $10^{-3} \text{ m}^3 \text{ kg}^{-1}$, they will hereafter be deleted in the text.

2. Results

For each month and the depths 10, 100, 200, and 500 m, each of the fields δ_T , δ_s , and δ_{st} were computed and plotted (see note 1). Generally, the specific volume anomaly field consists of a dome centered near 45° N, 124° W, a depression centered near San Francisco, and a ridge parallel and adjacent to the Baja California peninsula with axis south to north about 3° longitude from shore. In July (Figure 6) all three features are well established. The Columbia River outflow is at its peak during late June and early July (Huyer, 1983), and the warm, fresh surface plume results in enhancement of the northern dome. July is also a period of strong coastal upwelling (Huyer, 1983), and the cold, salty upwelled water results in intensification of the central depression. The horizontal gradient in δ decreases with depth, particularly in the northern region.

At 100 m (Figure 7) for example, there is no evidence of the warm, fresh core so prevalent on the surface. At 500 m (Figure 8) the gradient is very weak everywhere with dense cores centered about 2° off the coast at San Francisco and the northern Baja California peninsula. An important observation is that δ_{σ} (Figure 9) values are one to two orders of magnitude less than the sum of δ_T (Figure 10) and δ_S (Figure 11). This shows the steric anomaly to be very nearly equal to the sum of a temperature and salinity part so that this formulation is an effective linearization. In all cases δ_{σ} is negative, increasing slightly in absolute value with depth; values of -3 to -6 being common at 10 m and -6 to -9 more typical at 500 m (Figure 12). Gradients in δ_{σ} are everywhere small; however the cross term becomes more negative in areas where temperature and pressure act together to increase δ , and less negative when temperature and salinity act in conjunction to decrease δ . When salinity and temperature oppose change in specific volume anomaly, δ_{σ} remains nearly constant; the temperature-pressure interaction acts to mitigate change in specific volume anomaly that results from changes in either.

Advection of subarctic water south from the point where the North Pacific Current feeds the CC, results in cold (low δ_T) and fresh (high δ_S) tongue-like structures superimposed on the other characteristic features of the CCS described in part below. In the immediate vicinity of the coast, salinity and temperature act together to decrease steric anomaly. Near the surface this is most apparent just north of San Francisco Bay in July where large scale upwelling results in cold, salty water. The effects on density of temperature and salinity are positively correlated with specific volume anomaly near 45° N, 127° W, where the warm, fresh discharge of the Columbia River results in the geopotential dome described above. This feature is strongest in summer, weakest in winter, and most apparent in the δ_S field. Such seasonality is in keeping with the Columbia River's outflow cycle. There also persists a fresh dome at the mouth of the Strait of Juan de Fuca, but it is restricted to the immediate vicinity of the coast. (Since the fine scale salinity-temperature interplay associated with the drainage from Vancouver Island is not resolvable on the coarse scale used here, activity in that area is generally not included in discussion here.)

Near the surface, throughout the year, mean gradients of δ_T across the CCS (neglecting small scale features like those described above) are at least 50 percent greater than those of δ_S . At a depth of 10 m, absolute values of δ_T , which range from about 80 to 400 north to south through the year, fluctuate more season to season and are generally larger than values of δ_S which range typically from 50 to 250. However the gradient in δ_T diminishes more rapidly with depth than does that of δ_S ; the result is that at

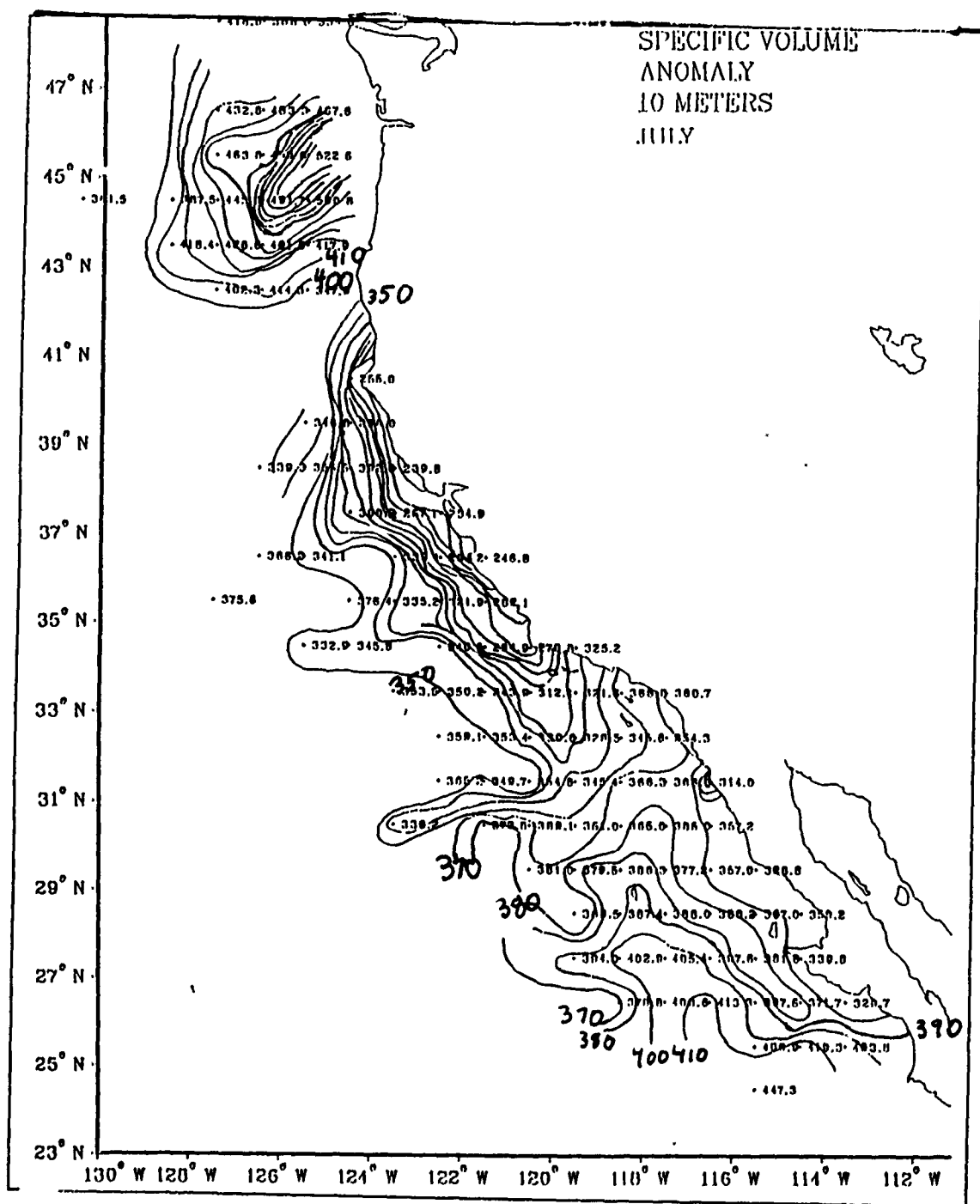


Figure 6. Steric Anomaly, July, 10 m: Units are $10^{-8} \text{ m}^3 \text{ kg}^{-1}$, and the contour interval is 10 units.

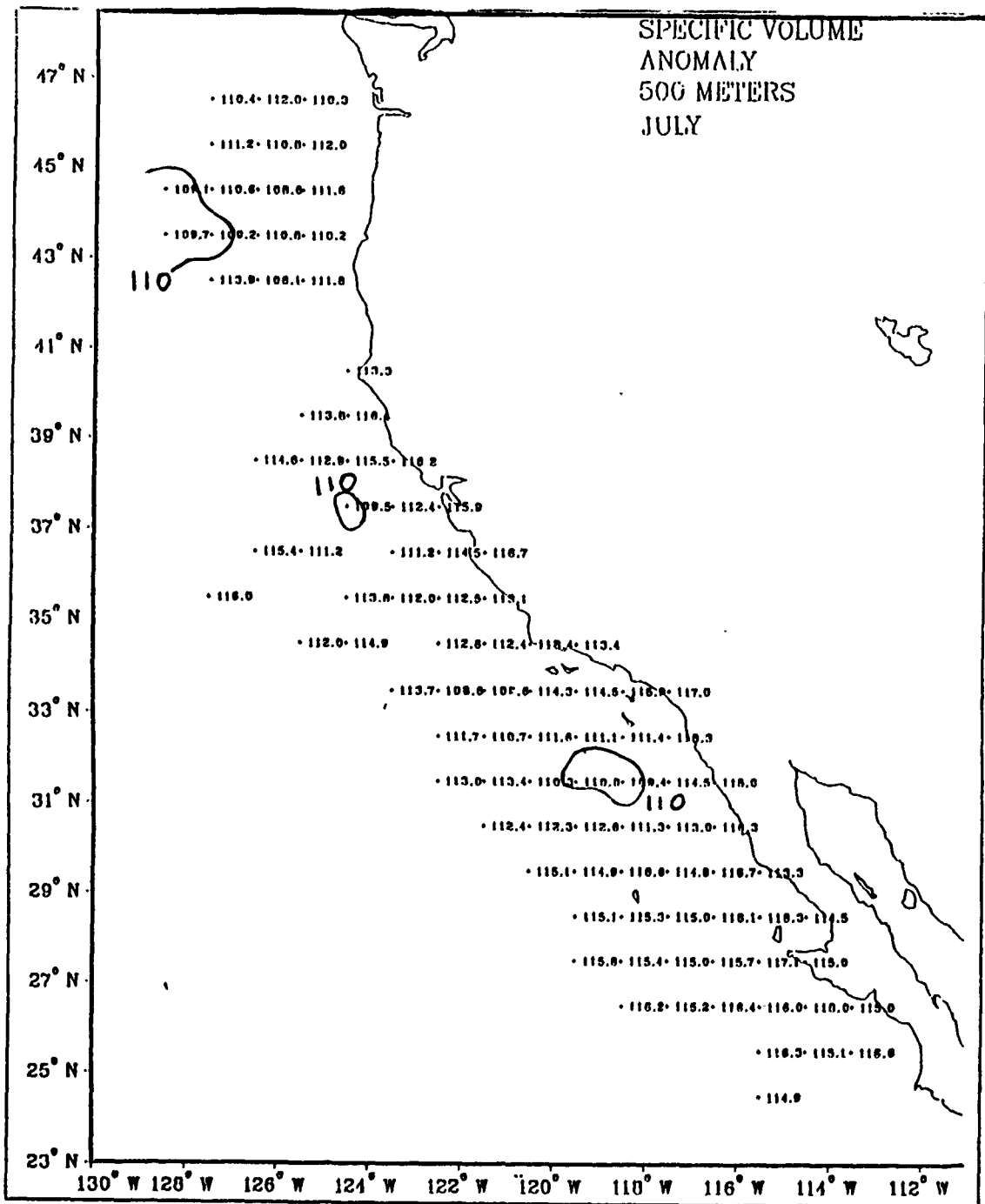


Figure 8. Steric Anomaly, July, 500 m: Units are $10^{-8} m^3 kg^{-1}$, and the contour interval is 10 units.

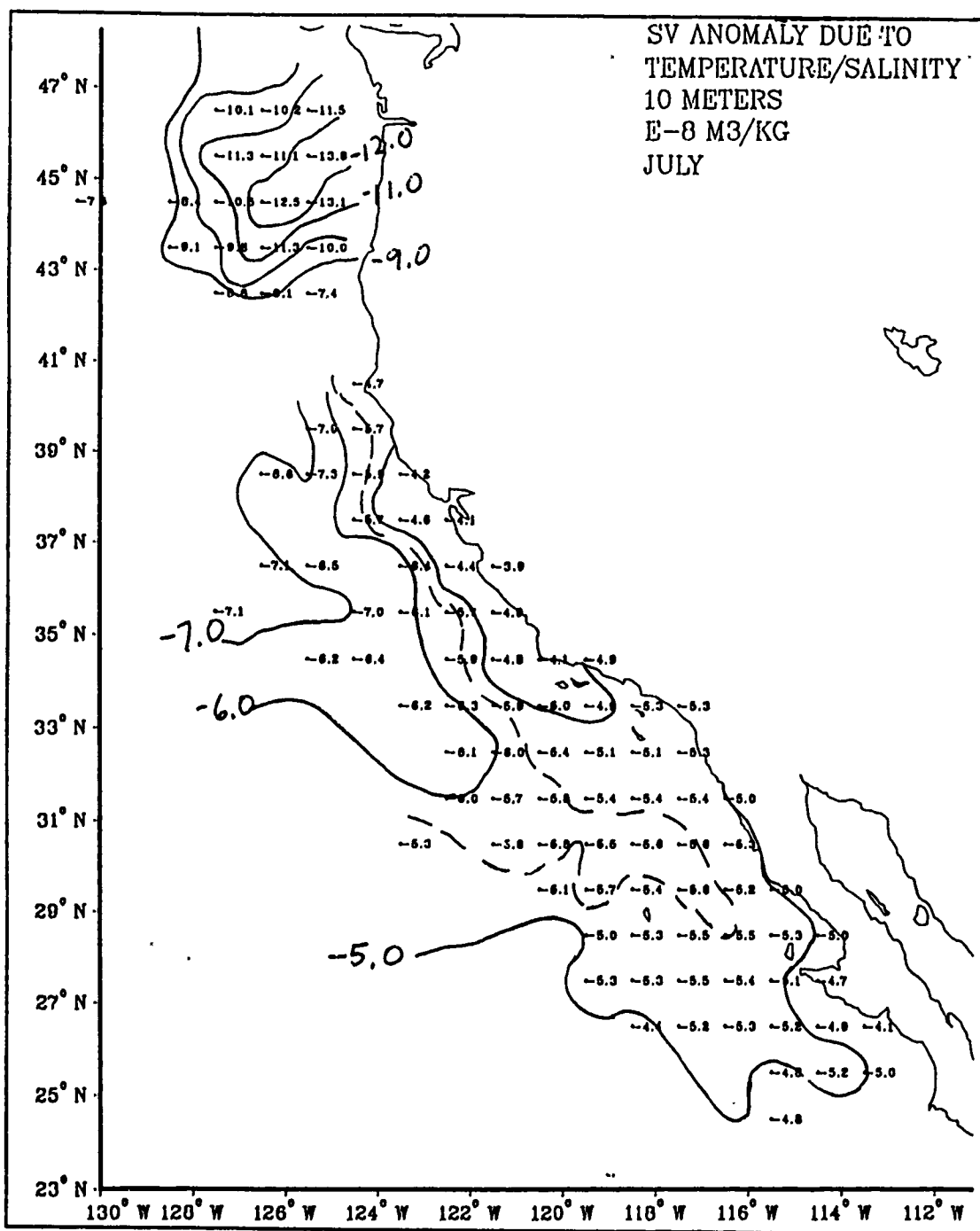


Figure 9. Specific Volume Anomaly (T-S), July, 10 m: δ_{σ_t} . Units are $10^{-3} \text{ m}^3 \text{ kg}^{-1}$, and the contour interval is 1 unit (dashed contour interval is 0.5 units from solid contours).

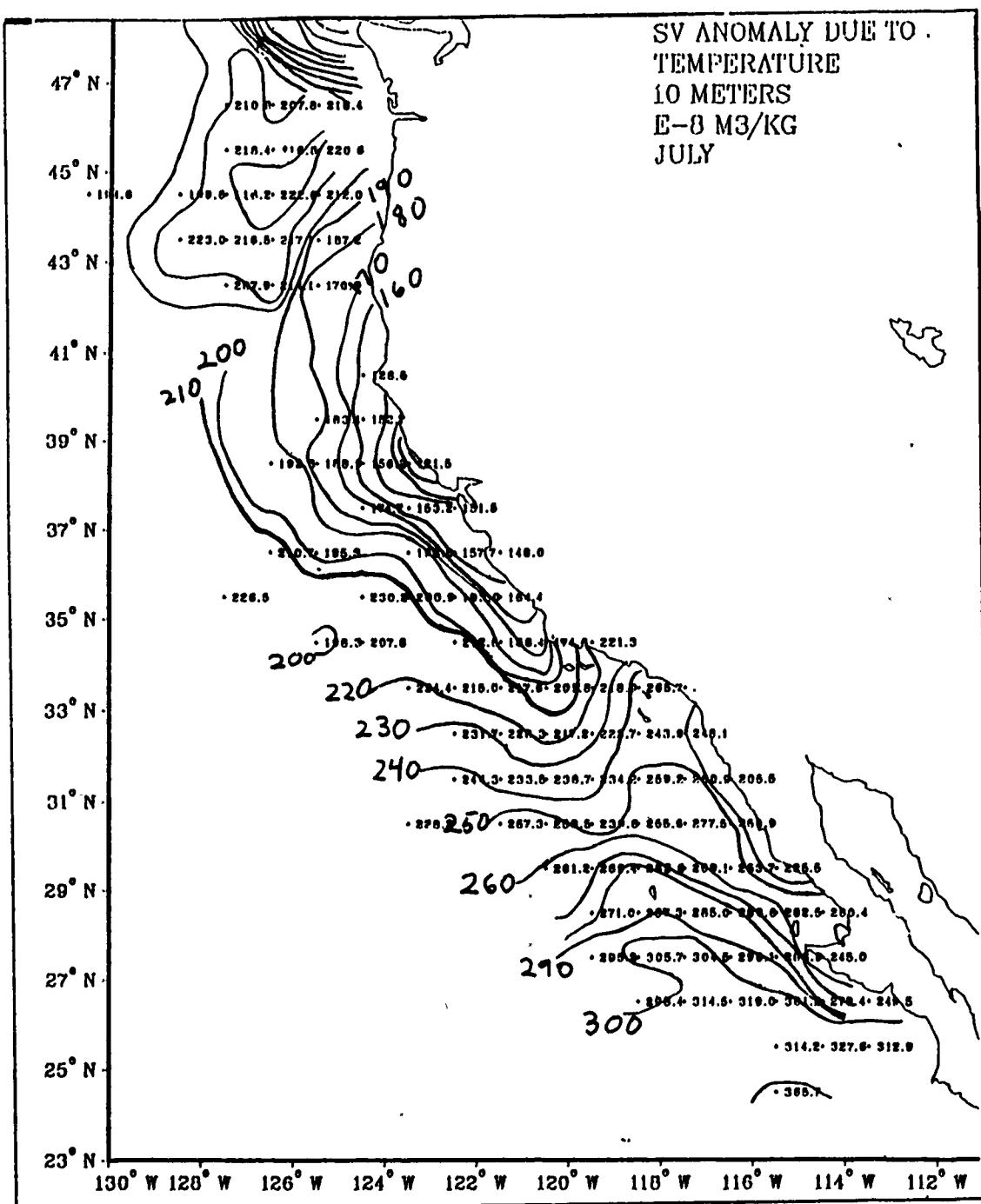


Figure 10. Specific Volume Anomaly (T), July, 10 m: δ_T . Units are $10^{-8} m^3 kg^{-1}$, and the contour interval is 10 units.

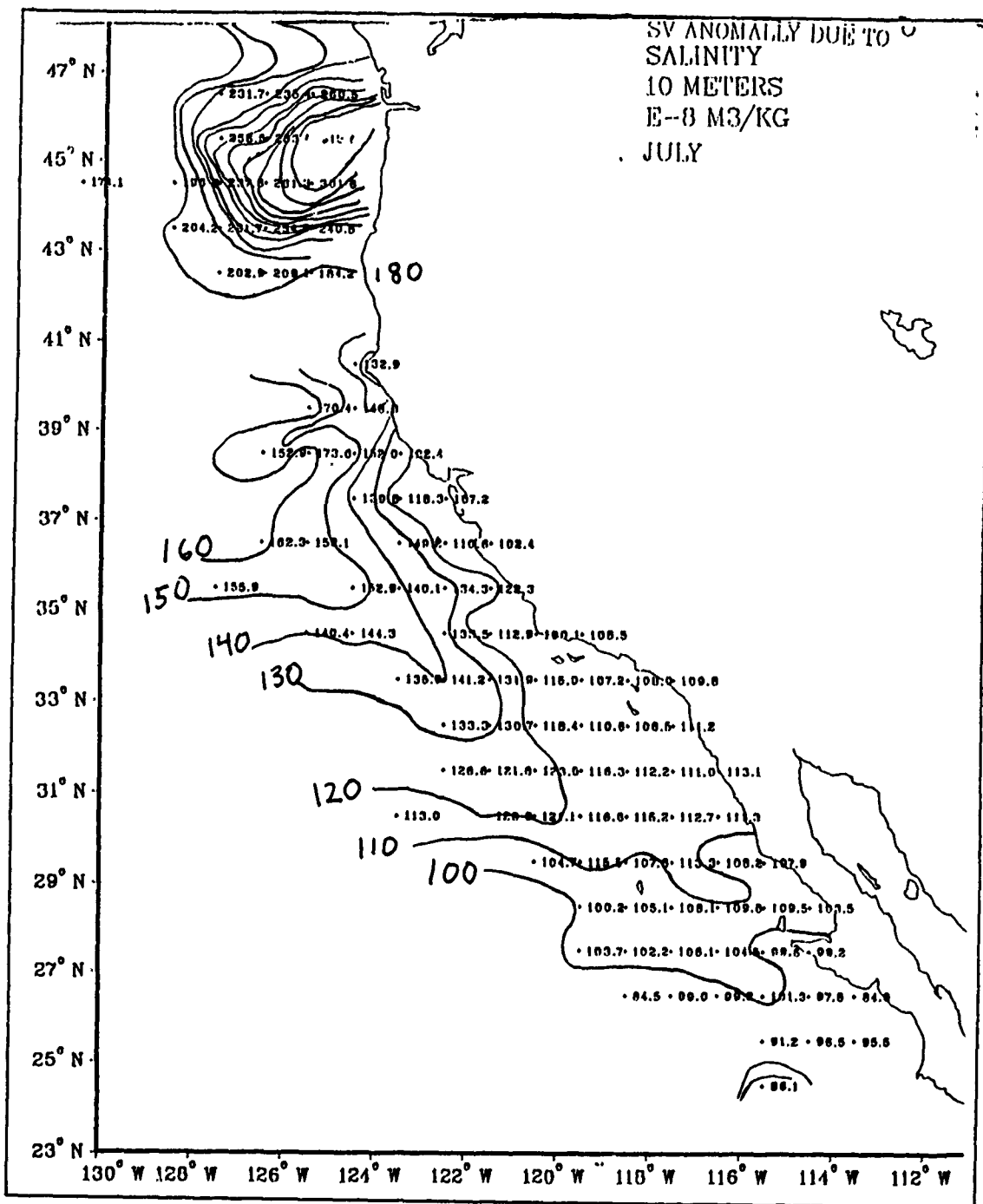


Figure 11. Specific Volume Anomaly (S), July, 10 m: δ_s . Units are $10^{-3} m^3 kg^{-1}$, and the contour interval is 10 units.

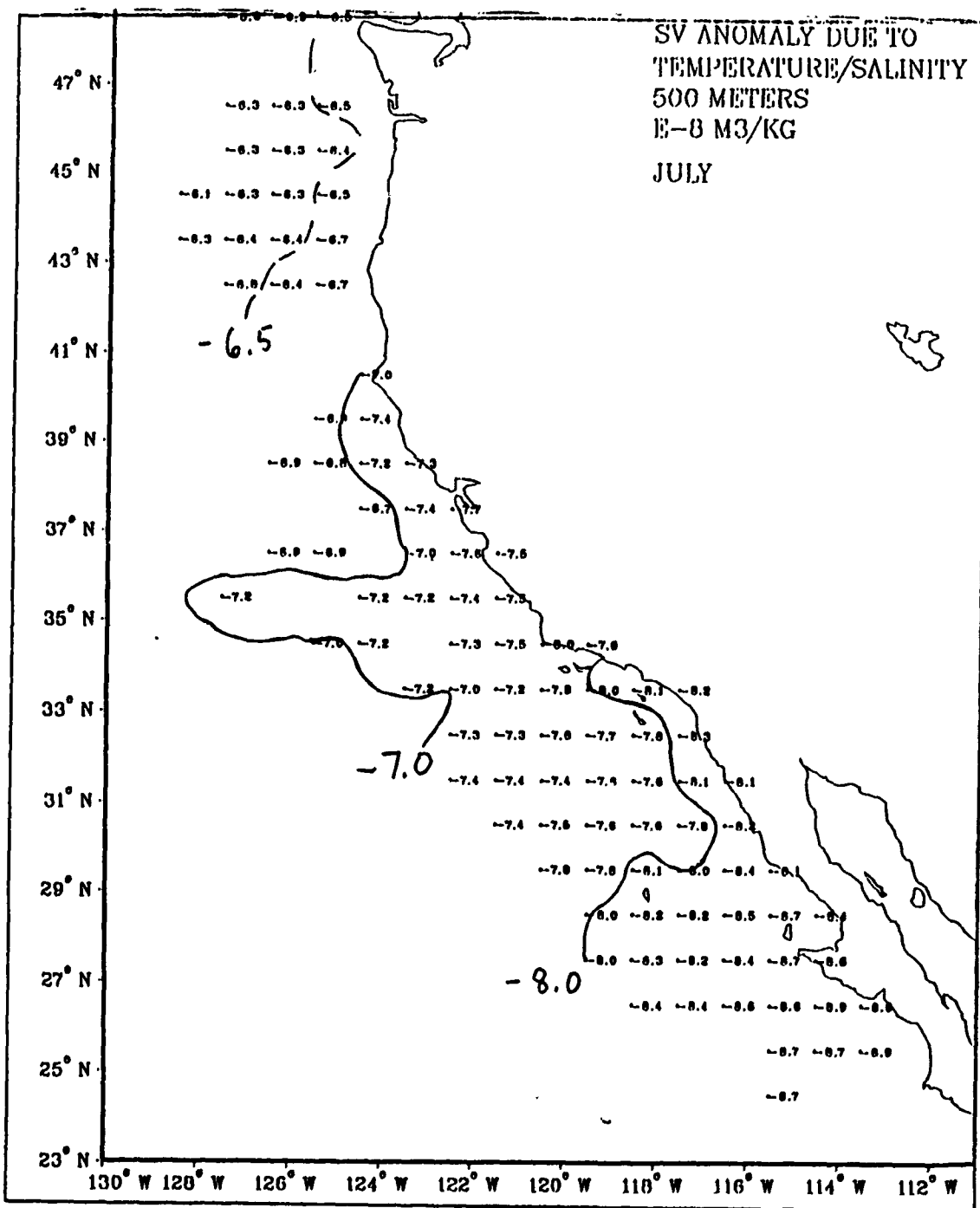


Figure 12. Specific Volume Anomaly (T-S), July, 500 m: δ_{σ} . Units are $10^{-8} \text{ m}^3 \text{ kg}^{-1}$, and the contour interval is 1 unit (dashed contour interval is 0.5 units from solid contours).

500 m, δ_T (Figure 13) and δ_S (Figure 14) fields are virtually mirror images of each other. At that depth, ranges of 40 to 70 are typical of δ_S , as compared to 45 to 75 for δ_T . At an intermediate depth of 100 m, ranges from 65 to 190 and 70 to 150 correspond to δ_T (Figure 15) and δ_S (Figure 16), respectively, while ranges of 60 to 135 and 40 to 85 are representative of δ_T (Figure 17) and δ_S (Figure 18) at 200 m. The salinity signature of the Columbia River is practically gone at 100 m. In fact, in the region north of 43° N, from 100 m down, gradients in both the δ_T and δ_S fields are with one exception considerably weaker than in southern areas. The exception is a δ_S maximum at 200 m during October in the data rich area near 44° N, 127° W (Figure 19). This unexplained, but possibly real (the central value is based on 22 observations although surrounding mean values are from as few as 10) mean feature supports a gradient of $8.2 \times 10^{-8} \text{ m}^3 \text{ kg}^{-1}$ in one degree of longitude, which is comparable to the strongest gradients anywhere in the CCS at that depth and much stronger than any other in the northern sector.

At 100 m, and to a lesser extent 200 m, a meridional tongue of δ_T with its axis just offshore is apparent. That is, there is a pronounced offshore cold core adjacent to the California coast. Cyclonic flow around this feature is consistent with nearshore subsurface poleward flow typical of the CCS.

C. VARIANCE AND CORRELATION OF THE SPECIFIC VOLUME ANOMALY CONSTITUENTS

1. Method

Often the absolute value of a quantity is of less importance than the nature of the temporal or spatial derivatives of that quantity. Statistics generated from a significant number of observations can provide information concerning those differentials. Deviation from local mean values can cause changes in local gradient or prevent change in local gradient when neighboring values change. In a flow supported by tight gradients, small meanders result in relatively large changes in local values. The actual variance² of a field is a descriptor of likely deviation; therefore, in a data block, large variance may indicate large gradient or large variability in the local gradient. The precise effect on instantaneous gradient, of course, depends on behavior of, and correlation with, neighboring data blocks. For example, if all nearby mean values change in tandem with each other, the gradient would remain constant and "no change" in gradient would result from variance. Without thorough knowledge of the nature of the field of interest,

² Whether or not the sample variances calculated here are valid representations of true variance in the various fields is a relevant question. Section IVF1 addresses this point in detail.

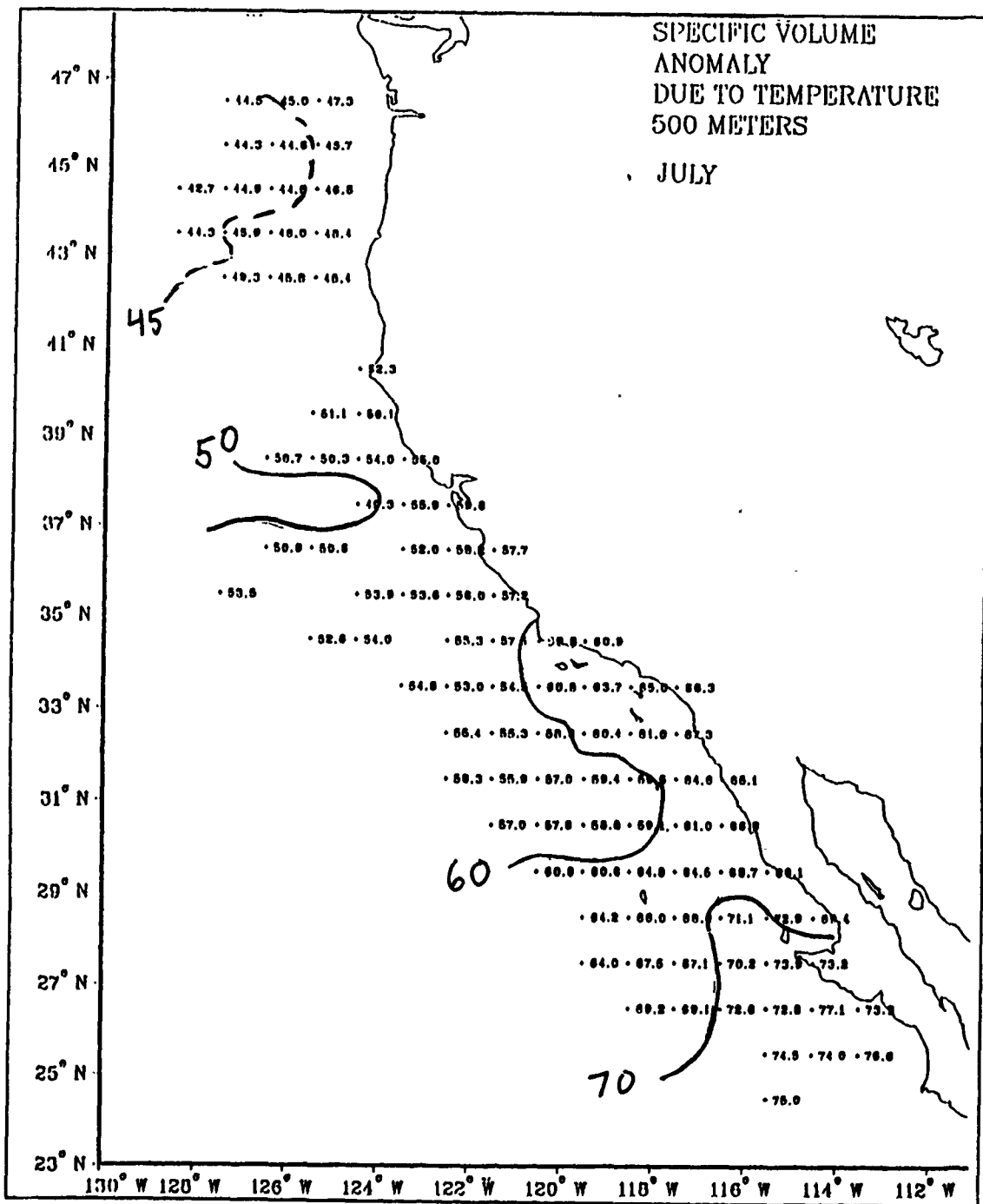


Figure 13. Specific Volume Anomaly (T), July, 500 m: δ_T . Units are $10^{-3} m^3 kg^{-1}$, and the contour interval is 10 units (dashed contour interval is 5 units from solid contours).

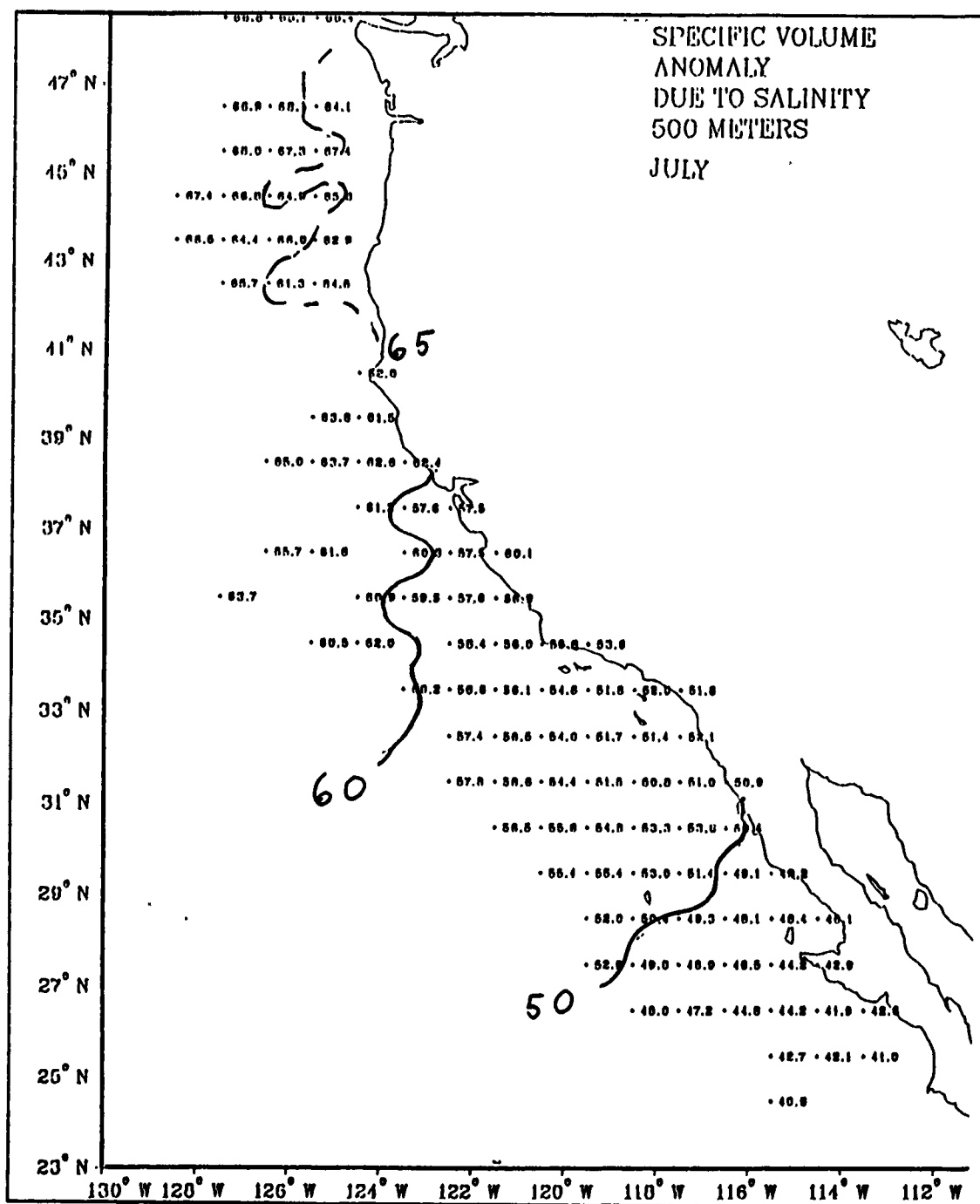


Figure 14. Specific Volume Anomaly (S), July, 500 m: δ_S . Units are $10^{-8} m^3 kg^{-1}$, and the contour interval is 10 units (dashed contour interval is 5 units from solid contours).

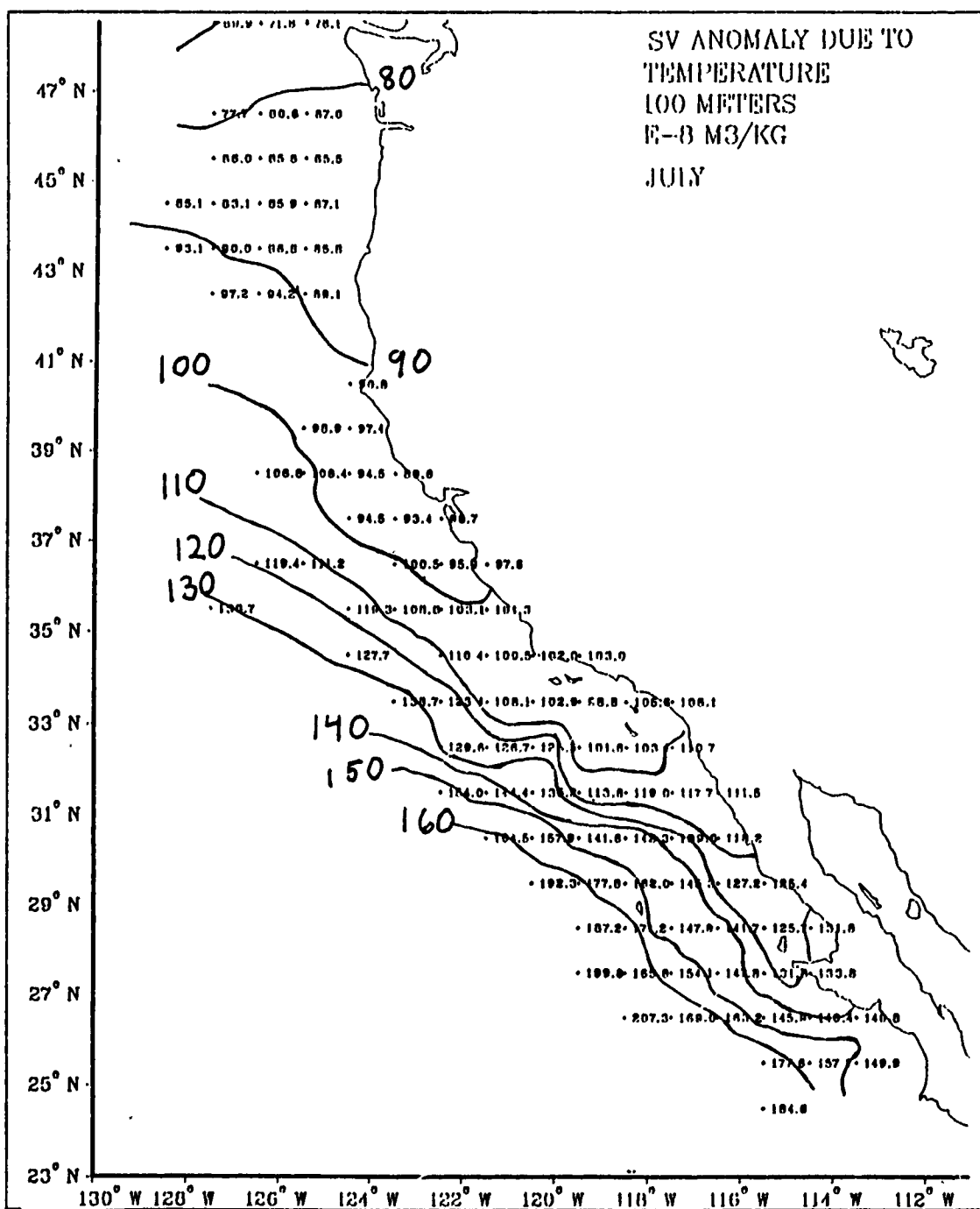


Figure 15. Specific Volume Anomaly (T), July, 100 m: δ_T . Units are $10^{-3} \text{ m}^3 \text{ kg}^{-1}$, and the contour interval is 10 units.

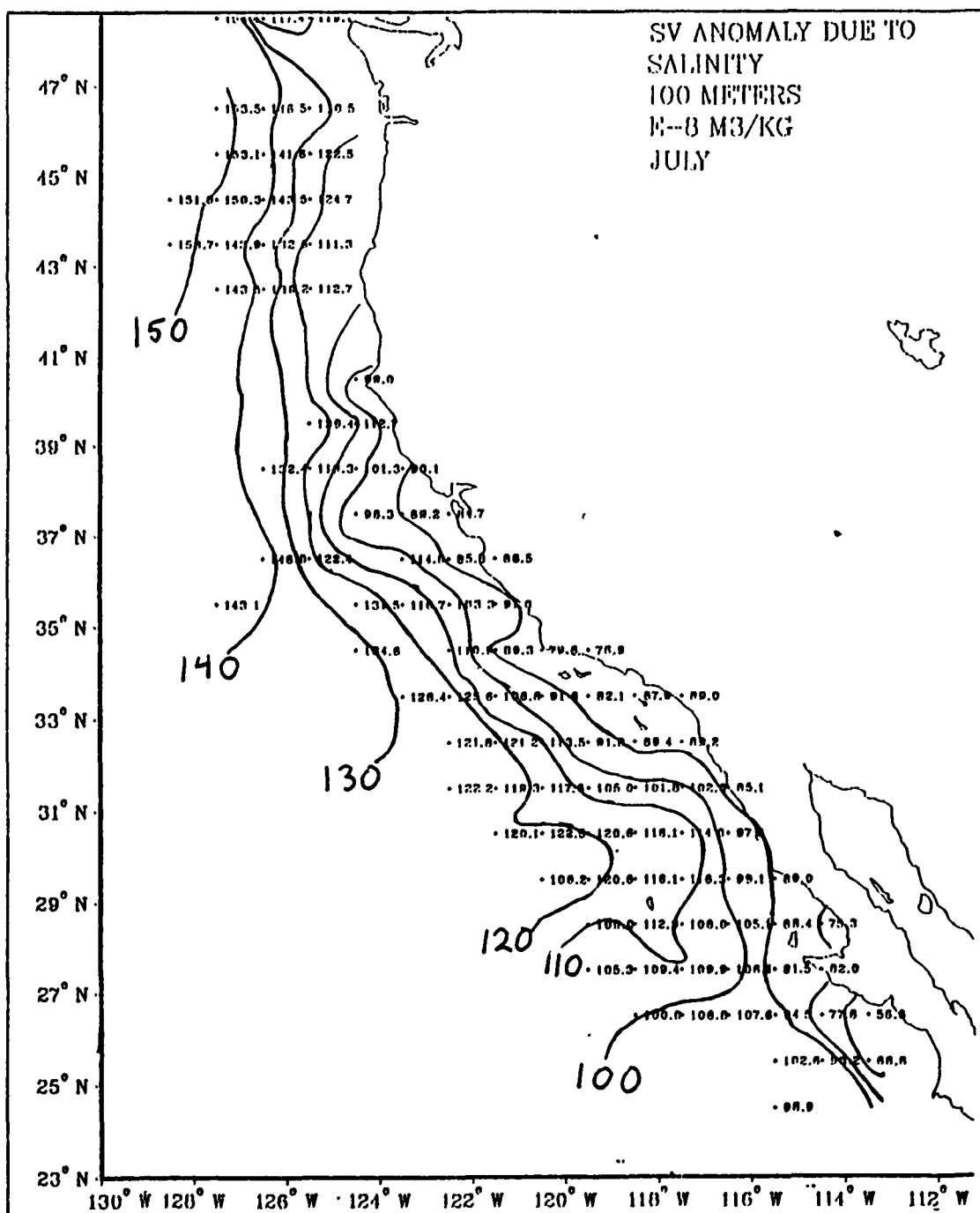


Figure 16. Specific Volume Anomaly (Sv), July, 100 m: δS . Units are $10^{-3} m^3 kg^{-1}$, and the contour interval is 10 units.

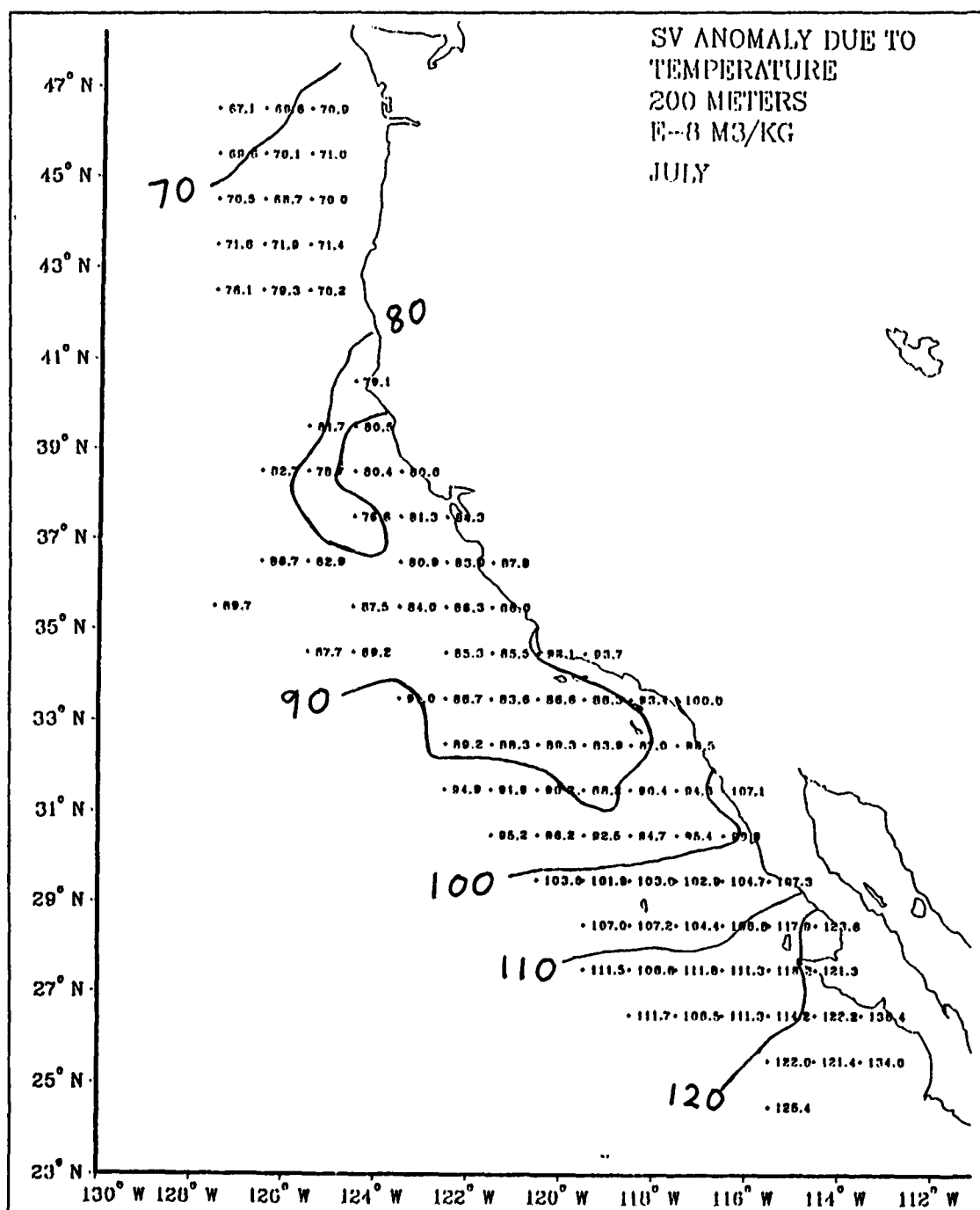


Figure 17. Specific Volume Anomaly (T), July, 200 m: δ_T . Units are $10^{-8} m^3 kg^{-1}$, and the contour interval is 10 units.

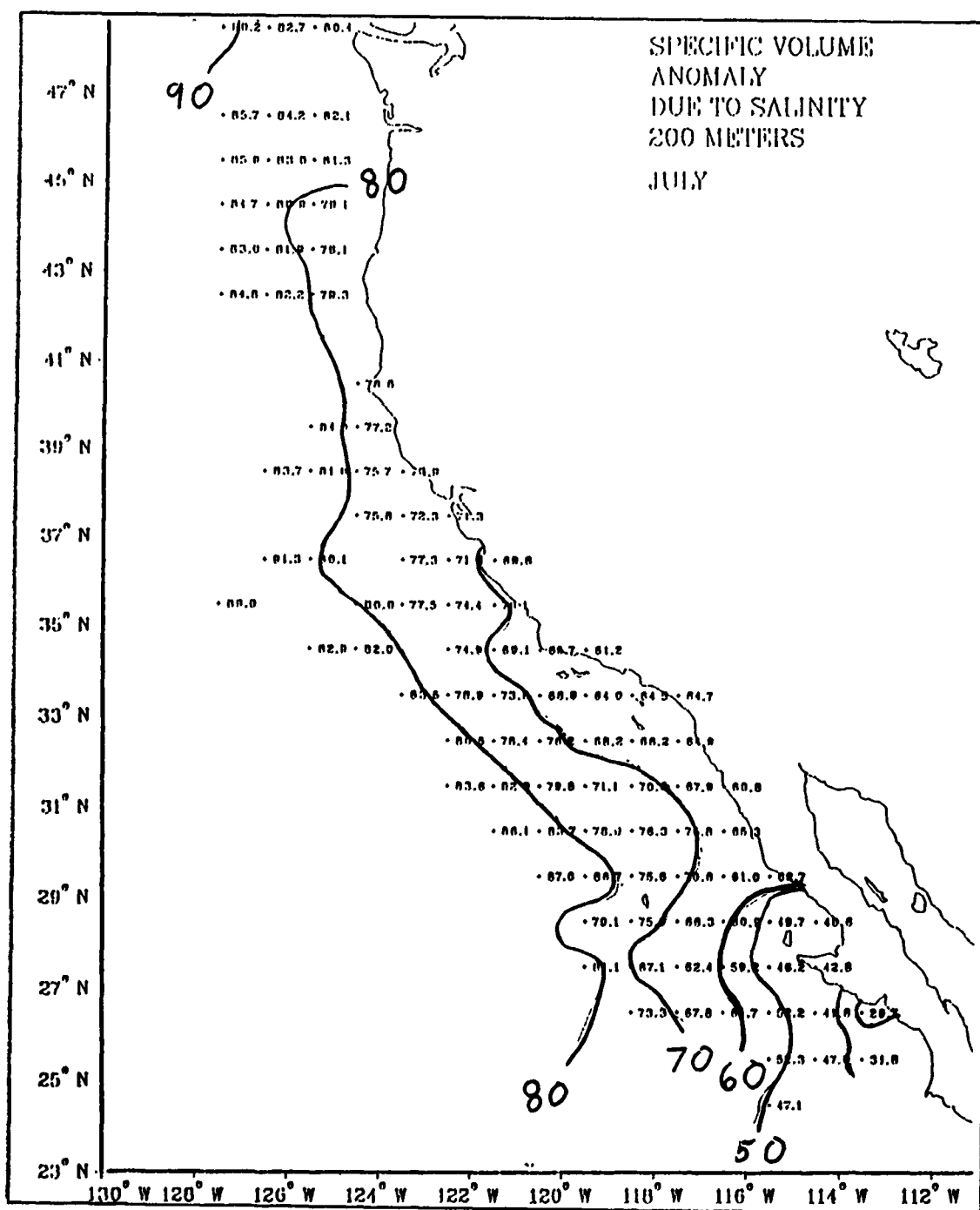


Figure 18. Specific Volume Anomaly (S), July, 200 m: δ_s . Units are $10^{-8} m^3 kg^{-1}$, and the contour interval is 10 units.

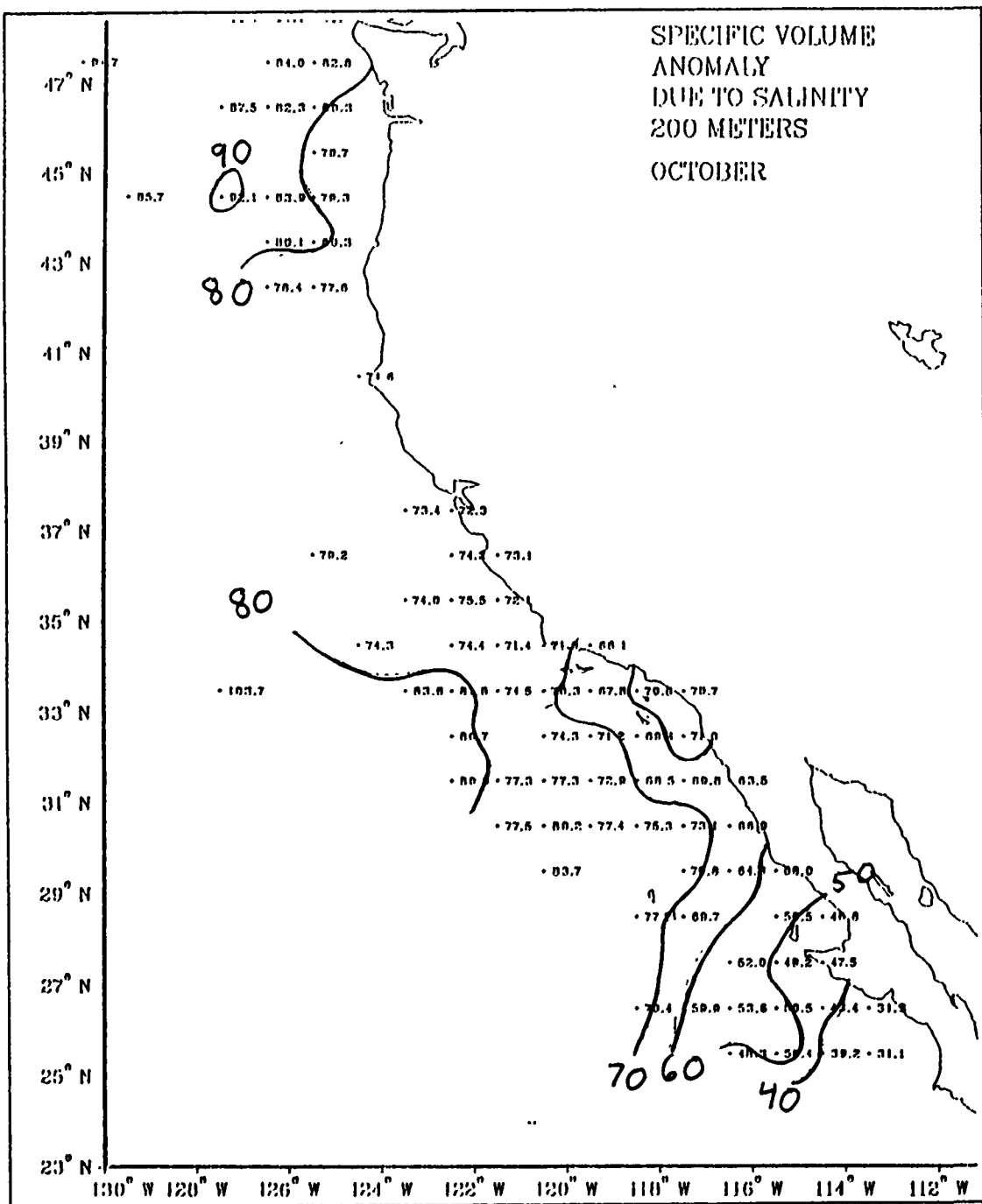


Figure 19. Specific Volume Anomaly (S), October, 200 m: δ_s . Units are $10^{-8} m^3 kg^{-1}$, and the contour interval is 10 units.

it is impossible to quantify gradient from sample variance calculation, and the fact that two data blocks have identical variance does not mean that they have identical gradient. However, determination of the contribution of various constituents to the total variance provides strong indication of the contribution of those constituents to the development of the field of interest. It is with this caveat that the following analysis technique is used.

Variance of the specific volume anomaly field results from the density changes that can be key to momentum balances. To evaluate the importance of saline variance to specific volume anomaly variance, $\sigma_{\delta_s}^2$ (variance in δ_s) should be compared to σ_{δ}^2 (variance in δ). Because equation (3) is linear, it is tempting to try to represent the variance of δ as the sum of the variances of the constituents. If this were possible, comparison of $\sigma_{\delta_T}^2$ (variance in δ_T) to σ_{δ}^2 , for example, would show at a glance how much of the total variance is due to temperature variance alone. That is, whenever the ratio $\sigma_{\delta_T}^2/\sigma_{\delta}^2$ remains constant and large, approaching one as an ideal limit, salinity variance could be deemed unimportant. Conversely if $\sigma_{\delta_T}^2/\sigma_{\delta}^2$ varies significantly over time or space intervals of interest, salinity variance could be considered important. However, because the constituents of specific volume anomaly are not independent of each other, this approach is not valid. The covariances play an essential role in determining the variance of the specific volume anomaly field. Therefore, to evaluate a term on the right hand side of equation (3) as a potential estimator of δ , in addition to variance comparison, it is necessary to determine how that term correlates with δ . If, for example, δ_T is highly correlated with δ , then most of the variance in δ can be accounted for by a linear relationship with δ_T . If also the variance of δ_T is of similar magnitude to that of δ , then δ_T can be considered a good estimator. After all, if δ changes when δ_T changes, in similar amounts and directions, then δ_T would be expected to model δ well. If that is the case, a similar look at the behavior of δ_s will probably show it contributes little to total variance, and salinity might be considered unimportant to the development of the specific volume field.

The correlation coefficient is useful as an indicator of the degree of correlation but more useful as an indicator of the sign of the correlation. The coefficient of determination, on the other hand, tells exactly how much of the variation in one variable is a result of a linear relationship with the other (e.g., Walpole and Myers, 1985).

These ideas can be used to evaluate the validity of the use of temperature alone to determine density. Wherever δ_T is highly correlated with δ , and has variance of similar magnitude, modeling δ with δ_T (or ρ with $\rho(T)$) should give acceptable results. If δ_T is highly correlated and its contribution to total variance nearly constant, even if not

precisely the same magnitude as total variance, a δ_T density model might still be acceptable because it will predict a representative gradient that will differ from the true gradient by a nearly constant factor.

2. Results

Variances of δ , δ_T , and δ_S were computed for each level of each data block, as were the covariances, $\sigma_{\delta_T\delta}$ (covariance between δ_T and δ) and $\sigma_{\delta_S\delta}$ (covariance between δ_S and δ). Correlation coefficients between δ and δ_T ($r_{\delta\delta_T}$) and δ and δ_S ($r_{\delta\delta_S}$) were also computed:

$$r_{\delta x} = \frac{\sigma_{\delta x}}{\sqrt{\sigma_{\delta}^2 \sigma_x^2}} \quad (12)$$

where x represents either δ_S or δ_T . In addition, coefficients of determination, $r_{\delta\delta_T}^2$, and $r_{\delta\delta_S}^2$ (as used in Figures 22-29) were calculated.

Maps of determination coefficients (given the sign of the correlation coefficient) for all months and the depths 10, 100, 200 and 500 m were evaluated (see note 1). Multiplication of the variance in δ_T , by $r_{\delta\delta_T}^2$, determines how much of the total variance in δ is due to variance in δ_T . Below about 100 m, variance in the δ field is very small, too small to allow confidence of statistical significance. Analysis of δ_T and δ_S correlations with δ is therefore limited to the upper 100 m. Generally δ_T (Figure 20, Figure 21) is more highly correlated with δ than is δ_S . Correlation between δ_S and δ (Figure 22, Figure 23) is usually quite weak on the surface and stronger, although not as large as $r_{\delta\delta_T}^2$, at 100 m. These statements are true only in a very general sense. For example, frequently in both fields very high or low correlations exist in the immediate vicinity of each other. Another exception is that, as expected, immediately offshore of a freshwater source, δ_T correlations are occasionally weak, or nonexistent. Usually when the δ_T correlation is weak, the δ_S correlation is very high. For example at 10 m in February at the mouth of San Francisco Bay, $r_{\delta\delta_T}^2$ (Figure 24) is 0.0 while $r_{\delta\delta_S}^2$ (Figure 25) is 1.0. Both correlations can be very high, predictably, for instance, in the Columbia River plume, where warm, fresh water results in high specific volume anomaly. On the other hand, the opposite situation exists well offshore of Baja California, near Guadalupe Island. There, in late winter and spring, very low δ_T correlations (Figure 26) coexist with very low $r_{\delta\delta_S}^2$ values (Figure 27). Variance in both δ_S and δ_T is very high in relation to

δ , but the two are so strongly in opposition that neither correlates well with the total variance.

Throughout the year, within a two or three degree radius of 31° N, 119° W in the upper 100 m, $r_{\delta\delta_T}^2$ (Figure 28) is consistently near 0.9 and the variance in δ_T (Figure 29) accounts for a reasonably consistent part of the variance in δ . Perhaps in this area, the assumption of constant salinity would introduce minimal error in a density model.

D. MEAN DIFFERENCES OF THE SPECIFIC VOLUME ANOMALY CONSTITUENTS

1. Method

If an observed quantity, x , is modeled by a predictor x' , then $(x - x')$ can be considered the error associated with a single observation. If that error is squared to eliminate sign bias and the sum of such squared error averaged, the square root of the result can be used as an indicator of the expected deviation and is termed the Root Mean Square Error (RMSE). The RMSE normalized by the mean value of x then provides an estimate of the magnitude of the expected error in terms of percent of the "correct" value. If δ is the observed quantity and δ_x the predictor:

$$\frac{\sqrt{\sum_{k=1}^n \frac{(\delta - \delta_x)_k^2}{(n)}}}{\bar{\delta}} = \text{RMSE}_{\text{normal}} \quad (13)$$

If for example x is T, the result, RMSE(T), provides an indication of how well δ_T approximates δ in a particular data block.

2. Results

Normalized RMSE values were calculated for δ_T and δ_S . As discussed in section IVB, both δ_T and δ_S are everywhere greater than zero and each greater than the absolute value of the sum of the remaining specific volume anomaly constituents. Therefore δ_T and δ_S are necessarily less than δ , and the sign of the expected error is known (the "root" and "squared" point of the RMSE technique is moot, and RMSE is equivalent to mean difference). The specific volume anomaly will always be underestimated.

As discussed earlier, it is the gradient in the error field that is likely more significant than magnitude of a single error. all, use of the actual mean salinity rather than standard 35 psu can remove a constant offset. The plots of RMSE(T) provide a

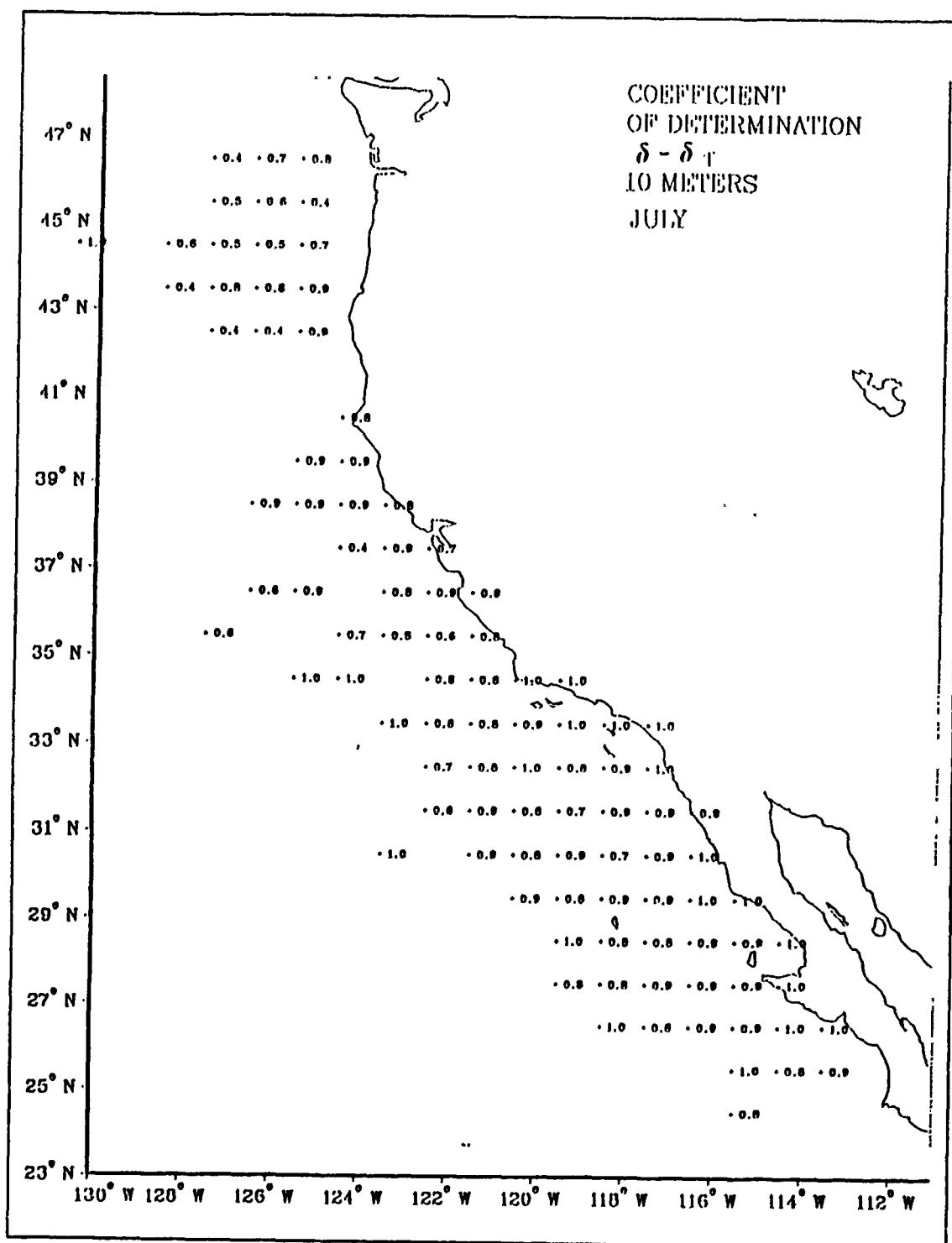


Figure 20. Specific Volume Coefficient of Determination (T), July, 10 m: $r^2_{\delta\delta_T}$

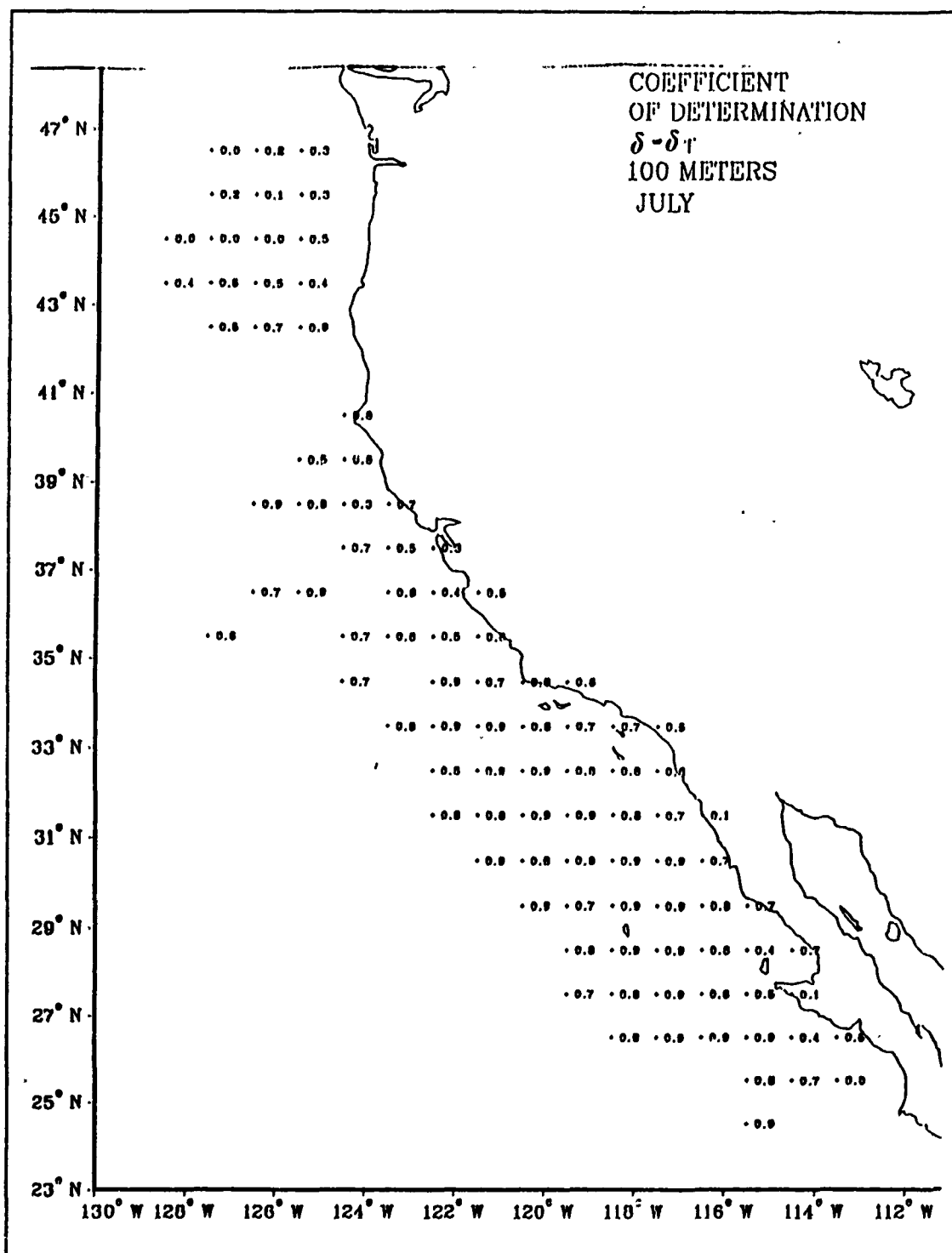


Figure 21. Specific Volume Coefficient of Determination (T), July, 100 m: $r_{\delta\delta_T}^2$.

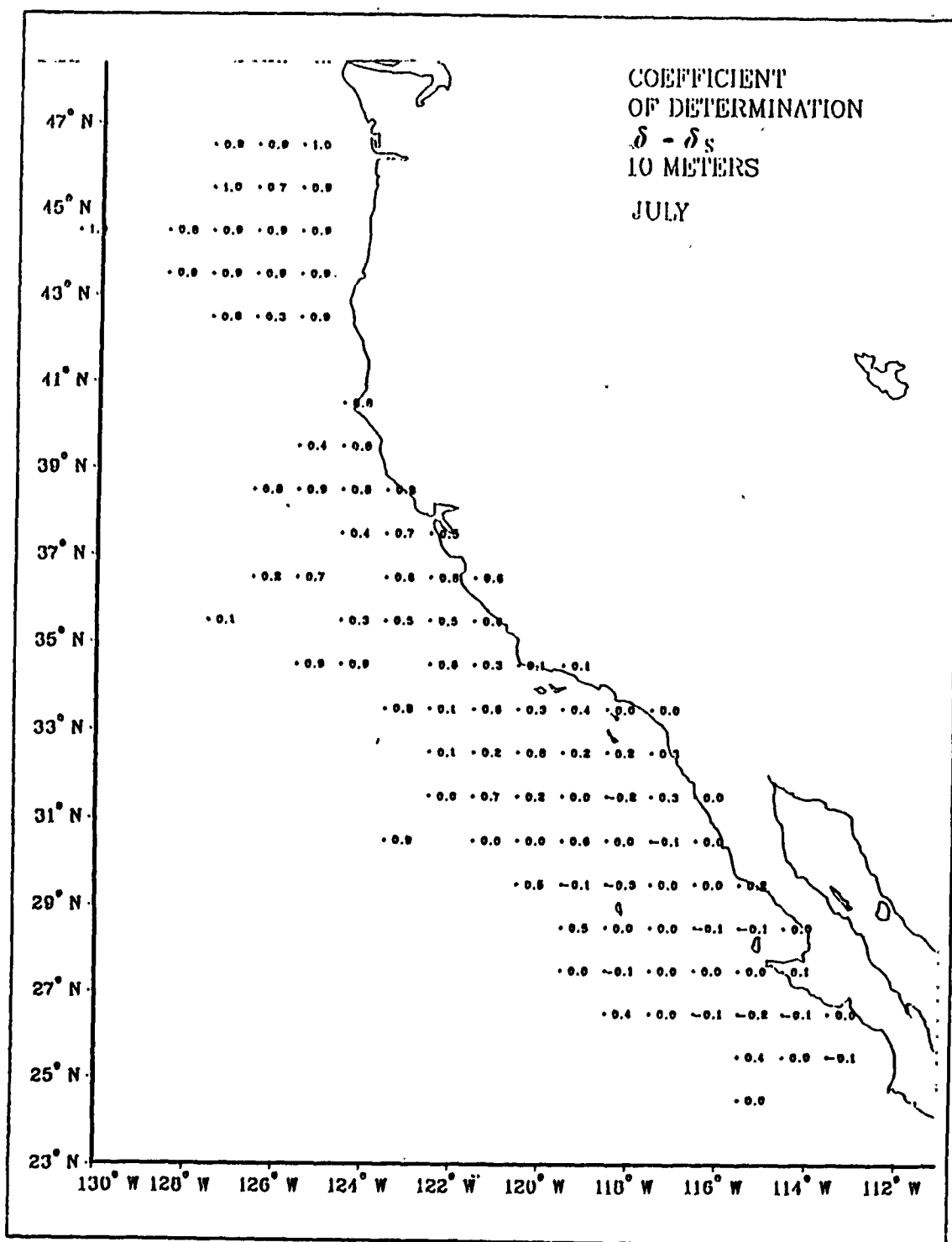


Figure 22. Specific Volume Coefficient of Determination (S), July, 10 m: $r^2_{\delta_s}$.

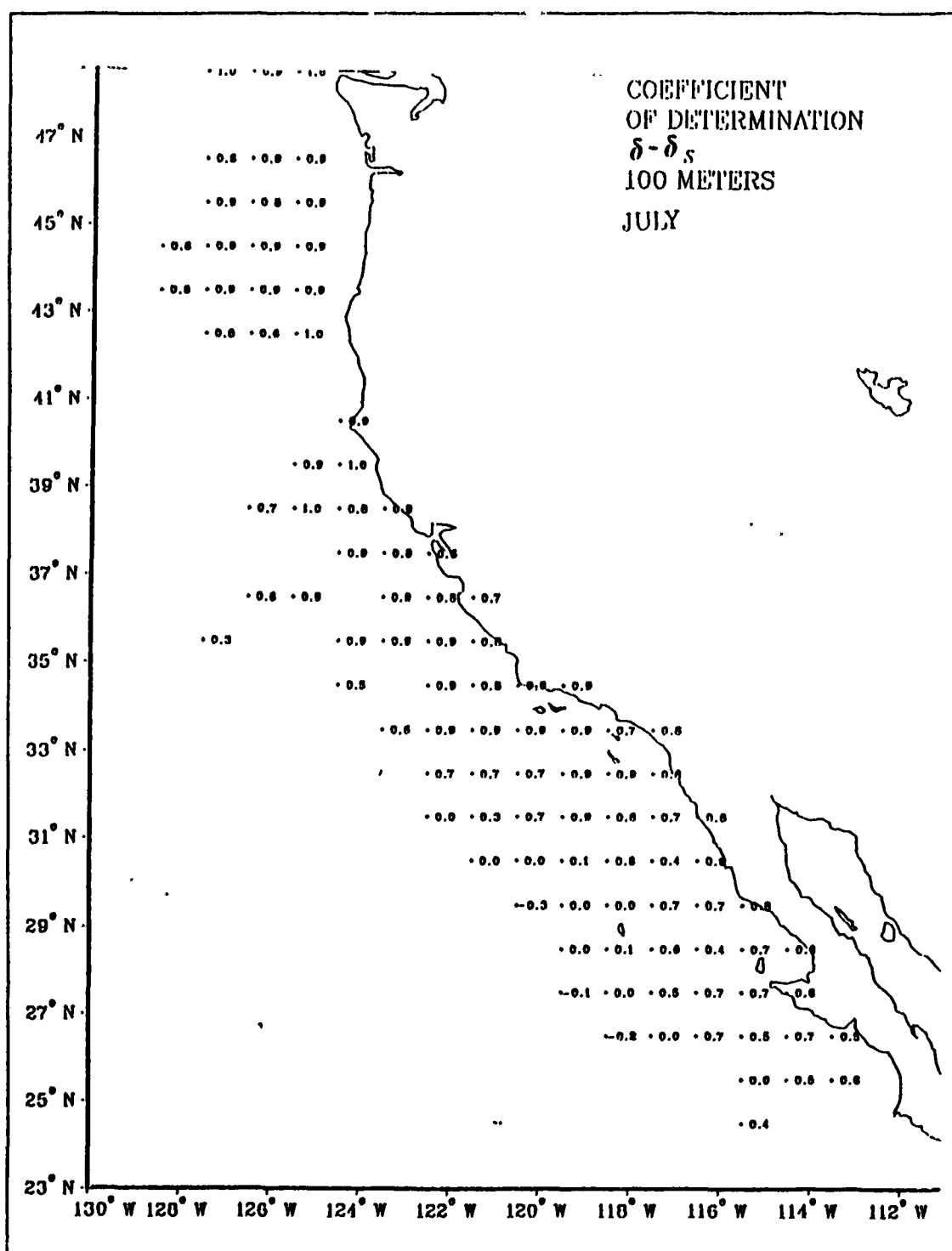


Figure 23. Specific Volume Coefficient of Determination (S), July, 100 m: $r_{\delta_s}^2$.

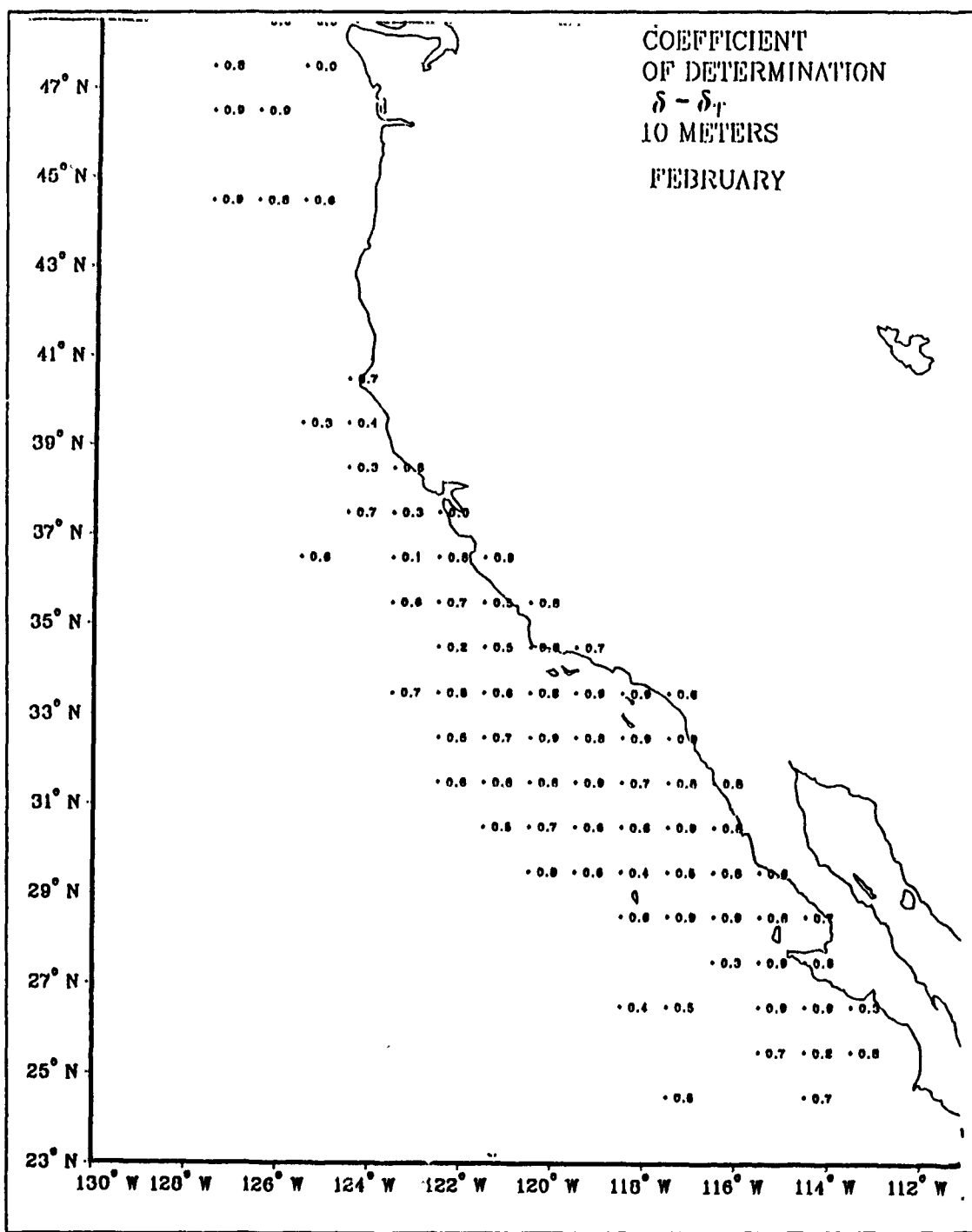


Figure 24. Specific Volume Coefficient of Determination (T), February, 10 m:

$$r_{\delta\delta_T}^2$$

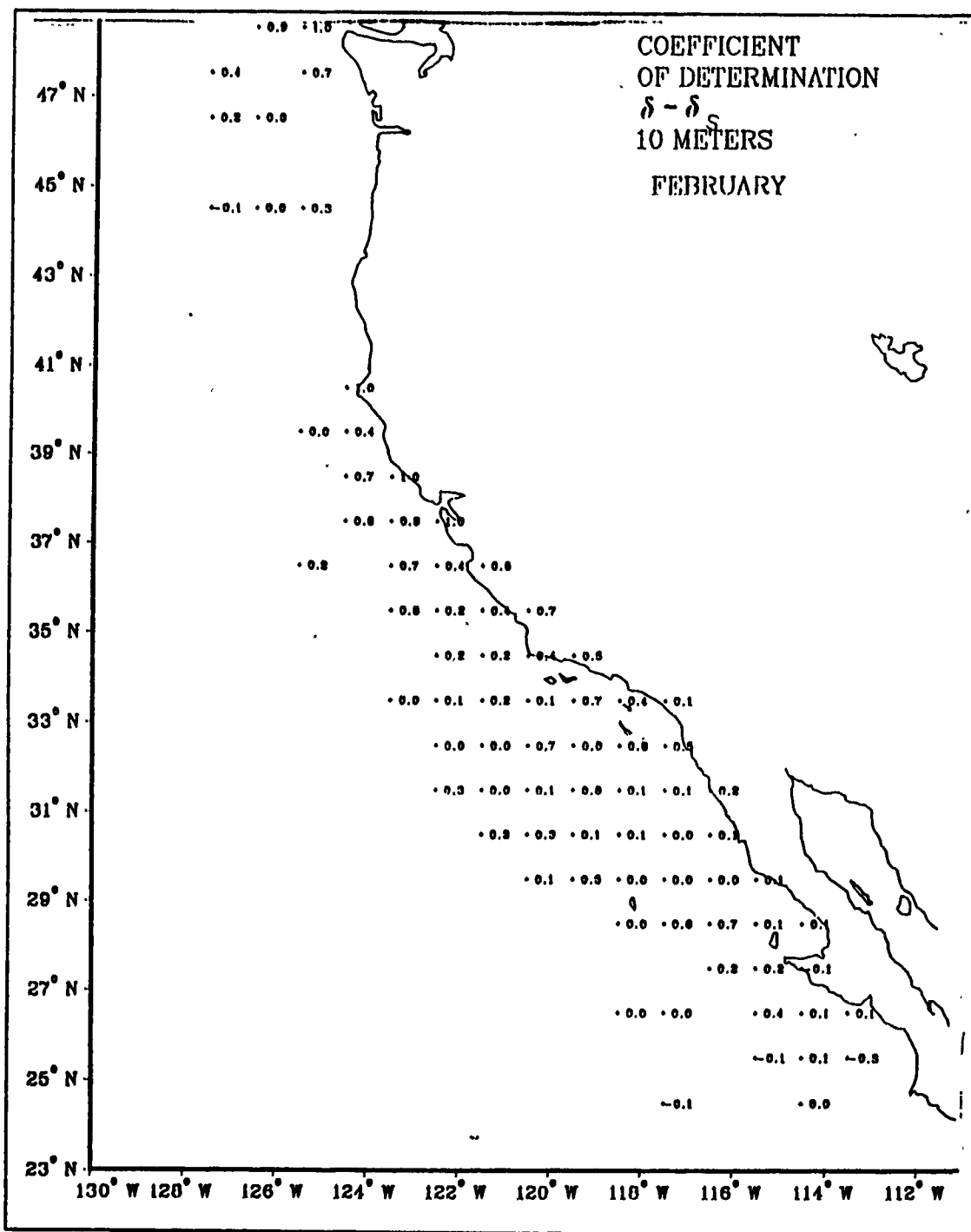


Figure 25. Specific Volume Coefficient of Determination (S), February, 10 m:

$r^2_{\delta\delta_S}$

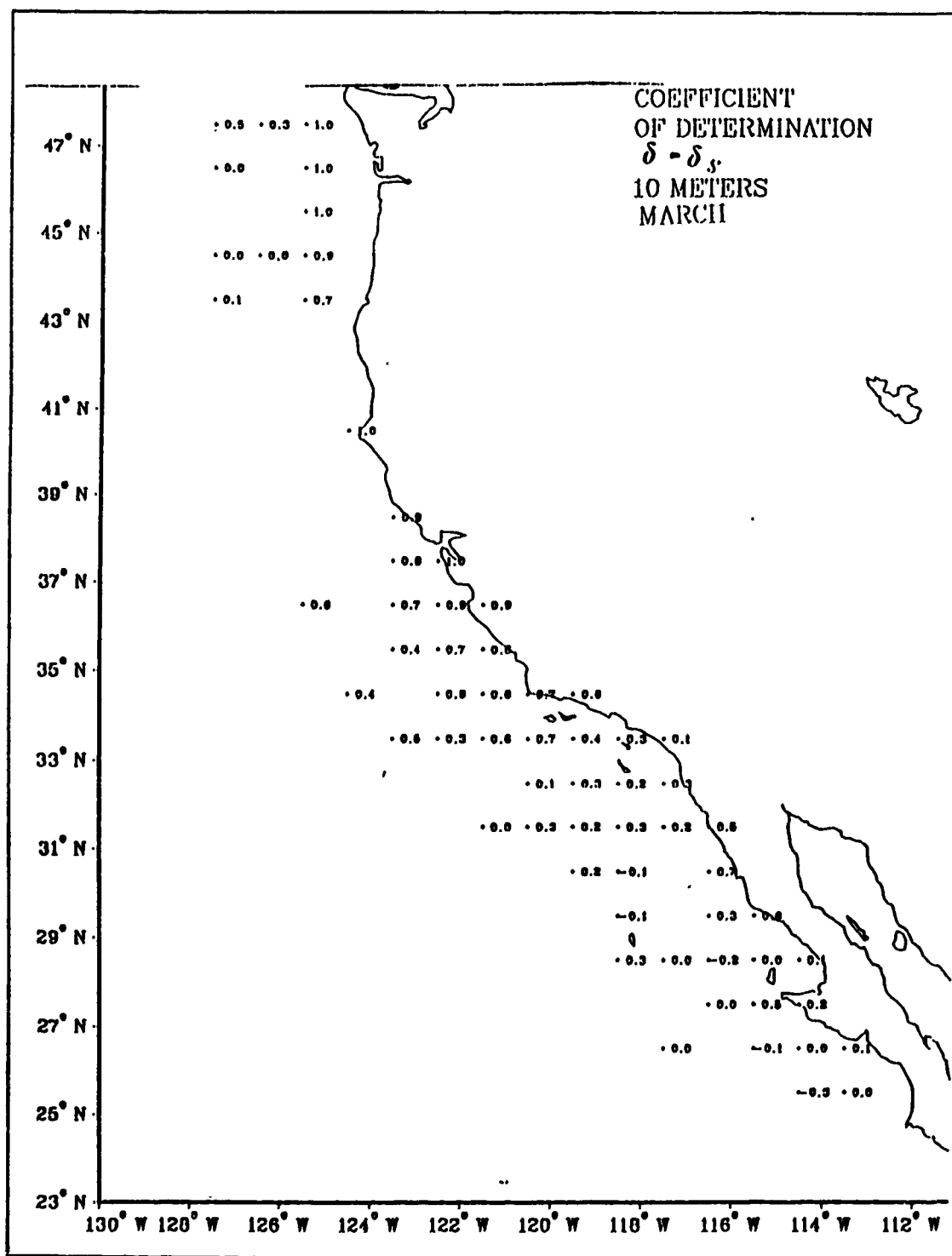


Figure 27. Specific Volume Coefficient of Determination (S), March, 10 m: r_{ss}^2 .

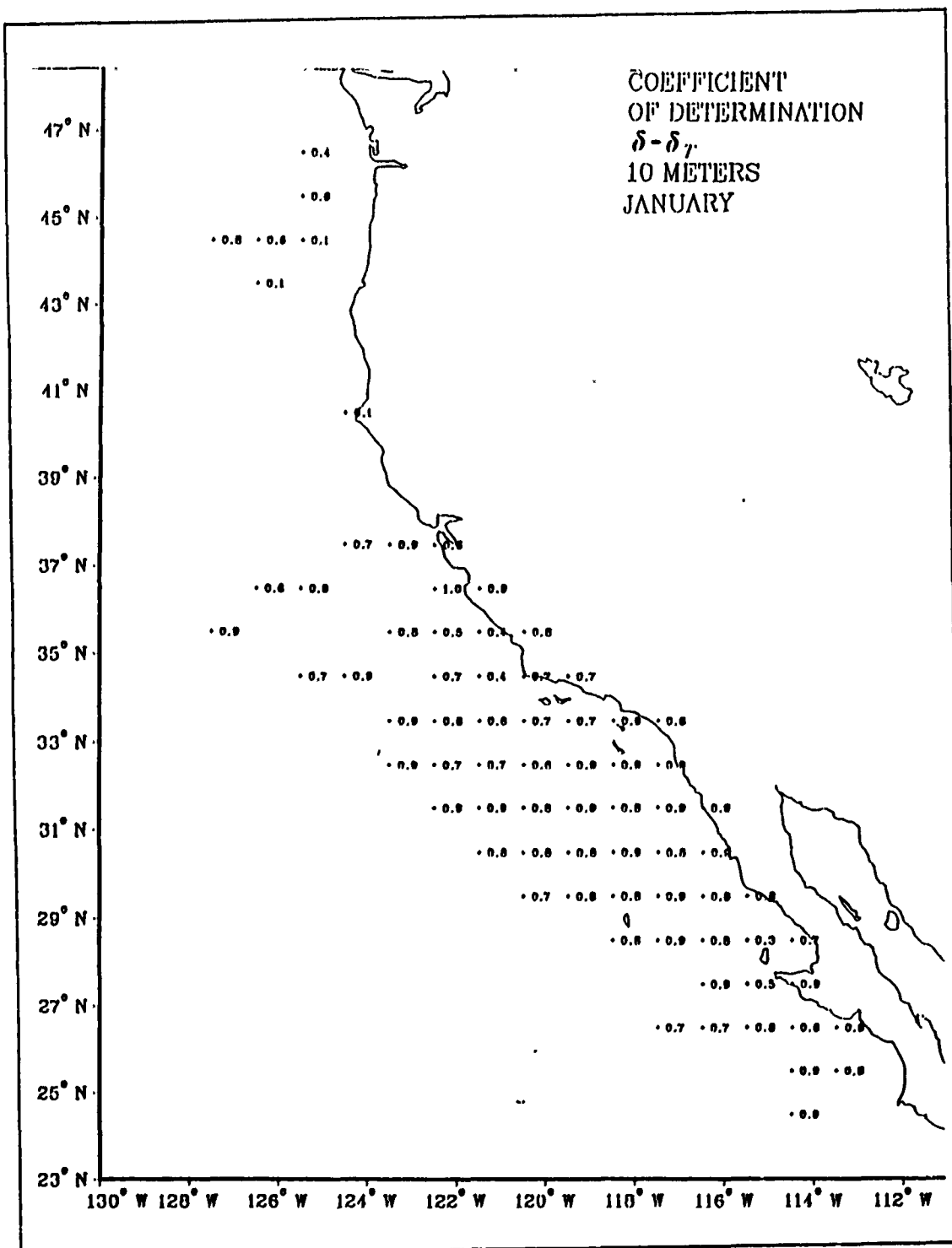


Figure 28. Specific Volume Coefficient of Determination (T), January, 10 m: $r_{\delta\delta_T}^2$.

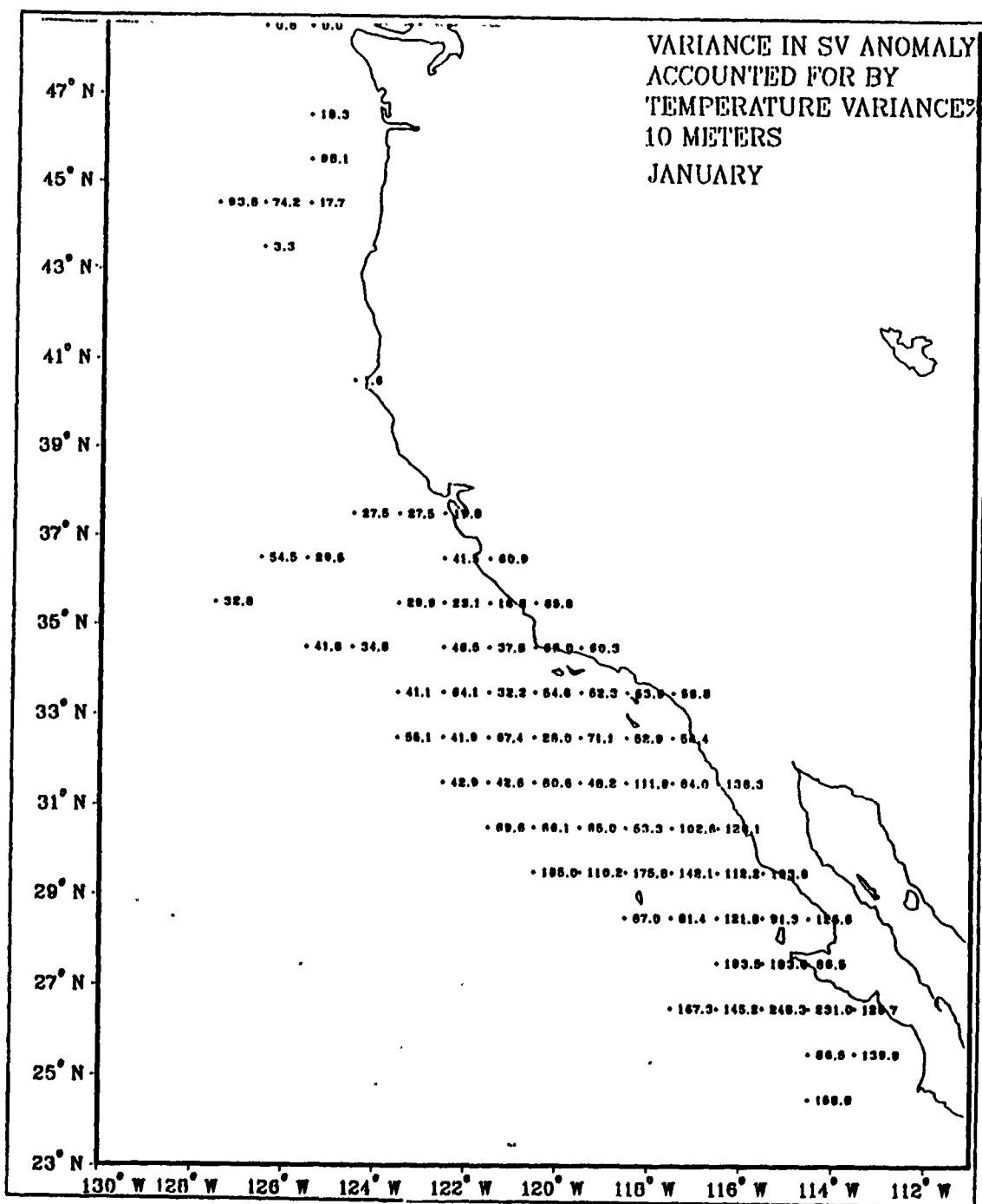


Figure 29. Variance in Steric Anomaly from Temperature, January, 10 m:
 $r_{st}^2 \times \sigma_{st}^2 \times 100$.

clear large scale picture of the price of neglecting salinity variation in specific volume anomaly calculations (e.g., Figure 30). Near the surface that neglect would result in a 40 to 50 percent underestimation in the north-south gradient, and a 10 percent underestimate west to east, with the largest errors tending to occur in winter months. The meridional gradient persists but decreases to a year-round 20 percent at 500 m (Figure 31).

Because δ_T and δ_S are by far the greatest contributors to total δ , data block values of RMSE(S) added to the corresponding values for δ_T usually are nearly equal to one (compare Figure 32 to Figure 30). Nevertheless, δ_S mean difference plots are illustrative of the part δ_S plays in determining total steric anomaly. The large scale opposition of gradients in δ_S and δ_T , in virtually every direction, is clear from analysis of these distributions. At 500 m, in the southern section of the CCS there is a pronounced increase in the zonal gradient in the δ_S RMSE field (Figure 33), salinity making a larger contribution to δ offshore than nearshore. Some smaller scale complexities are also discernible. For instance, near the surface, across the mouth of San Francisco Bay in September (Figure 34), there is a twenty percent change in the δ_S contribution to δ , accompanied by a very flat gradient in RMSE for δ_T . This phenomenon is illustrative of the local nature of saline variability, and temperature-salinity interaction in the CCS.

An interesting result of this analysis is that there are large areas, virtually any six degree latitude by four degree longitude block, where the assumption of no salinity variation would apparently result in less than a ten percent error in the resultant specific volume gradient. That is particularly true if areas immediately adjacent to the coast are excluded.

E. DYNAMIC HEIGHT

1. Method

Dynamic height, Φ , is a measure of how the density of a column of water differs from the density of a standard column of the same depth and is calculated by integrating the specific volume anomaly over depth from an assumed layer of no motion to a depth of interest. It is the horizontal gradient in dynamic height that determines the geostrophic velocity field. If the contributions to that gradient from salinity are significant, they should be considered when momentum calculations are performed. If the mean differences $(\overline{\delta} - \overline{\delta_T})$, where $(\overline{\quad})$ denotes the mean, in columns are integrated with respect to pressure, the resulting horizontal distribution is a good measure of the effect of salinity on the geostrophic velocity field. That is, contours of $\overline{\Phi} - \overline{\Phi}_{3517} = \overline{\Phi}'$ define

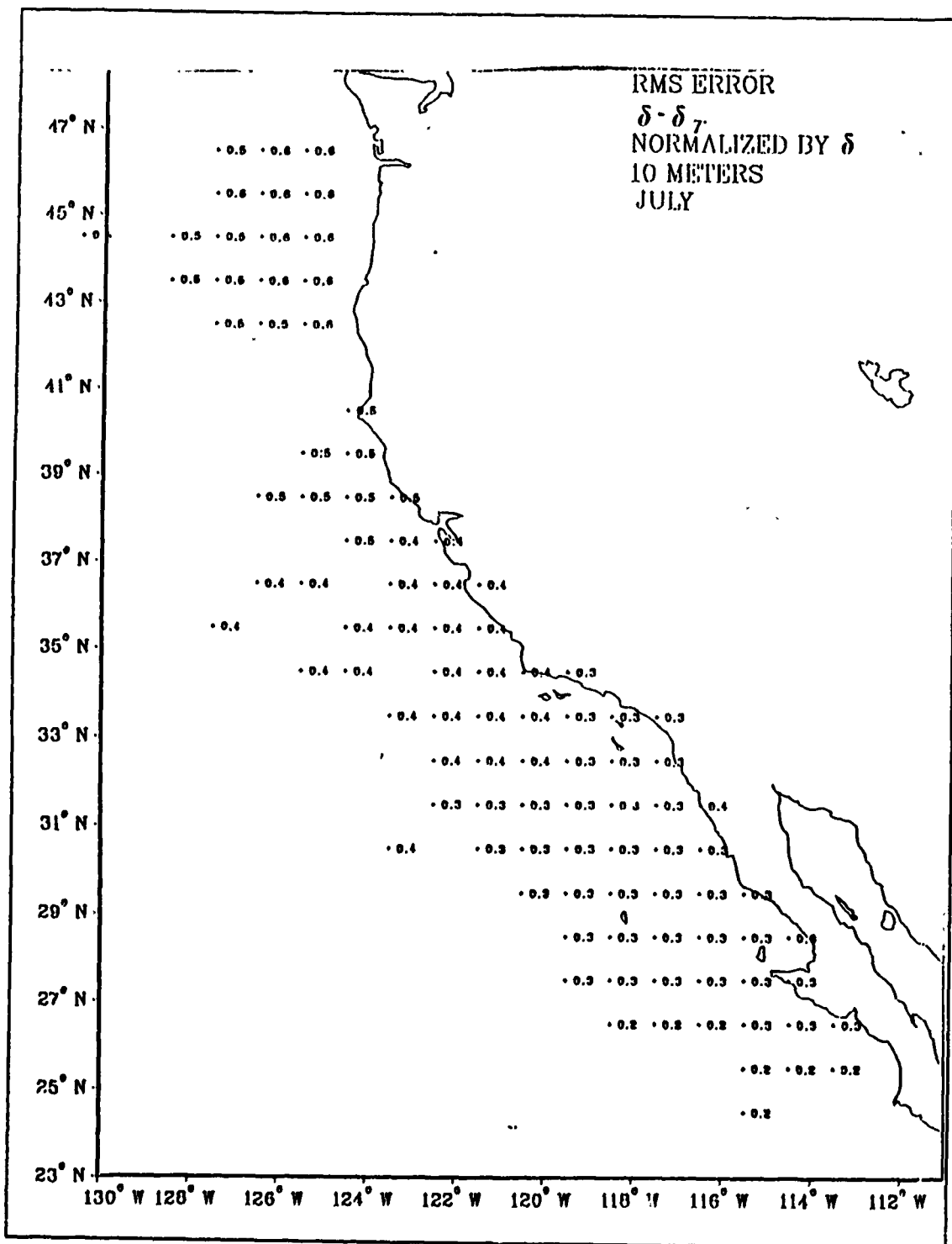


Figure 30. Specific Volume Anomaly RMSE (T), July, 10 m.

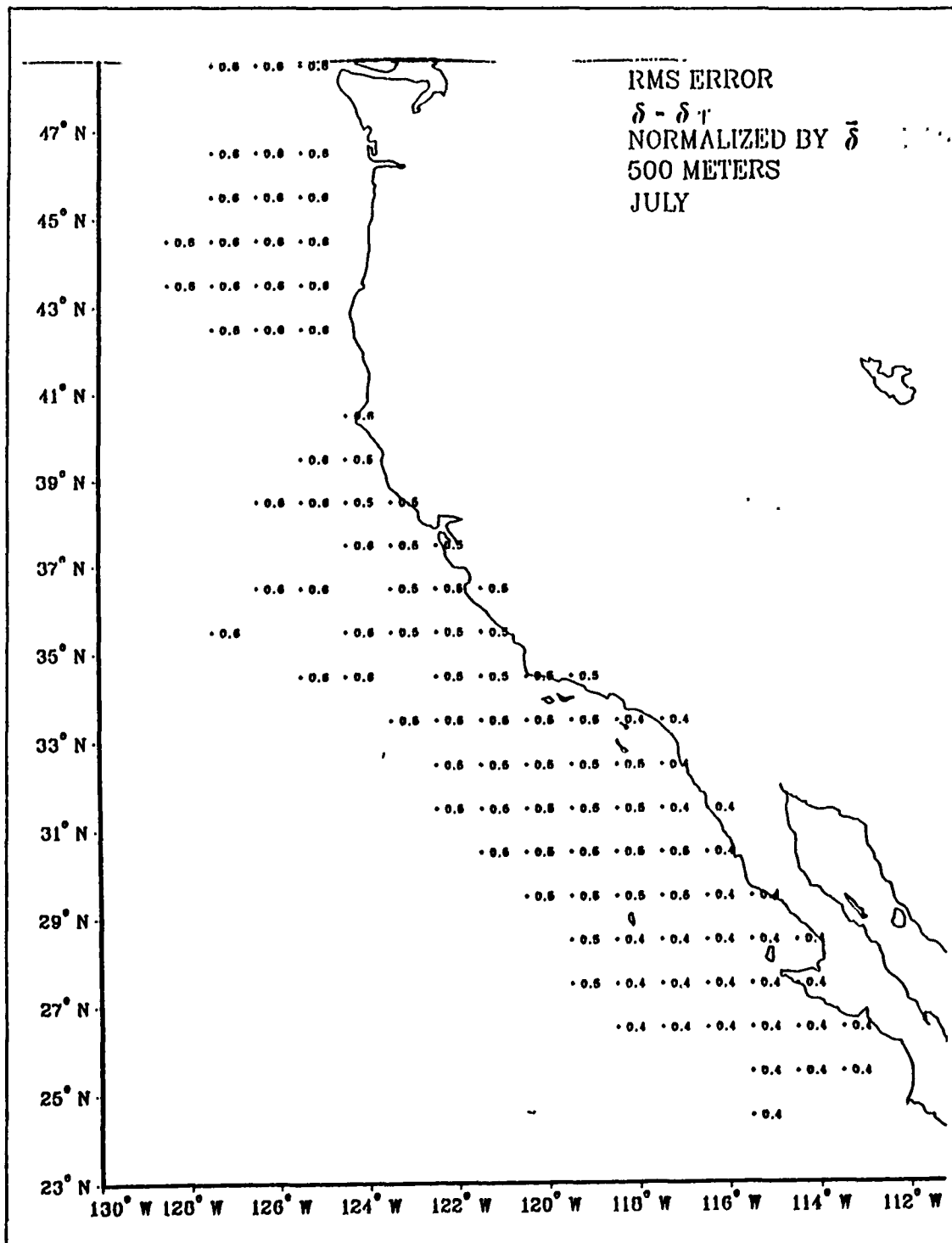


Figure 31. Specific Volume Anomaly RMSE (T), July, 500 m.

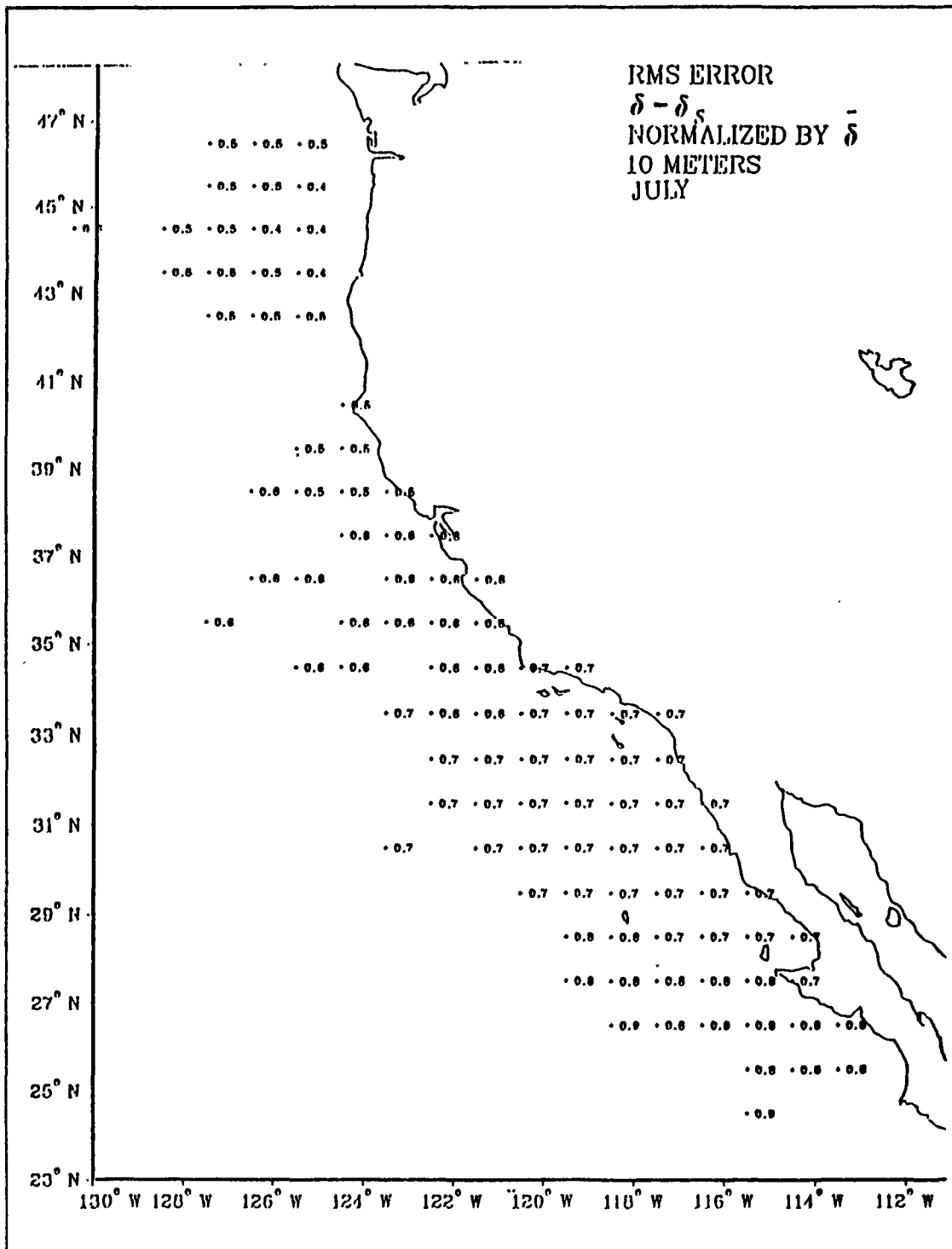


Figure 32. Specific Volume Anomaly RMSE (S), July, 10 m.

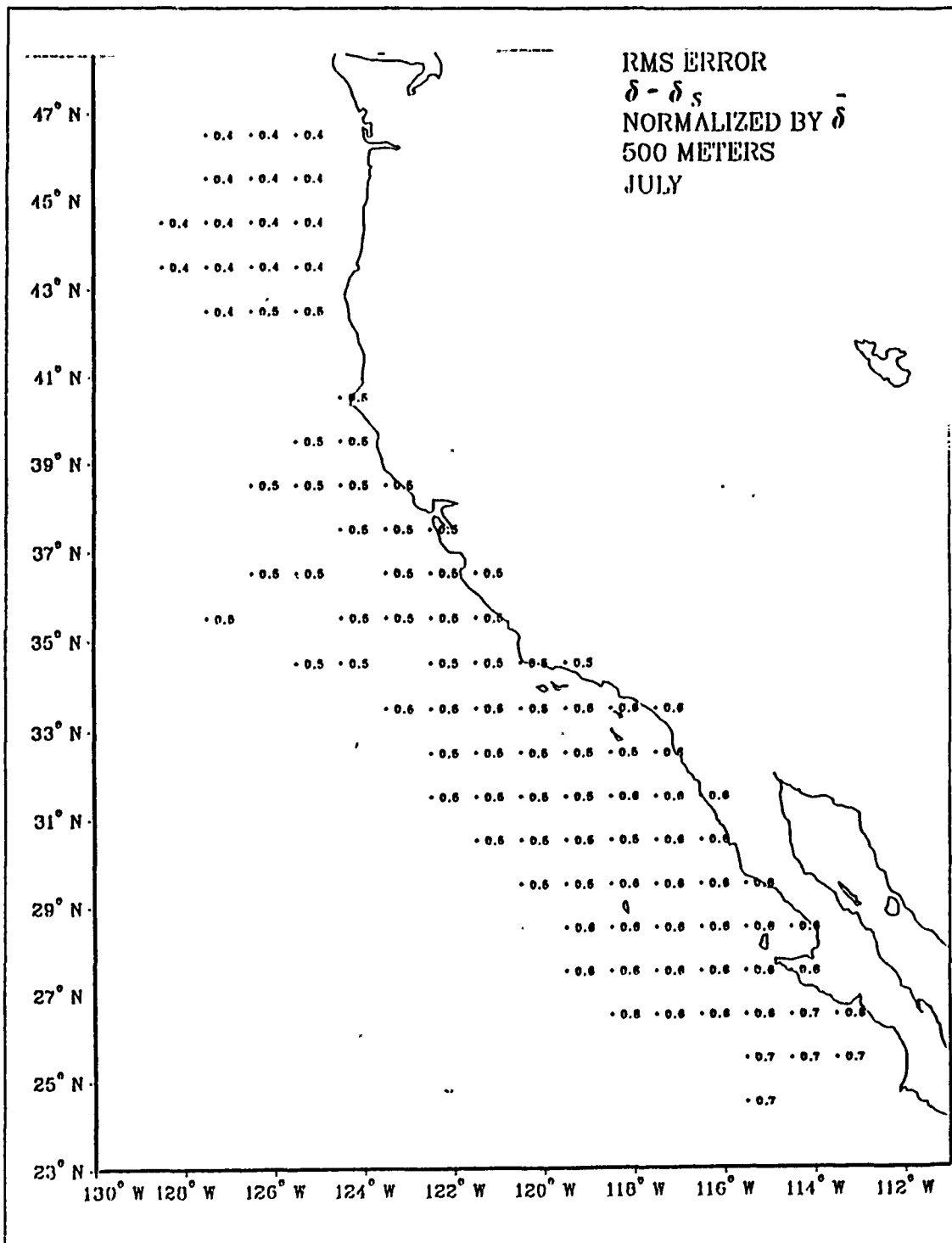


Figure 33. Specific Volume Anomaly RMSE (S), July, 500 m.

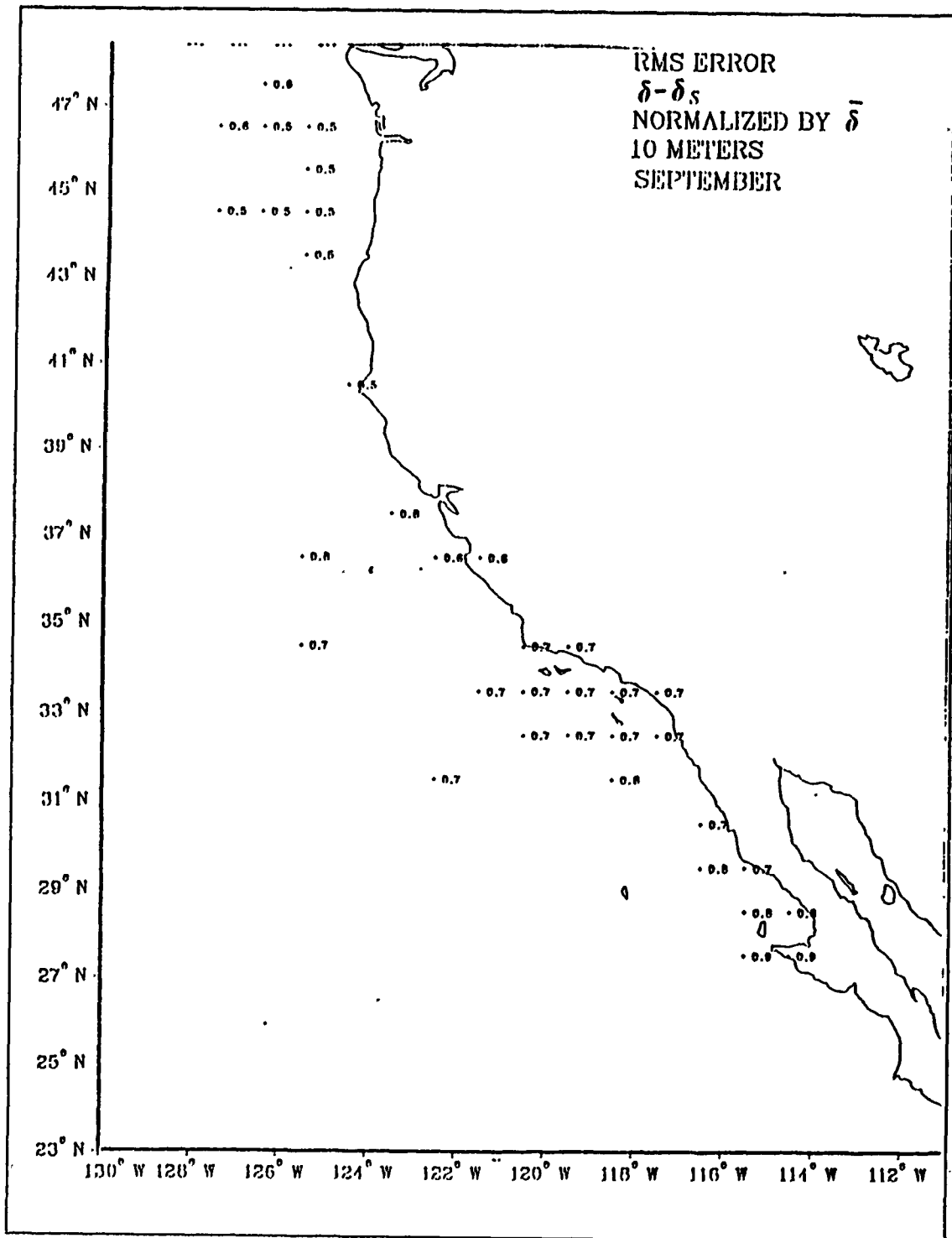


Figure 34. Specific Volume Anomaly RMSE (S), September, 10 m.

mean geostrophic flow that will not be accounted for if δ_T is used as an estimator of δ . Therefore, if gradients in the difference field are large, salinity is important.

2. Results

Plots of monthly mean values of Φ , $\Phi_{3\sigma}$, and Φ' , obtained by integrating from an assumed layer of no motion at 500 m, to 200 m (200/500), 100 m (100/500), and the surface (0/500) were plotted and evaluated. The Φ results, where they overlap, are in very close agreement with those of Wyllie (1966). Standard deviations are in virtually every case considerably more than an order of magnitude less than mean values. Even so, this small variance still indicates that contour locations are doubtful by more than the width of a contour interval on these maps. Therefore, any conclusions drawn concerning small scale features are suspect. It should also be remembered that these are maps of mean fields, representing climatology rather than instantaneous flows.

Examination of the 0/500 dynamic height field of the CCS (e.g., Figure 35 and Figure 36), leads to division of the area into three regions. North of 43° N the divergence of the North Pacific Current and freshwater discharges from the Columbia River and Strait of Juan de Fuca result in disorganized mean geostrophic gradients. A split of the flow toward the north and south is superimposed on weak circulations around warm, freshwater plumes. The area along the U.S. coast from 30° to 38° N is dominated by cyclonic geostrophic circulation inshore, and flow generally to the southeast offshore. The strength of the southward flow and degree of cyclonic turning onshore is seasonal. Southward flow is strongest in summer and weakest in winter. Conversely, onshore cyclonic turning is least in summer, greatest in winter. There is another cyclonic center just offshore of Baja California near 25° N. Again the cyclonic departure from a generally southeastward flow is seasonal as described above. For each month the dynamic height difference fields (Φ') (Figure 37) show inclusion of horizontal salinity gradients to be responsible for a nearshore, equatorward geostrophic component from San Francisco to San Diego and a southwestward flow along the coast of Baja California. This predictable geostrophic pattern is due to the persistent salinity pattern: fresh to saline, offshore toward shore, with a more meridional, fresh to salty north to south, gradient in the southern section. What is even more interesting is the fact that throughout the year, the magnitude of the anomalous flow implied by the Φ' field is on the same order as flow associated with $\nabla\Phi$ itself, and perhaps greater in some areas than the magnitude of the flow predicted by $\nabla\Phi_{3\sigma}$ (compare figures 36-38).

In the northern region, in each month, $\nabla\Phi_{3\sigma}$ fails to account for a persistent south-southwestward component from the mouth of the Columbia River that varies in

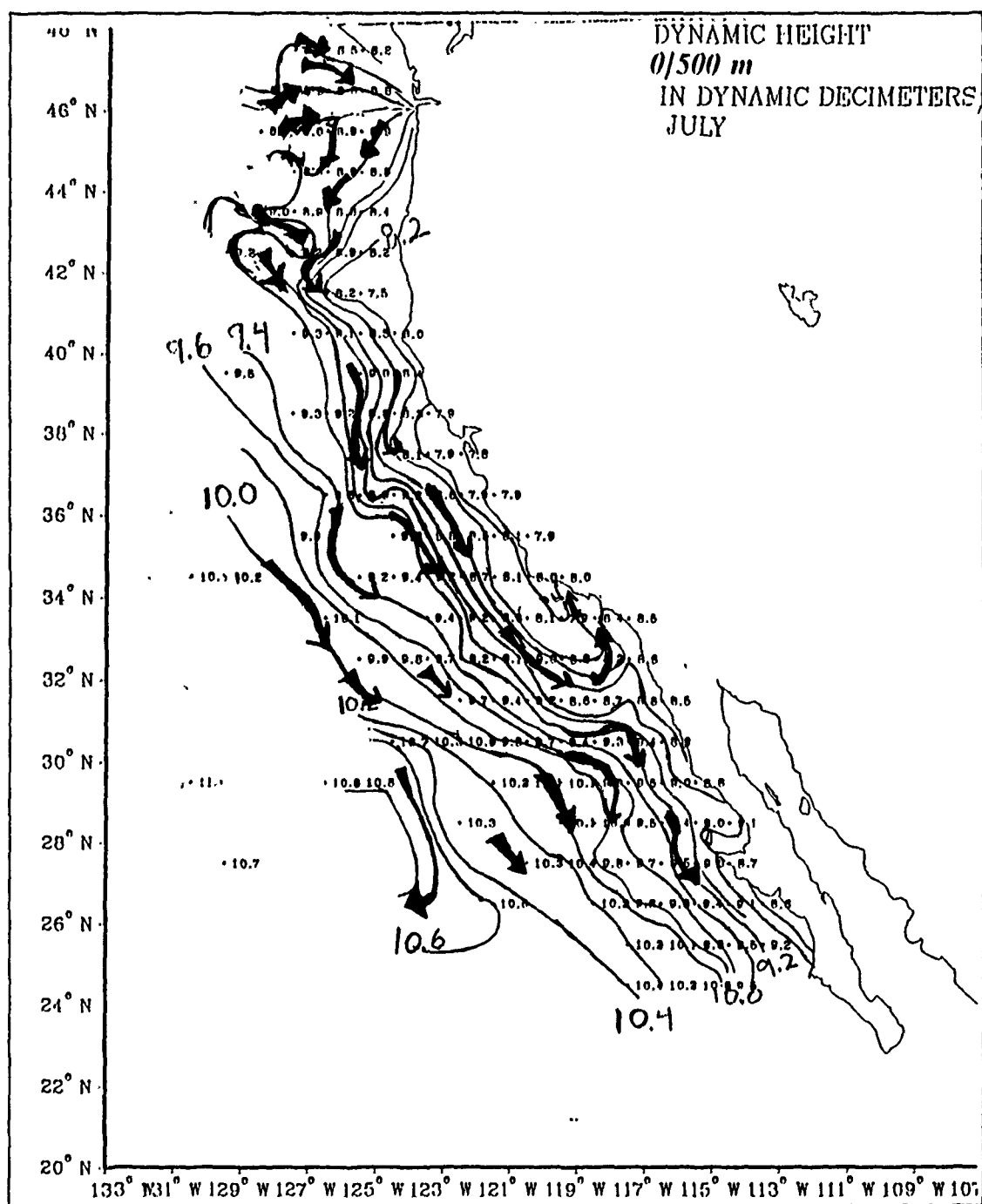


Figure 36. Dynamic Height, 0/500 m, July: Φ , the contour interval is 0.2 and units are dynamic decimeters.

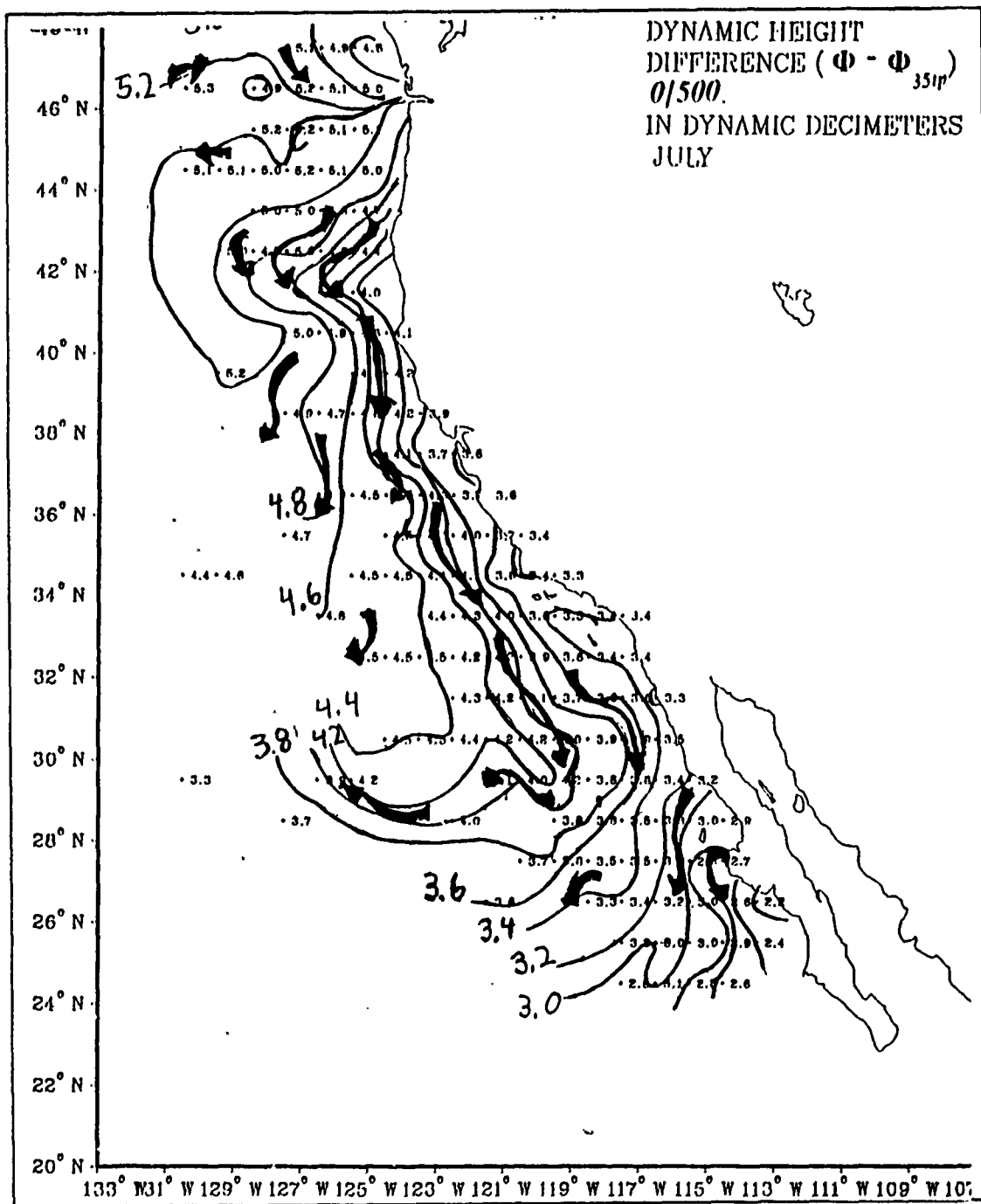


Figure 37. Dynamic Height Difference, 0/500 m, July: $\Phi' = \Phi - \Phi_{351p}$, the contour interval is 0.2 and units are dynamic decimeters.

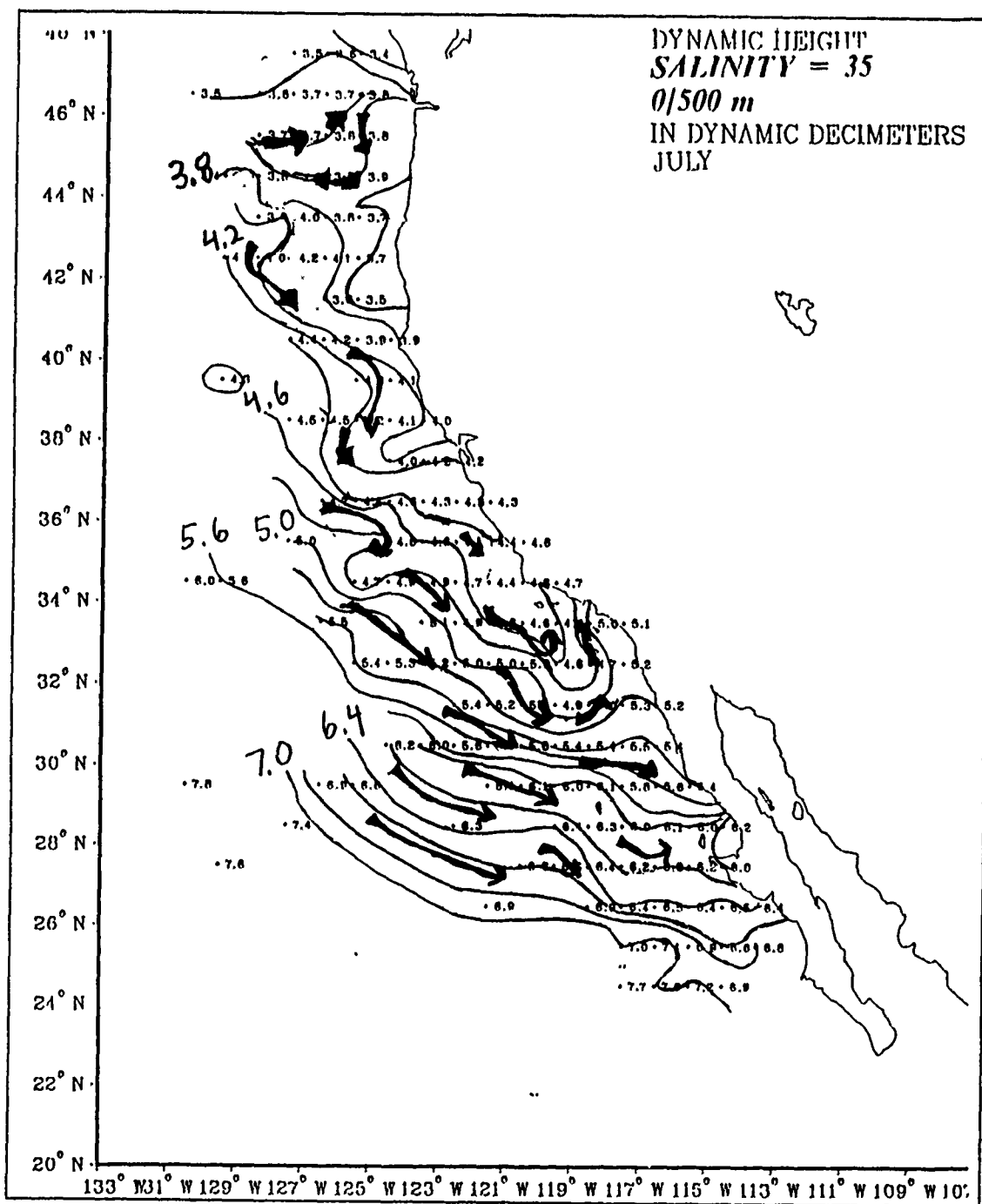


Figure 38. Dynamic Height (Salinity 35), 0/500 m, July: $\Phi_{35\sigma_t}$, the contour interval is 0.2 and units are dynamic decimeters.

intensity with the magnitude of discharge from that river. However, seaward of that southward component the difference field is very slack. That is, the dynamic height field estimated from temperature gradient alone very nearly accounts for the geostrophic flow pattern in the region where surface salinity has the largest annual variance. This apparent contradiction is explained by the fact that the horizontal salinity gradient here decreases rapidly with depth. At depth, throughout the year, there is virtually no significant salinity gradient in this northern area. At 200 m for example, over a distance where mean temperature may vary by 0.4°C , salinity changes less than 0.1 psu . In the southern area, by contrast, a 0.5°C temperature change is accompanied typically by a change of 0.3 psu . The result is that in the north, the depth integrated effect of salinity on geostrophic flow only approaches that of temperature in the immediate vicinity of the sharpest upper level salinity gradient.

Analyses of dynamic height and geostrophic flow at other levels (*e.g.*, 200/500 and 100/500 m, Figures 39-44) show relative gradients very similar to those previously discussed. $\nabla\Phi'$ is of similar order as $\nabla\Phi$ and $\nabla\Phi_{35\sigma_t}$ at all depths, and the general pattern of the difference field persists with depth. North of northern Baja California, the difference field shows a strong offshore-onshore gradient indicative of higher salinities inshore in the poleward flow. This result is consistent with the idea that the poleward flow can be traced by its high salinity (*e.g.*, Lynn and Simpson, 1987). That is, the inshore poleward undercurrent may carry the saline signature of Equatorial water which is to the south of the CCS. That salinity increases significantly toward the south is evident from the fact that south of about 34°N there is a strong alongshore north to south gradient in the difference field. The southward salinity increase is also apparent in the salinity fields (Figure 4). The 100/500 and 200/500 m dynamic height calculations show increased cyclonic turning associated with the large scale California coastal features described earlier. That is, the dense cores associated with what look like "c" shaped troughs centered at the California coast and Baja California peninsula on the 0/500 m plots move offshore with depth so that at 200 m, and possibly even at 100 m, a closed geostrophic circulation with coastal poleward flow exists. Because of the neglected zonal salinity gradient, $\Phi_{35\sigma_t}$ greatly overestimates the strength and horizontal extent of the poleward flow.

Due to the absence of the freshwater runoff below the surface, the divergence of the North Pacific Current is relatively clear on the 100/500 and 200/500 m plots. This divergence area seems to be farther south in the winter than summer, as noted by Pickard and Emery (1982). Although the divergence occurs in a region of generally poor

data coverage, the seasonal migration seems to be from near 40° N in the winter to 45° N in summer, rather than the 45° N to 50° N range reported by Pickard and Emery (1982).

The focus of this thesis is large scale; however, using the rule of thumb that features whose wavelengths exceed 2 grid points in extent may be resolved, it may be possible to use these calculations to gain insight into some relatively small scale features. In Appendix B, discussion of some smaller scale effects of salinity on dynamic height in the CCS is provided.

F. PROPAGATION OF T-S VARIANCE THROUGH THE EOS

1. Method

An alternate approach to examine the relative importance of constituent variance to density variance is to propagate the variance associated with each of the independent variables through the complete nonlinear equation of state. By the chain rule, if density is strictly a function of salinity, temperature, and pressure then:

$$\Delta\rho = \frac{\partial\rho}{\partial t} \Delta t + \frac{\partial\rho}{\partial s} \Delta s + \frac{\partial\rho}{\partial p} \Delta p, \quad (14)$$

where (Δ) indicates departure from mean values and ρ is mean density. Because all observations are on standard depth levels and pressure changes on those levels are small, even in comparison to error associated with depth determination, Δp can be neglected. Squaring both sides of (14), summing over a number of observations, and dividing by the number of observations less one (e.g., Greenwalt and Shultz, 1962) leads to :

$$\sigma_\rho^2 = \left(\frac{\partial\rho}{\partial t}\right)^2 \sigma_t^2 + \left(\frac{\partial\rho}{\partial s}\right)^2 \sigma_s^2 + 2\left(\frac{\partial\rho}{\partial s}\right)\left(\frac{\partial\rho}{\partial t}\right) \sigma_{st}, \quad (15)$$

where σ^2 represents variance (either sample or population), σ denotes covariance, and subscripts represent variables to which the statistic applies. As demonstrated by Lillibridge (1989), the equation of state, EOS(80), a polynomial, is relatively easy to differentiate. Therefore the contribution to σ_ρ^2 from temperature, salinity, and their interaction is easily determined over any interval of interest. This technique can be as readily applied to specific volume or any of the specific volume anomaly constituents and is desirable because it employs the full nonlinear equation of state. Insofar as the statistics used are accurate estimators, the equation of state itself accurate, and the pressure levels constant, the expression is valid. The method is particularly useful when

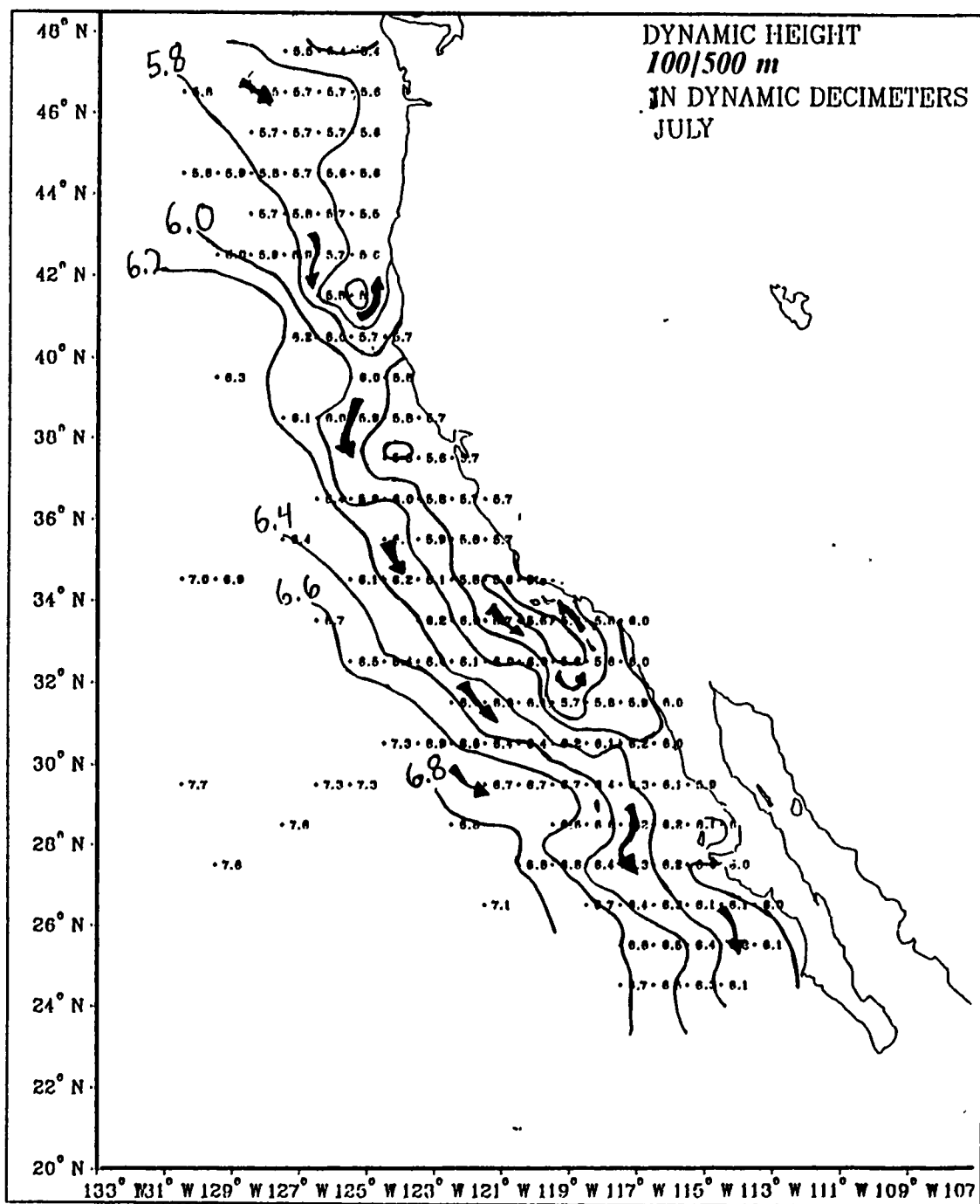


Figure 39. Dynamic Height, 100/500 m, July: Φ , the contour interval is 0.2 and units are dynamic decimeters.

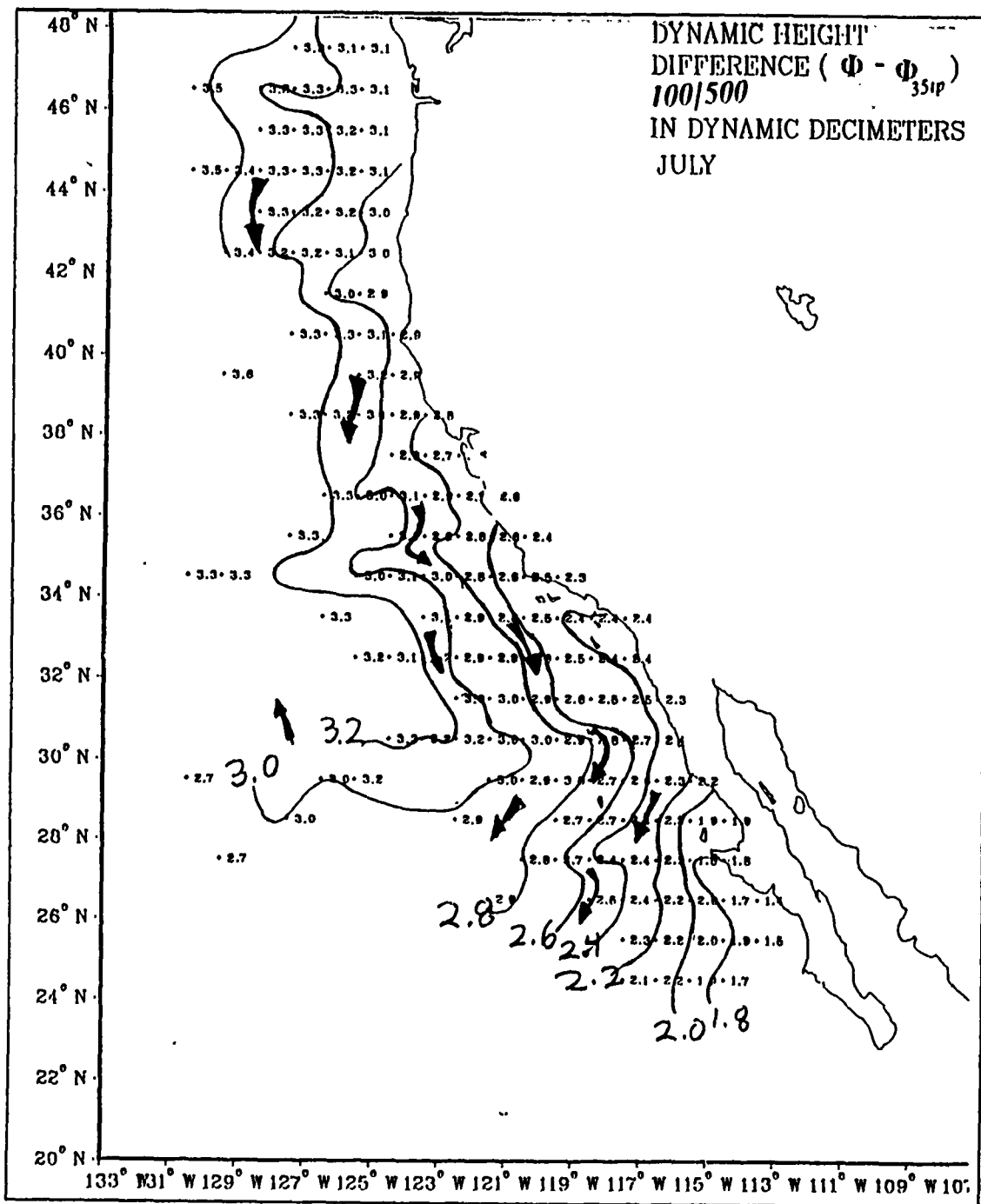


Figure 40. Dynamic Height (Salinity 35), 100/500 m, July: Φ_{35sp} , the contour interval is 0.2 and units are dynamic decimeters.

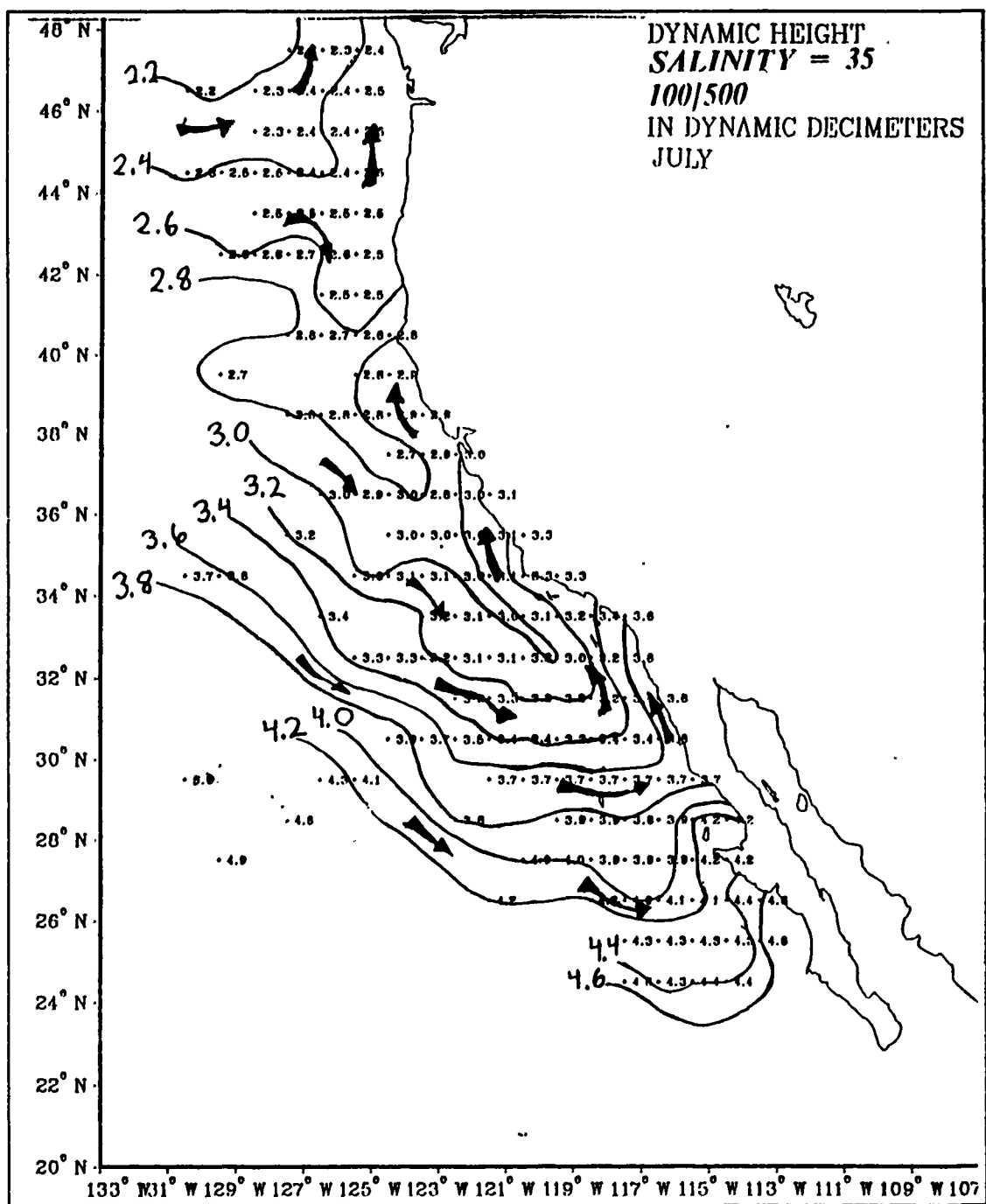


Figure 41. Dynamic Height Difference, 100/500 m, July: $\Phi' = \Phi - \Phi_{35/r}$, the contour interval is 0.2 and units are dynamic decimeters.

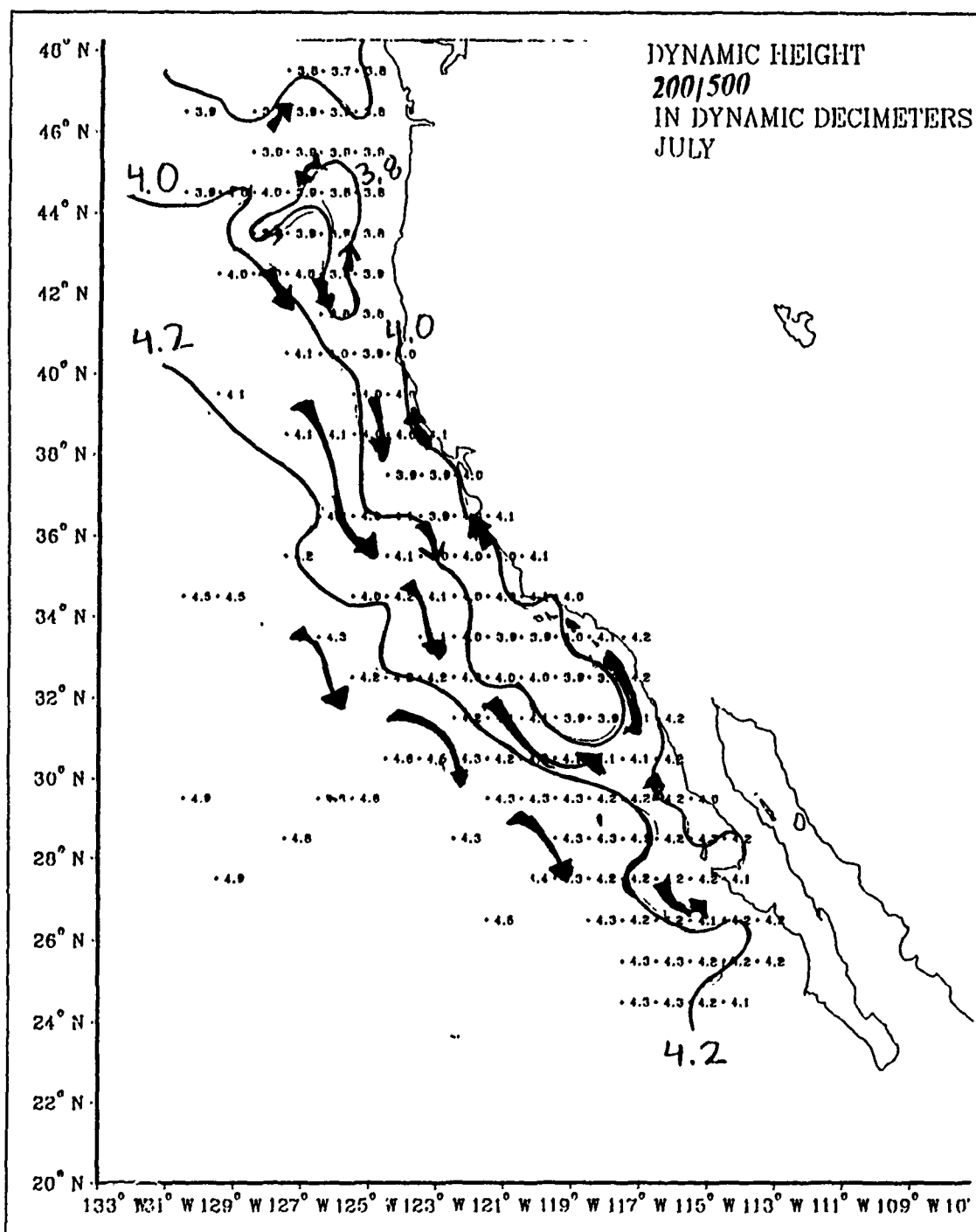


Figure 42. Dynamic Height, 200/500 m, July: Φ , the contour interval is 0.2 and units are dynamic decimeters.

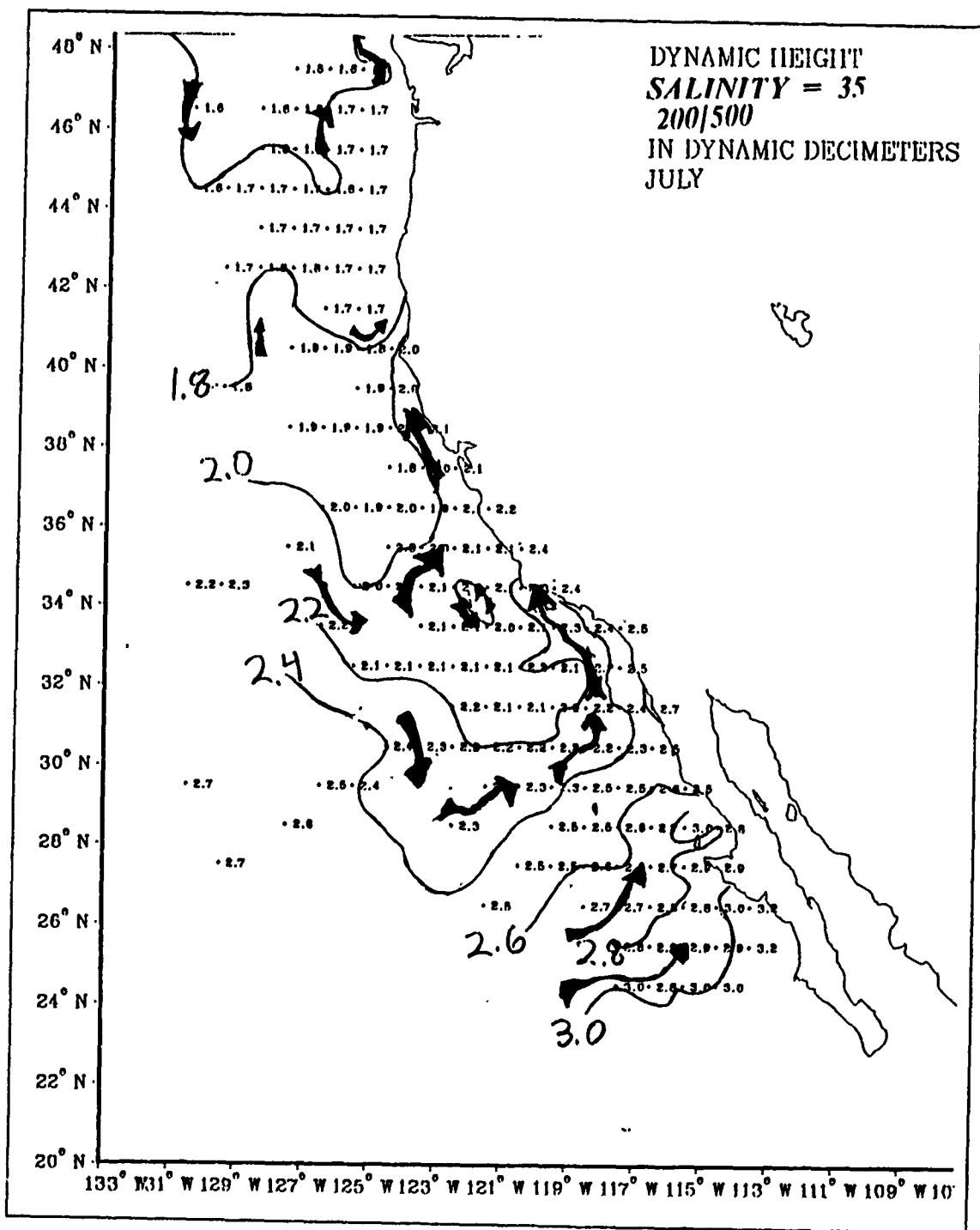


Figure 43. Dynamic Height (Salinity 35), 200/500 m, July: $\Phi_{35/200}$, the contour interval is 0.2 and units are dynamic decimeters.

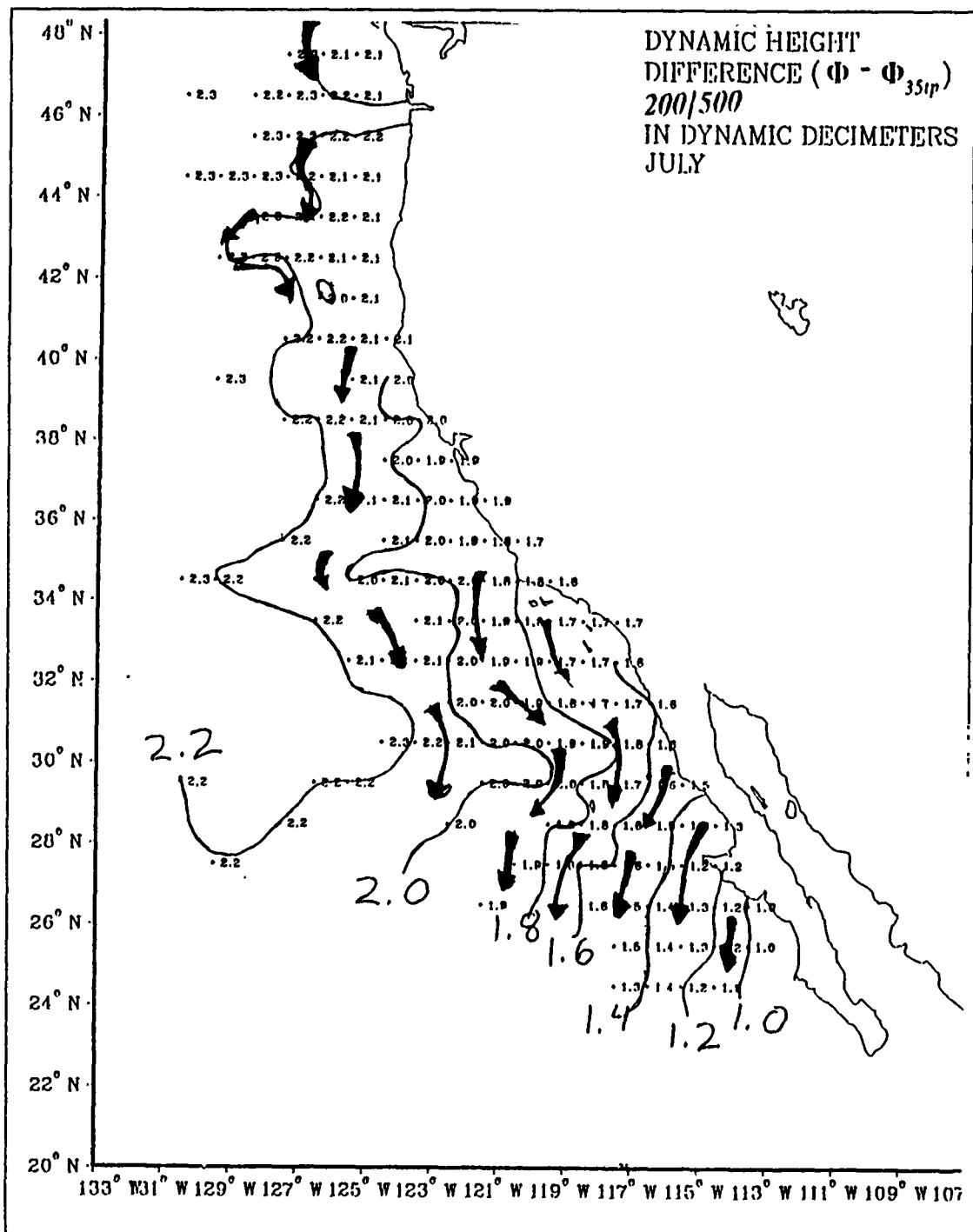


Figure 44. Dynamic Height Difference, 200/500 m, July: $\Phi' = \Phi - \Phi_{351p}$, the contour interval is 0.2 and units are dynamic decimeters.

temperature and salinity ranges over a time-space interval of interest are reasonably well known and a quick assessment of the relative importance of constituent variances desired. It also is computationally quite efficient because the equation of state need only be invoked once to determine total and constituent variance over a sample of interest.

Let the terms on the right hand side of equation (15) be represented as:

$$\begin{aligned}\sigma_{\rho_t}^2 &= \left(\frac{\partial \rho}{\partial t} \right)^2 \sigma_t^2 \\ \sigma_{\rho_s}^2 &= \left(\frac{\partial \rho}{\partial s} \right)^2 \sigma_s^2 \\ \sigma_{\rho_{st}}^2 &= 2 \left(\frac{\partial \rho}{\partial s} \right) \left(\frac{\partial \rho}{\partial t} \right) \sigma_{st}\end{aligned}\tag{16}$$

As mentioned earlier, to increase the number of observations and hence statistical validity, these data block variance estimates were computed over three-month seasons, with winter defined as January, February, March.

Potential energy (*PE*) of a column of water can be determined by integrating $PE = \rho g z$, where g is the acceleration due to gravity, considered constant, and z is height above some reference level, over depth (e.g., Fosonoff, 1962). It follows that on a constant depth level (or very thin layer) ρ is the only variable in *PE*, and the horizontal density field can be used to represent potential energy. Change in the density field, either over time or distance, then represents change in the potential energy field. Equivalently, variance from the mean density field can be considered as an indication of energetic activity or potential. In general, relatively high density variance should correspond to relatively high energetic activity. Therefore, if sample variance computed over some time or space interval is an accurate estimator of the true density variance, sample variance may provide indication of energetic activities. Dantzer (1977) used similar statistical techniques applied to vertical excursions of the thermocline to calculate North Atlantic potential energy levels.

2. Results

Maps of σ_ρ^2 and percent contributions of salinity, $(\sigma_{\rho_s}^2/\sigma_\rho^2 \times 100)$, temperature, $(\sigma_{\rho_t}^2/\sigma_\rho^2 \times 100)$, and covariance, $(\sigma_{\rho_{st}}^2/\sigma_\rho^2 \times 100)$, were evaluated. Near the surface, large density variance occurs in areas of maximum fluctuation in precipitation, heating, or freshwater influx for example. Accordingly, Figure 45 indicates high variance near the Columbia River outflow, and in the upwelling region along the coast of California. As expected, salinity variance is dominant in the Columbia River plume (Figure 46). Also

as anticipated, in the upwelling region, temperature and salinity effects (compare Figure 47 and Figure 46) are positively correlated and of similar relative importance to total density variance. These near-surface observations are consistent with results already presented and so provide evidence that this technique may be valid.

Away from the surface, areas of highest indicated variance may be dynamically active regions in the CCS. Regions of maximum σ_p^2 might correspond to the mean positions of currents or eddies. If so, equation (15) can be used to determine the relative contributions of temperature, salinity, and their interaction, to the CCS itself. In support of this idea, the locations of maximum σ_p^2 seem to more closely correspond to CC and CU locations as depth increases. For example areas with σ_p^2 at least twice as high as neighboring data blocks at 200 m (Figure 48) correspond reasonably well with the areas of tight gradient in Φ (200/500 m) apparent in Figure 42. In the regions of high variance, salinity, with variance ratios $(\sigma_s^2)/\sigma_p^2$ typically from 50 to 200, seems to contribute more to total variance than temperature, with variance ratios $(\sigma_t^2)/\sigma_p^2$ in the high total variance region of 5 to 150. At 500 m, salinity contributes virtually all of the density variance (Figure 49) in a region that resembles the characteristic cyclonic circulation of the CCS. The high correlation of saline contribution to density variance indicates that the density gradient is largely due to salinity gradients at this depth. Figure 50 shows some areas at 500 m with total density variance values on the same order as at 200 m and these areas have values at least twice as high as neighboring data blocks. The location of these regions match the location of some of the energetic portions of the CCS discussed above. These observations provide evidence that the density gradient at 500 m may be significant and is largely induced by salinity gradients. This speculation is consistent with that of Lynn and Simpson (1989).

If quarterly mean values of salinity and temperature are substituted for t and s in equation (15), and statistics are generated from these mean values by summing across the length or width of the CCS, equation (16) will represent contributions of salinity, temperature, and their covariance to the total density variance and may indicate their importance to the mean density gradient. Such calculations were performed to obtain statistics cross-shore at each latitude that had at least five seasonal means of at least 10 observations, and alongshore, across data blocks equidistant from the coast. Alongshore lines are numbered 1 to 8 from inshore out, and cross-shore lines are identified by latitude (Figure 51). The results at the surface and 100 m were plotted as histograms. Inshore, alongshore lines 1 (Figure 52) and 2 (Figure 53) show large year-round total variance at the surface. In the northern sector where line 1 crosses the

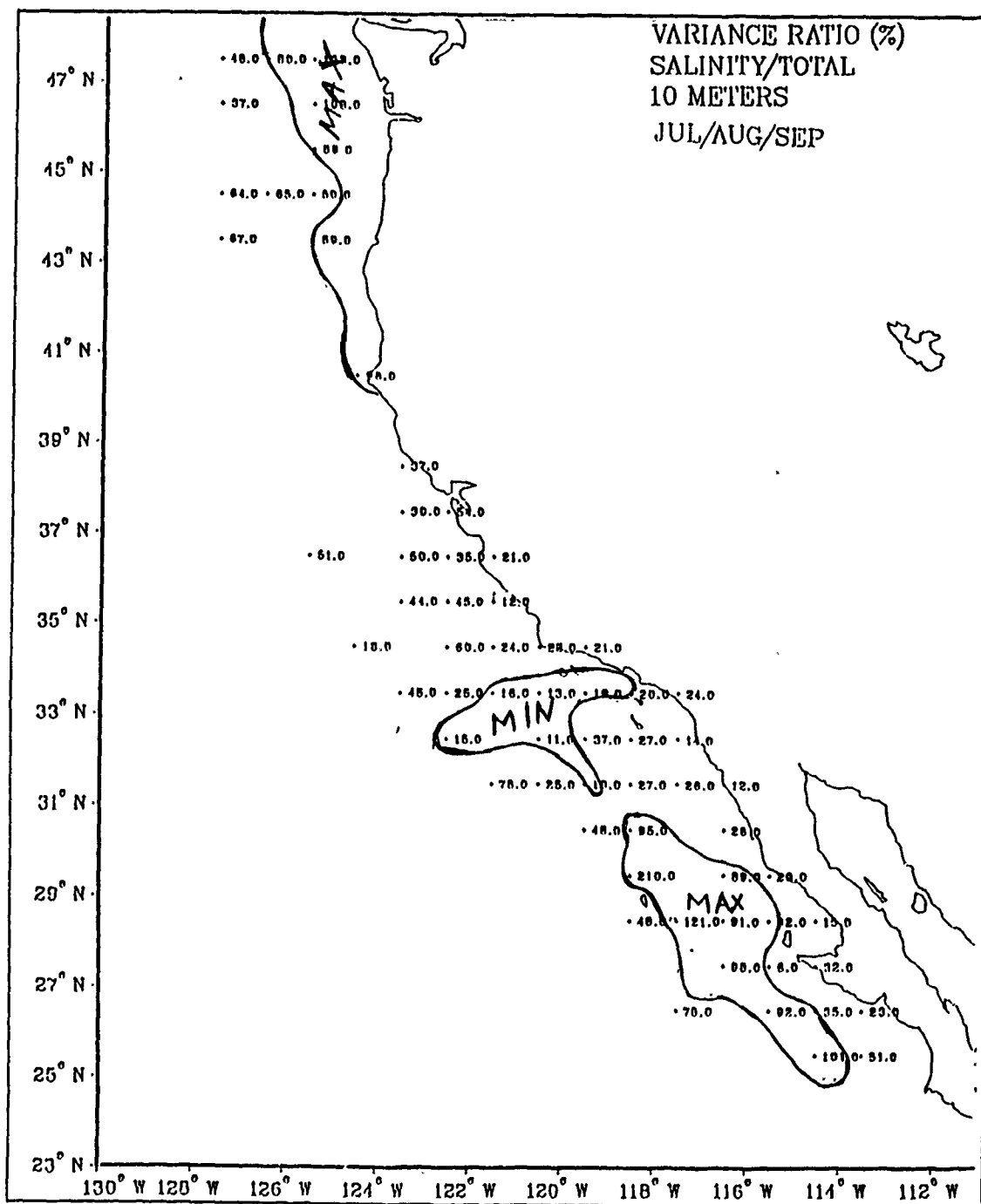


Figure 46. Salinity Contribution to Total Density Variance, 10 m, Summer:

$$\sigma_{\rho_s}^2 / \sigma_{\rho}^2 \times 100.$$

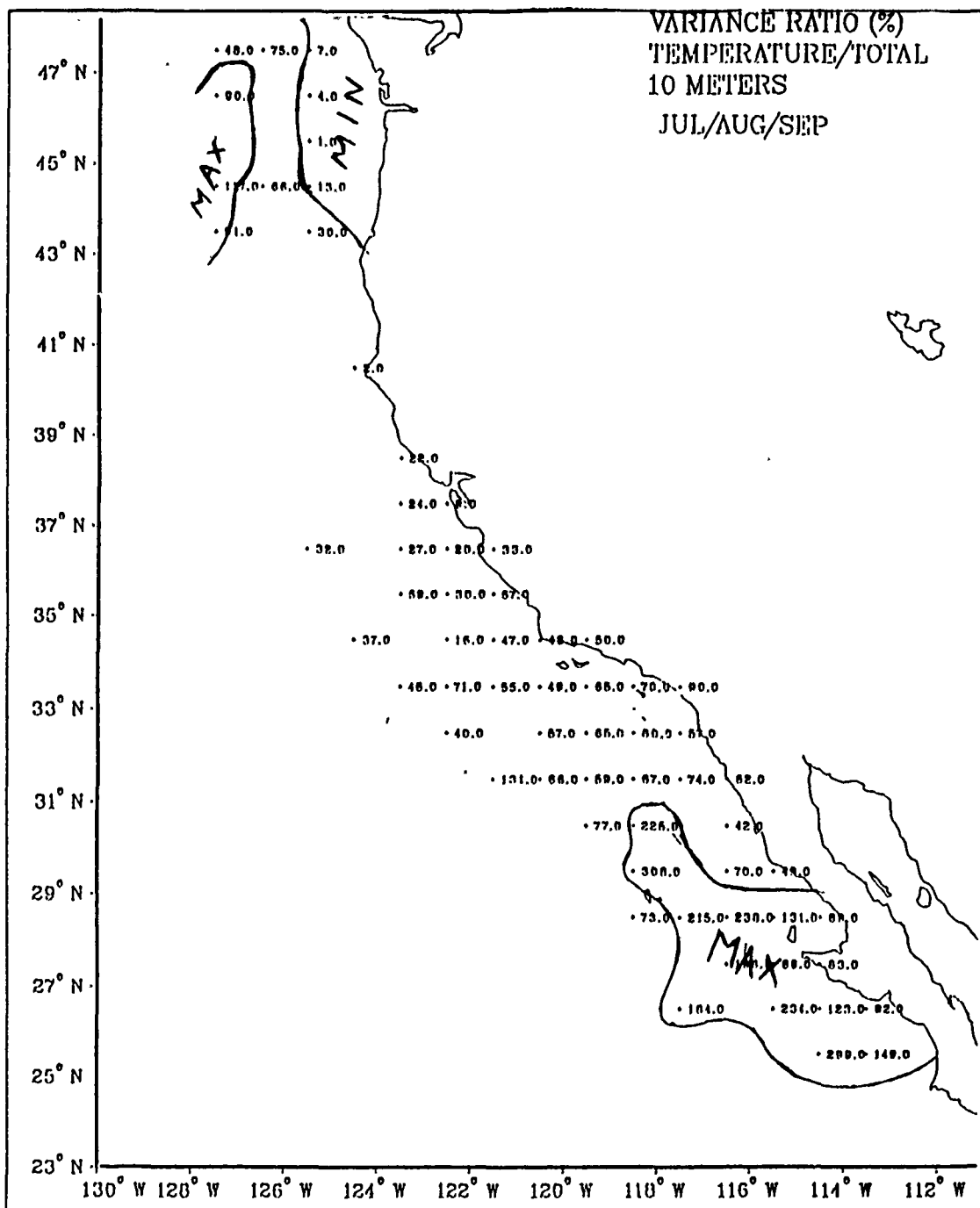


Figure 47. Temperature Contribution to Total Density Variance, 10 m,
Summer: $\sigma_{\rho}^2 / \sigma_{\rho}^2 \times 100$.

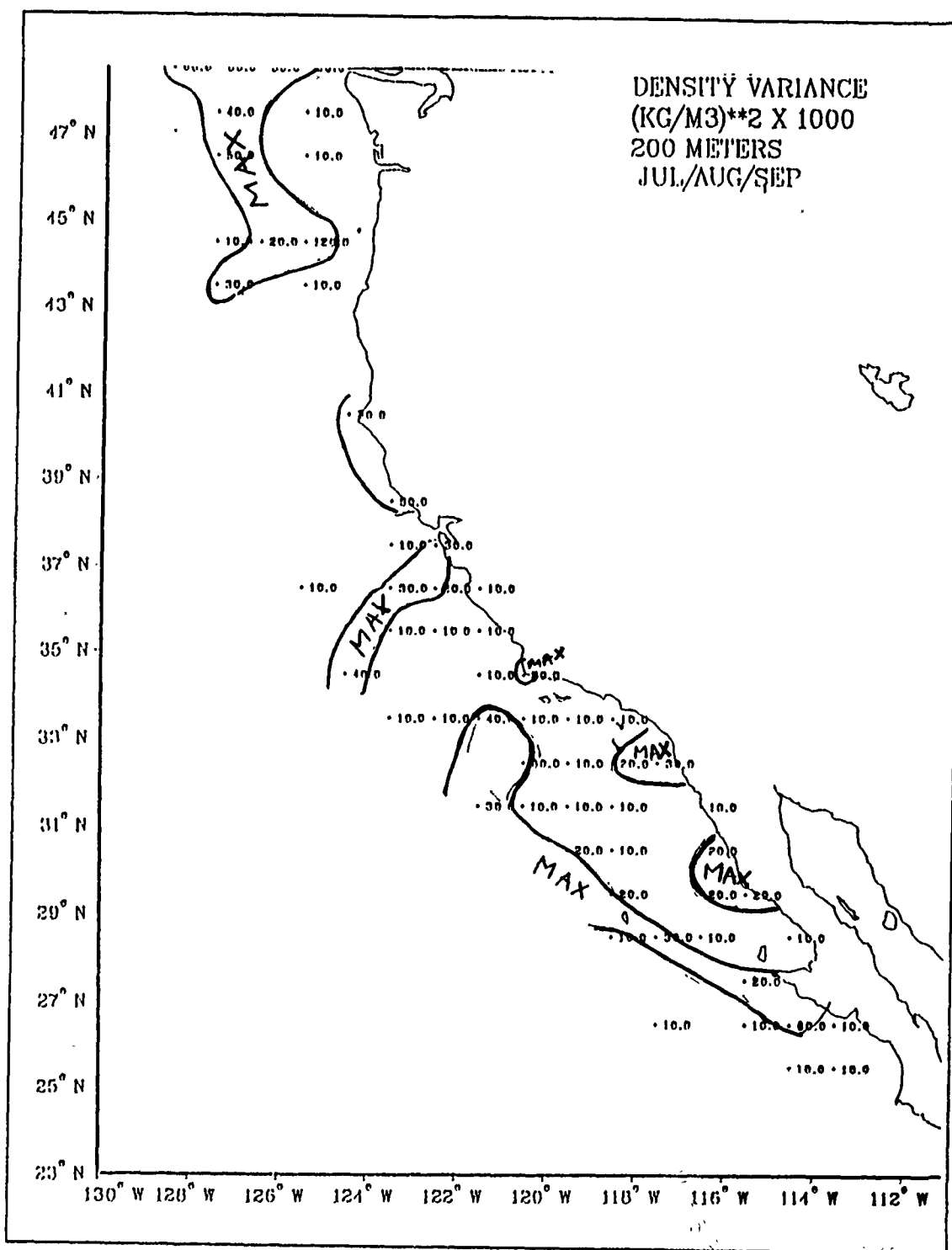


Figure 48. Total Density Variance, 200 m, Summer: Units are $(\text{kg/m}^3)^2 \times 10^3$.

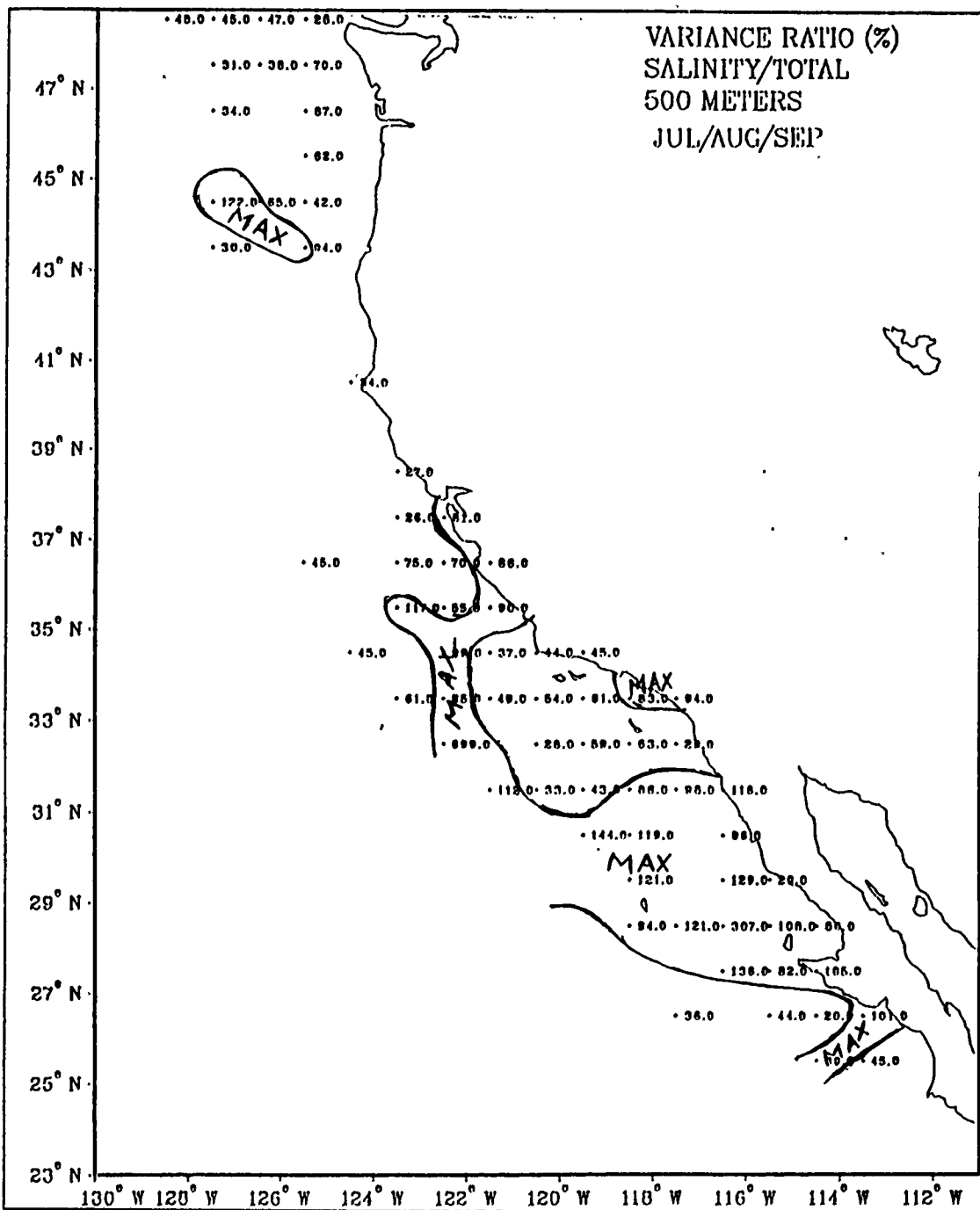


Figure 49. Salinity Contribution to Total Density Variance, 500 m, Summer:
 $\sigma_s^2 / \sigma_\rho^2 \times 100$.

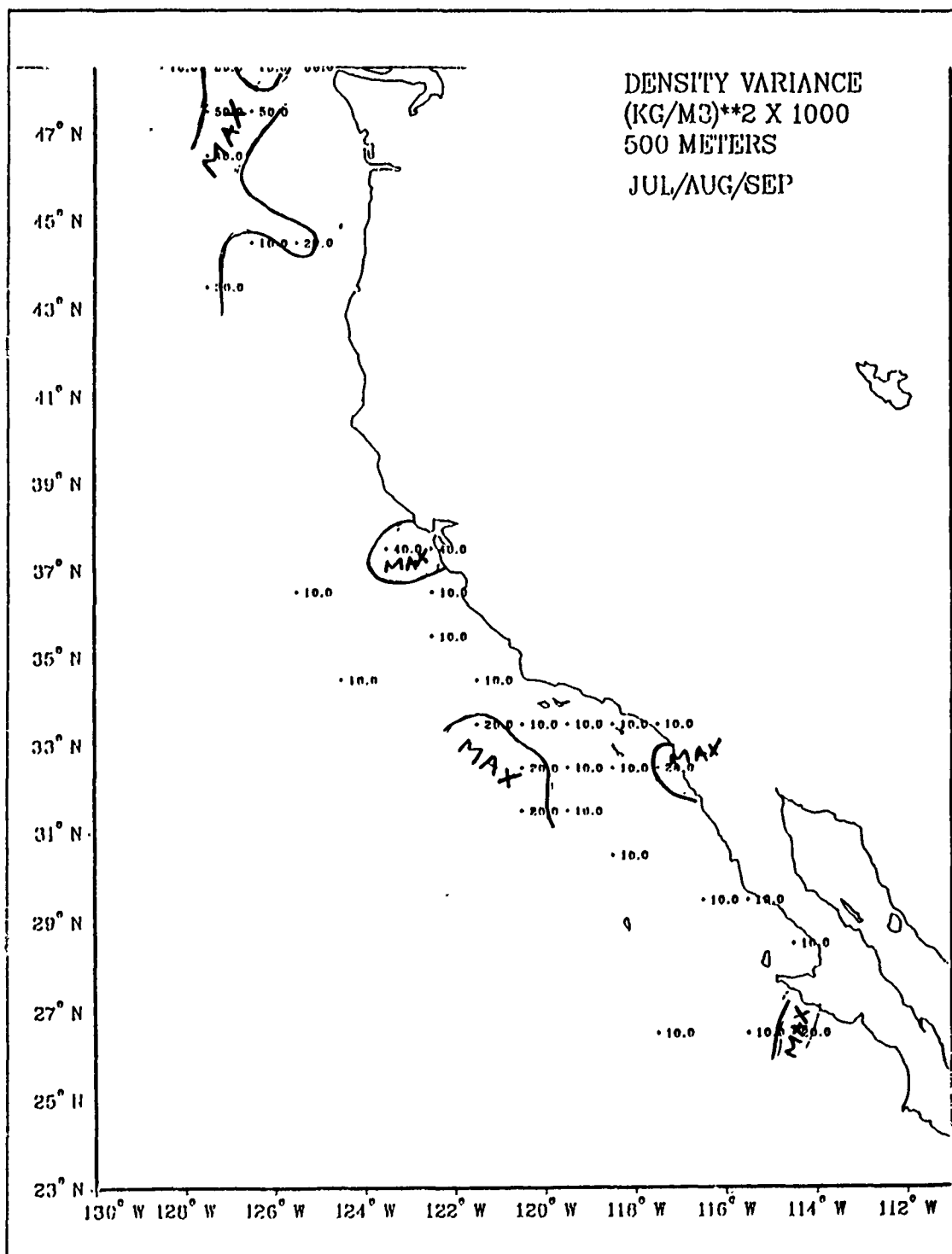


Figure 50. Total Density Variance, 500 m, Summer: Units are $(\text{kg m}^{-3})^2 \times 10^3$.

Columbia River outflow region, the greatest surface contribution is clearly from salinity. On this line even at 100 m, salinity variance dominates alongshore except in winter when temperature variance is apparently slightly more important. Line 2, which is influenced by runoff the length of the California coast, as well as by Columbia River outflow, shows surface salinity as most important in fall, and a strong saline signature year round. At 100 m, temperature is clearly dominant in the low runoff, winter season, and at least of equal importance the rest of the year. Northern cross-shore sections (only sections at 46°, 47°, 49° N in the autumn, and 26°-35° N met the minimum number of observations criterion) show salinity variance as key during the fall (e.g., Figure 54).

Alongshore, the covariance is always negative, as must be expected when the large scale opposing meridional trends in temperature and salinity are considered. Cross-shore, except in the northern area where warm, fresh Columbia River outflow results in strong positive interactions, covariance tends to be less important and of either sign, reflecting the variability of the nearshore waters (e.g., Figure 55).

Cross-shore variance at 100 m is very small in the north, generally an order of magnitude less than the 0.1 to 0.5 ($kg\ m^{-3}$)² typical at the surface. In the south, cross-shore variance at 100 m is of comparable magnitude to that at the surface.

Histograms generated for areas where relative contributions to density variance of temperature, salinity, and their interaction are the same will have similarly shaped histograms. Therefore, it is reasonable to expect that, in the same water mass, areas undergoing similar energetic processes will have similarly shaped histograms. This reasoning implies that if the shape of the histogram for a particular section is the same at the surface and 100 m, the two levels may well be undergoing the same dynamics and/or thermodynamics; that is, they are dynamically coupled. In the autumn, the graphs for areas south of 31° N at both depths are very similar in shape (e.g., Figure 56), indicating such coupling may exist. Perhaps surface cooling which occurs during the months of October through December results in deeper mixed layers south of 31° N.

In this southern region, except when total variance is very low, temperature provides the largest contribution to cross-shore gradients. There is a tendency for greatest temperature variance, and therefore total variance, to occur in fall, further evidence that surface cooling is greatest during that period.

Alongshore lines also show a noticeable, if less pronounced, increase in variance during the autumn. During that season, the alongshore sections seaward of line 2 show the surface and 100 m layers to be well coupled the length of the CCS (e.g., Figure 57).

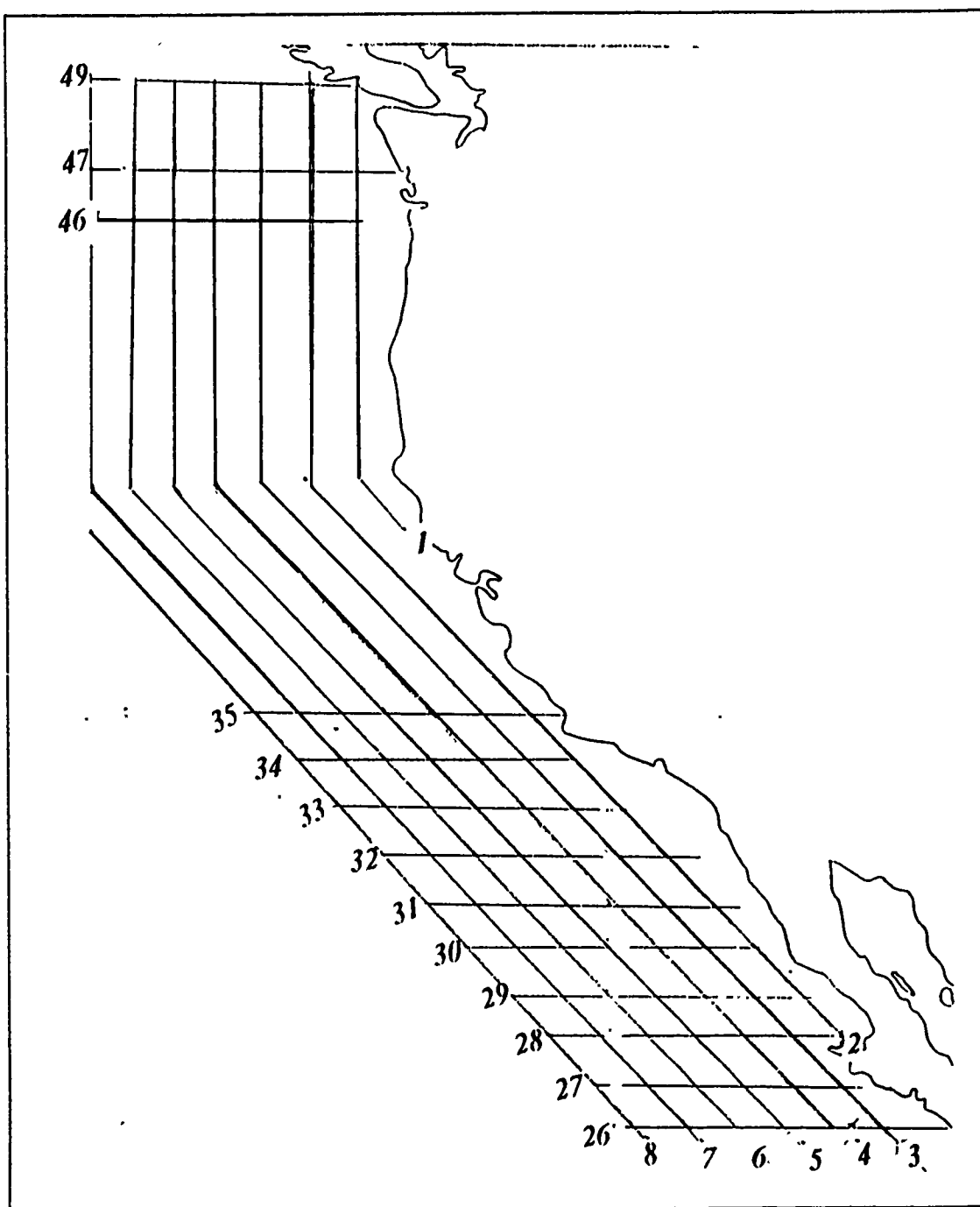


Figure 51. Alongshore and Cross-Shore Density Variance Contribution: Contributions to total density variance by temperature, salinity, and their interaction were calculated along the lines shown.

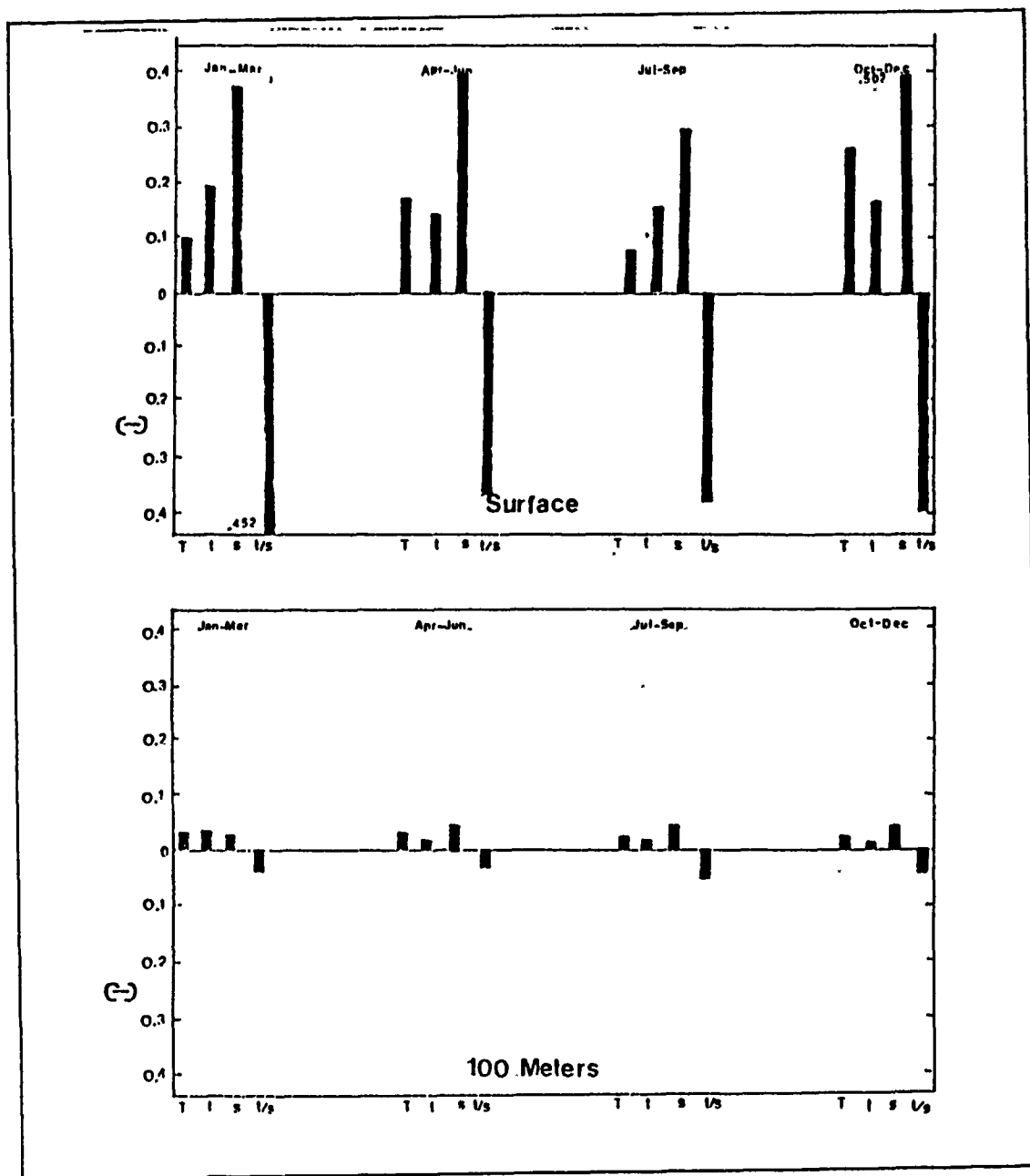


Figure 52. Alongshore Line 1, Contributions to Density Variance: Contribution to total density variance (labeled T) by temperature (t), salinity (s), and their interaction (t/s) are depicted here by season at the surface and 100 m. Units of density variance here are $(kg\ m^{-3})^2$.

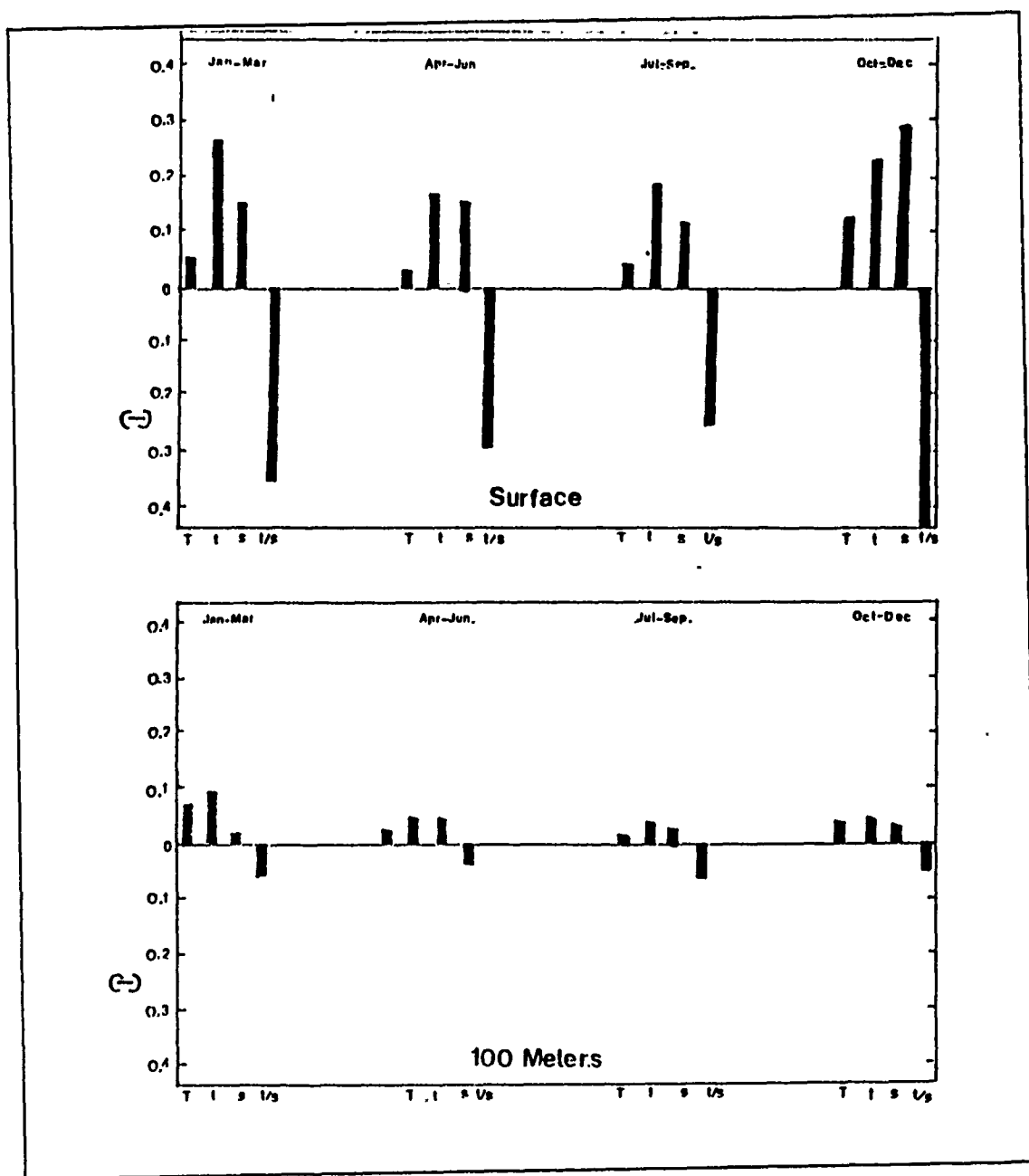


Figure 53. Alongshore Line 2, Contributions to Density Variance: Contribution to total density variance (labeled T) by temperature (t), salinity (s), and their interaction (t/s) are depicted here by season at the surface and 100 m. Units of density variance here are $(kg\ m^{-3})^2$.

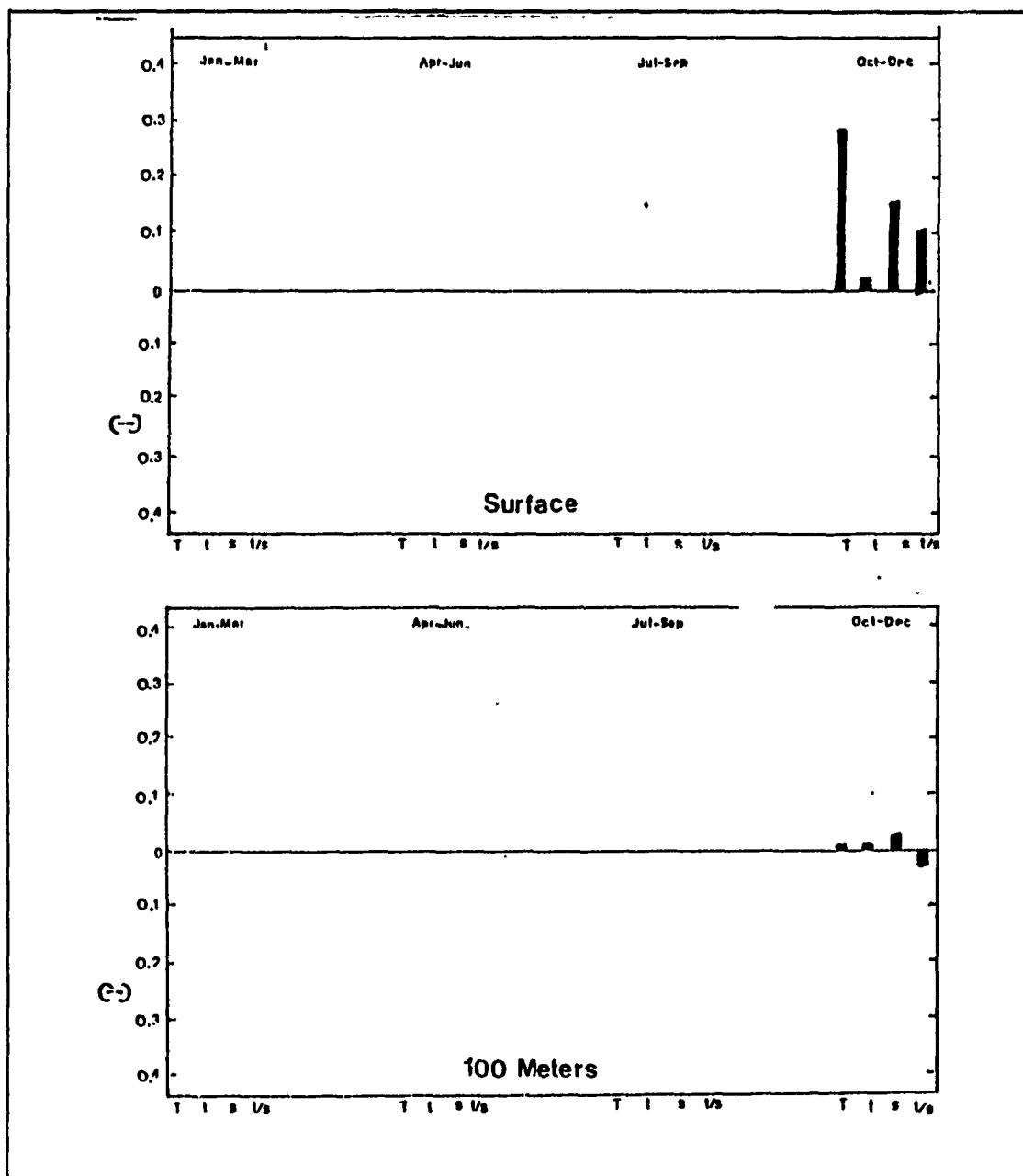


Figure 54. Cross-shore Line 46, Contributions to Density Variance: Contribution to total density variance (labeled T) by temperature (t), salinity (s), and their interaction (t/s) are depicted here by season at the surface and 100 m. Units of density variance here are $(kg\ m^{-3})^2$.

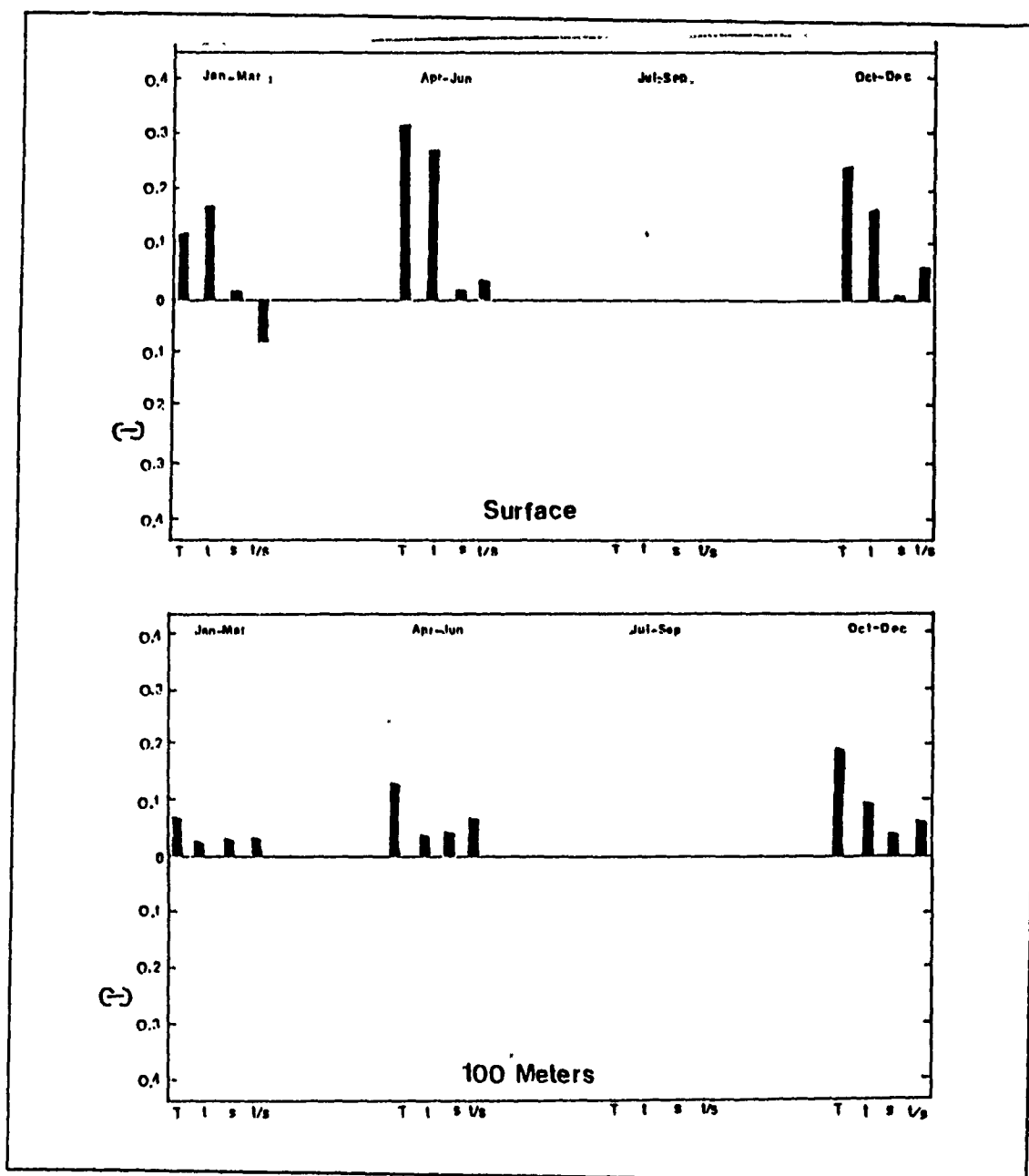


Figure 55. Cross-shore Line 26, Contributions to Density Variance: Contribution to total density variance (labeled 'T') by temperature (t), salinity (s), and their interaction (t/s) are depicted here by season at the surface and 100 m. Units of density variance here are $(kg\ m^{-3})^2$.

Again a possible interpretation is that surface cooling in the fall results in deeper mixing. If this interpretation is valid then mixing occurs offshore for the length of the CCS.

It may be argued that over any areas or periods where the relative contributions to total variance remain constant, a density model based on temperature alone can accurately represent gradients, erring only by a constant factor. In that case, intersections of a group of adjacent alongshore sections sharing a characteristic histogram shape, with a group of cross-shore sections that have a common histogram shape, will highlight such regions. Subject to individual interpretation, some seasonal combinations of lines 2-5 and 26-31 may meet the criteria. For example, the autumn histograms for lines 3 (Figure 58) and 4 (Figure 59) are nearly the same shape, as are the autumn graphs of lines 27, 28, and 29 (Figure 60, Figure 56 and Figure 61, respectively). The implication here is that during October through December, at least in the upper 100 m, within an area 2° - 4° from shore, between 27° and 30° N, a temperature-only density model would overestimate the alongshore gradient by a constant small factor and underestimate the cross-shore gradient by a similar amount. Again the indication is that offshore, in select three or four degree blocks, salinity variance may not be essential to an accurate model of the dynamic field. (Using this technique to generate shorter alongshore cuts, of lengths similar to the cross-shore cuts for example, might result in the identification of more of these areas.)

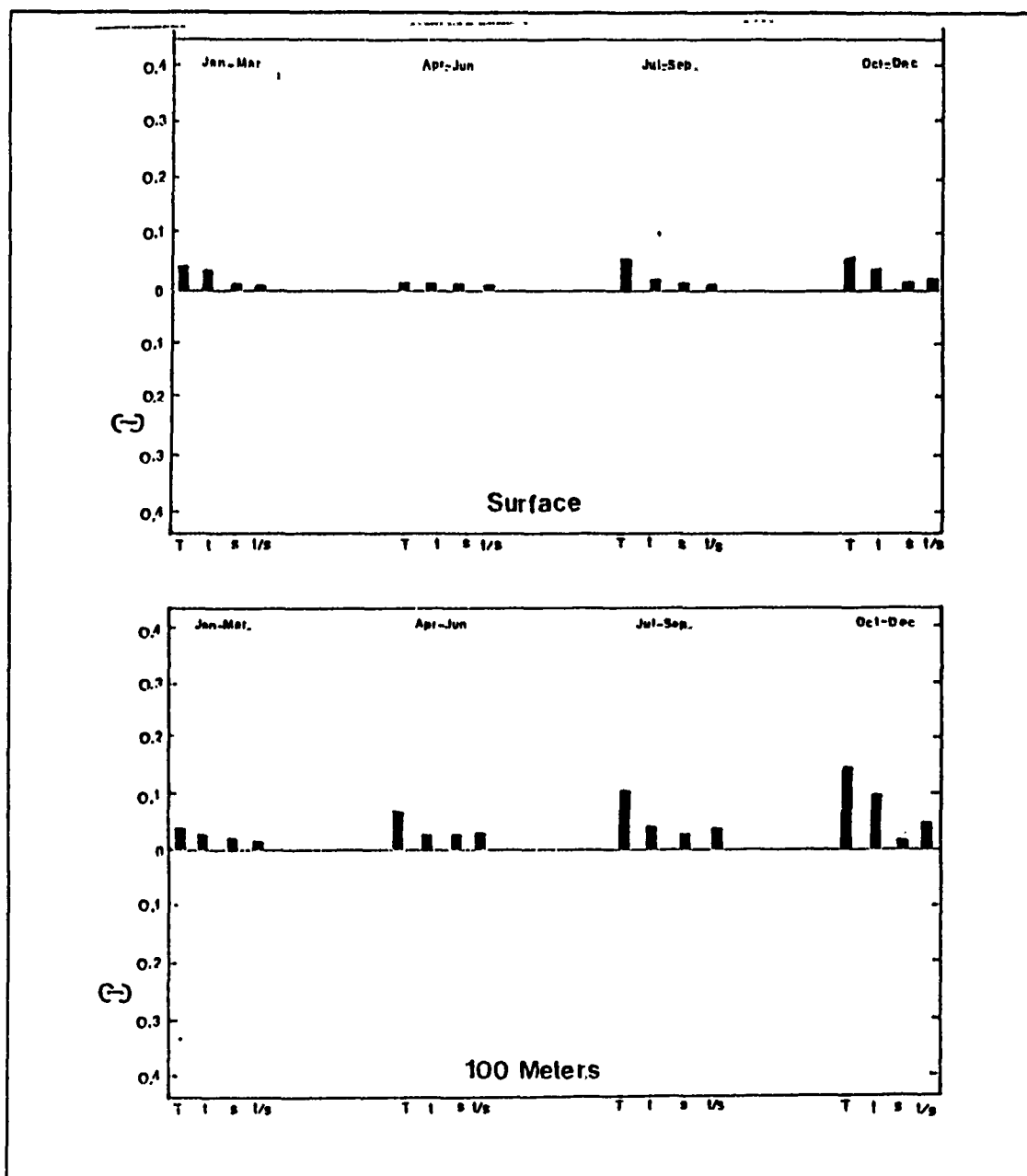


Figure 56. Cross-shore Line 28, Contributions to Density Variance: Contribution to total density variance (labeled T) by temperature (t), salinity (s), and their interaction (t/s) are depicted here by season at the surface and 100 m. Units of density variance here are $(kg\ m^{-3})^2$.

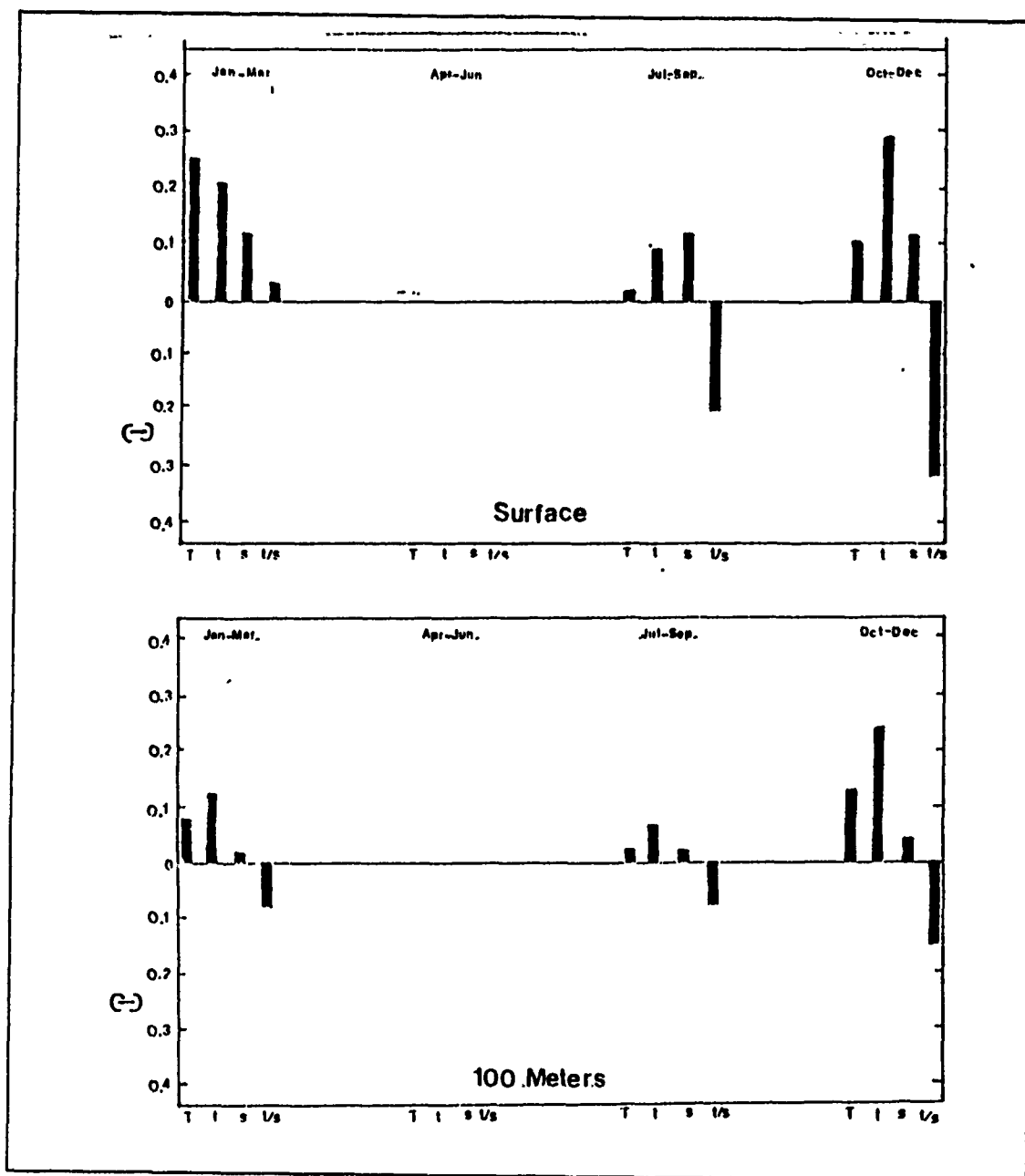


Figure 57. Alongshore Line 6, Contributions to Density Variance: Contribution to total density variance (labeled 'T') by temperature (t), salinity (s), and their interaction (t/s) are depicted here by season at the surface and 100 m. Units of density variance here are $(kg\ m^{-3})^2$.

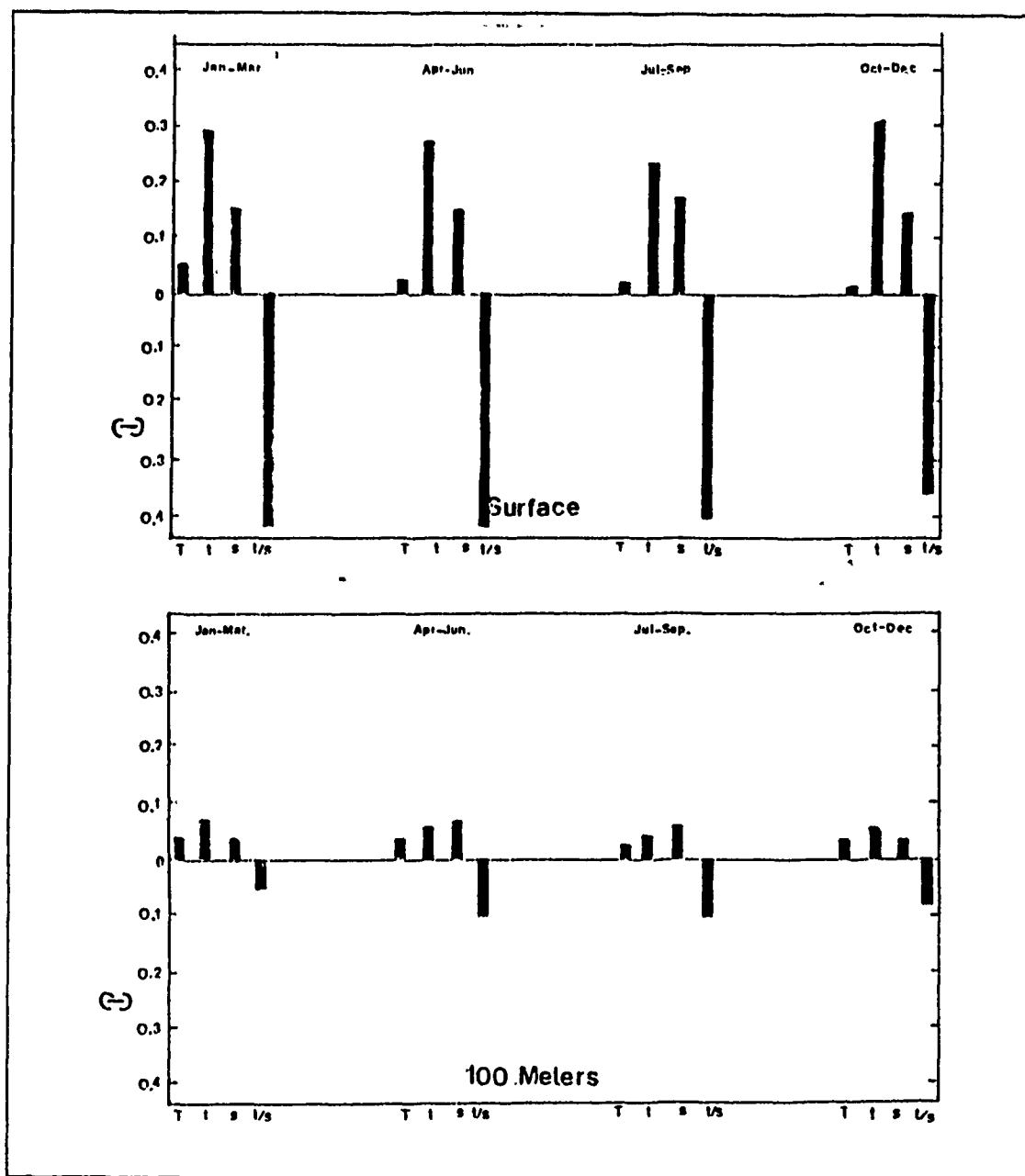


Figure 58. Alongshore Line 3, Contributions to Density Variance: Contribution to total density variance (labeled T) by temperature (t), salinity (s), and their interaction (t/s) are depicted here by season at the surface and 100 m. Units of density variance here are $(kg\ m^{-3})^2$.

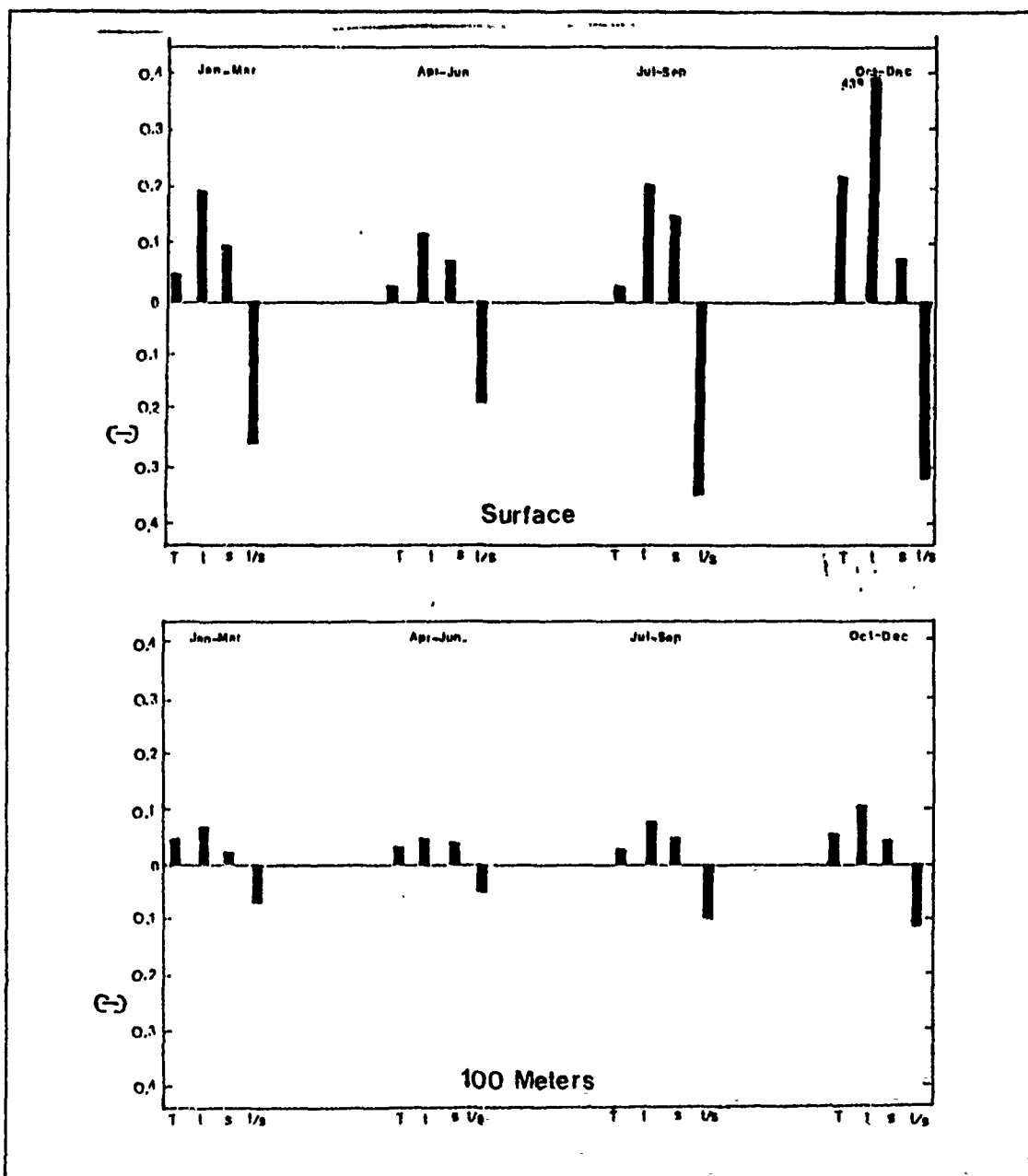


Figure 59. Alongshore Line 4, Contributions to Density Variance: Contribution to total density variance (labeled T) by temperature (t), salinity (s), and their interaction (t/s) are depicted here by season at the surface and 100 m. Units of density variance here are $(\text{kg m}^{-3})^2$.

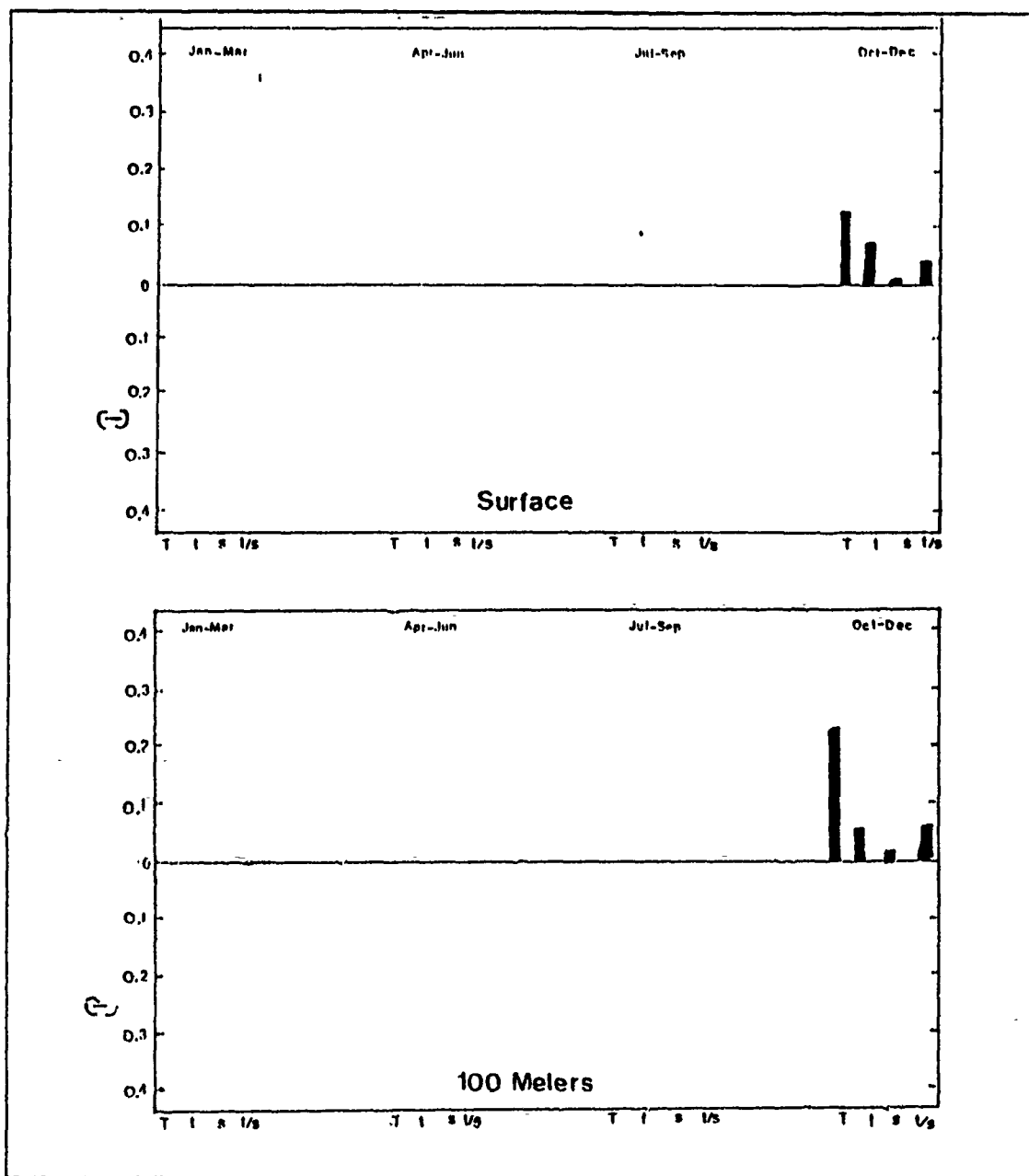


Figure 60. Cross-shore Line 27, Contributions to Density Variance: Contribution to total density variance (labeled T) by temperature (t), salinity (s), and their interaction (t/s) are depicted here by season at the surface and 100 m. Units of density variance here are $(kg\ m^{-3})^2$.

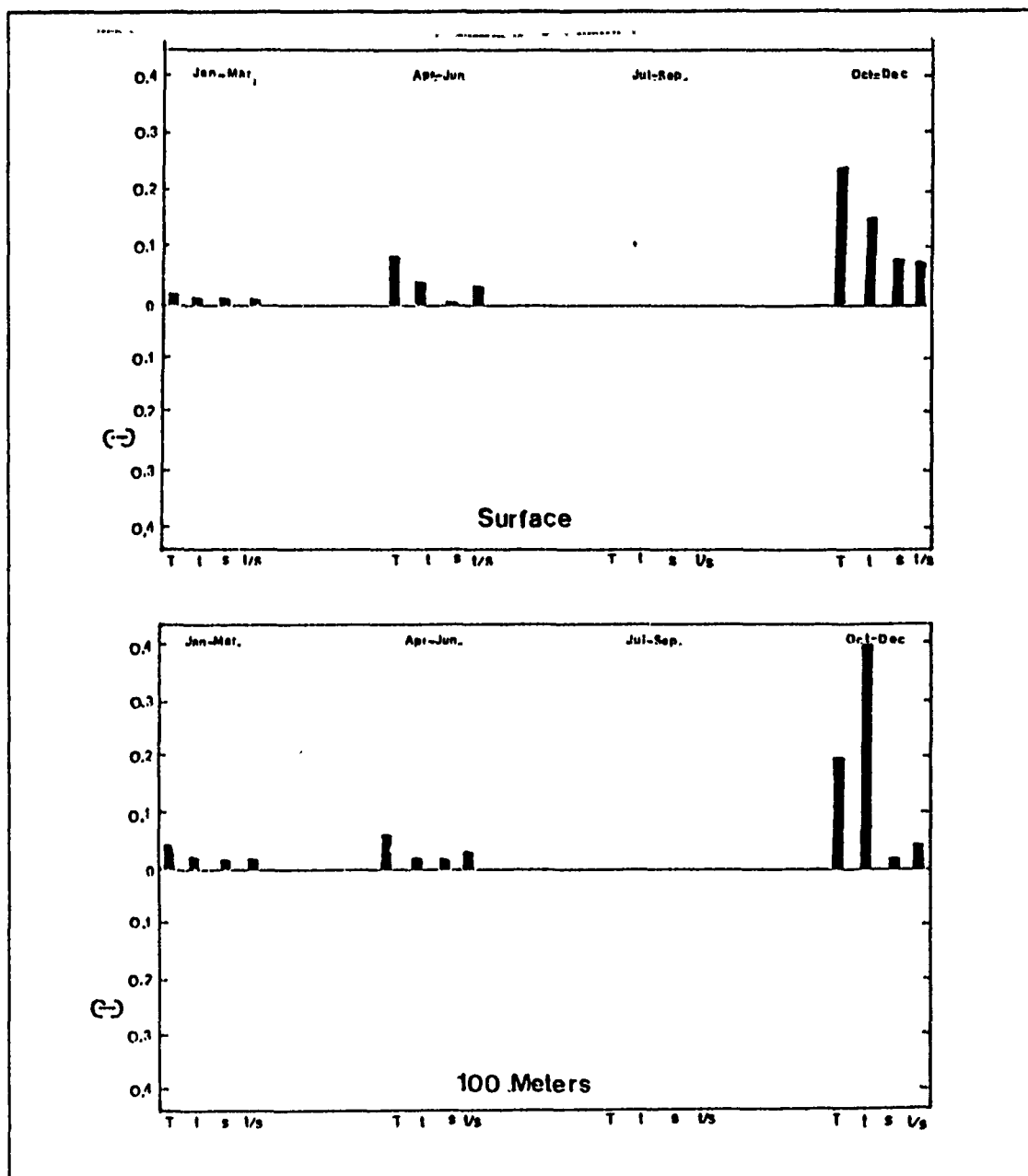


Figure 61. Cross-shore Line 29, Contributions to Density Variance: Contribution to total density variance (labeled T) by temperature (t), salinity (s), and their interaction (t/s) are depicted here by season at the surface and 100 m. Units of density variance here are $(kg\ m^{-3})^2$.

V. SUMMARY AND CONCLUSIONS

Salinity has a profound impact on the CCS, with structure that is complex and variable. In the region of the Columbia River's outflow, surface salinity may vary an entire *psu* in 100 km, or 1 *psu* over the course of a year; yet in this region the depth integrated importance of the salinity gradient is less important than anywhere else in the CCS. Off the coast of Baja California, where thermal expansion coefficients are high, saline contraction coefficients low, and surface salinity gradients have minimal impact on the density field, the importance of salinity variability 100 m below the surface is often equal to the importance of temperature variance. The mean salinity field has been shown to have a pronounced effect on the large-scale geostrophic circulation of the CCS. On the other hand, there seem to be regions on the order of 3° squares where the assumption of constant salinity might not cause significant errors in the estimation of density gradients. Relative importance of temperature and salinity often changes seasonally. Areas where mean gradients in temperature and salinity have positive correlation in terms of their effect on density border areas of negative covariance of the T-S gradients. Despite the existence of correlation in mean gradients, there seems to be little correlation between simultaneously observed values of temperature and salinity.

Based on these observations, it is reasonable to conclude that careful work concerning the CCS should include haline description. Descriptively and dynamically, salinity is essential to accurately characterize the large-scale structure of the CCS. Evidence has been developed in this study that indicates salinity may play significant roles in many smaller scale phenomenon as well. There is some indication that there may be areas where salinity variation may be neglected in process-oriented models, but regions to be so modeled must be carefully selected.

A. STERIC ANOMALY

A comparison of the constituents of the steric anomaly due to salinity and temperature showed that the gradients in δ_T and δ_S oppose generally, major exceptions being on the surface off the coast of Oregon where the warm, fresh discharge of the Columbia River leads to large values of δ_T and δ_S , and off the coast of northern California in summer, when upwelling of cold, salty water leads to low values for both δ_T and δ_S .

In areas where δ_T is highly correlated with δ , and has similar variance, δ_T might be considered an adequate estimator of δ . A small, shallow region with these characteristics was identified off the coast of northern Baja California.

Using the idea of RMSE to calculate mean differences from the steric anomaly, δ , of δ_S and δ_T , the contributions to mean gradient in δ associated with δ_S and δ_T were compared. On the large scale, δ_S is quite important and certainly should not be ignored. On the other hand, the contribution of salinity is fairly evenly distributed and so, as the amount of area considered decreases, the relative magnitude of error in gradient resulting from the assumption of constant salinity also decreases. For example, assumption of a constant value of salinity for the entire CCS in July would result in an approximate overestimate of 40 percent in the alongshore south to north mean δ gradient. However, if only the area adjacent to the California coast is considered, a 10 percent error results.

B. DYNAMIC HEIGHT

Calculating dynamic height, Φ , by integrating δ over depth, and comparing it to $\Phi_{35\sigma_\theta}$, calculated by integrating δ_T , provided insight concerning the importance of salinity variation to the geostrophic flow field. At all depths, the mean variability of salinity in the CCS is responsible for a significant equatorward component along the coast of California and a strong offshore component adjacent to Baja. Additionally mean local salinity gradients can play a major role in the structure of small scale features.

C. VARIANCE IN THE DENSITY FIELD

By calculating temperature and salinity variances and covariances and differentiating the equation of state, contributions to local variation in density due to salinity, temperature, and their interaction were computed directly. Temperature variation provided the major contribution year-round on the surface. Salinity's importance generally increased with depth so that at 500 m, salinity variance might actually be most significant. Substantial variance in the density field existed even at 500 m in locations that correspond to the CC and CU, indicating dynamic activity was occurring at 500 m, and perhaps that, as Lynn and Simpson (1989) have suggested, the CCS can extend deeper than 500 m, and that at deeper depths it may be traceable by salinity variance.

By applying this technique to the mean temperature and salinity field, the relative contribution to longshore and cross-shore gradient was determined. Nearshore, or elsewhere in the vicinity of river drainage (Figure 52), variance is generally high and saline contribution considerable. There is a tendency for high variance to occur in the

autumn (defined here as October through December, Figure 57) due apparently to surface cooling. Offshore this cooling and associated mixing tend to decouple the surface layer and allow greater density variation at deeper depths, at least 100 m.

VI. RECOMMENDATIONS

A. PROFILE

The information developed in this research should be displayed in vertical sections. The organizational techniques employed here would allow alongshore, cross-shore, or diagonal lines to be displayed easily in vertical cross section. Study of these sections would allow fuller appreciation of the three dimensional interaction of temperature and salinity in the CCS. Perhaps sections of the contribution of salinity to density variance could be used with the ideas of Lynn and Simpson (1989) concerning "spiciness" to gain a fuller understanding of the water mass structure of the CCS.

B. FINER RESOLUTION

This analysis has been carried out at a 1° spatial by 1 month temporal scale, and so allows only large-scale resolution. A much finer scale approach, perhaps $1/2^\circ$ by 2 weeks, might be possible in certain regions. Using similar processing techniques and finer resolution, if every depth level were analyzed, rather than the few depths emphasized here, the T-S interplay associated with small scale phenomena such as coastal upwelling might be characterized.

C. MODELING CONSIDERATIONS

Speculation has been offered here concerning the validity of the assumption of constant salinity for the purpose of dynamic modeling. Ideally, the mean salinity data processed for this study should be incorporated into a CCS model run and results compared to similar runs in which salinity was held constant. On the other hand, indications of the effects of salinity might be achieved with less effort by using a temperature-driven linearization of density that simulates saline variability. For example, increasing the magnitude of the thermal expansion coefficient, α , in an upwelling process model may capture the effect of a positive T-S covariance on density. Entering different values of α for different regions and depths (higher values where covariance is positive, lower values where negative) would simulate salinity's variation over regions where salinity or temperature effects change sign. Use of a constant value of α over a range of temperatures, in addition to ignoring saline contribution, can superimpose a false smoothing tendency, resulting in an underestimation of the magnitude of positive $\Delta\rho$ in cold water, and negative $\Delta\rho$ in warm water. Forcing α to change more or less uniformly

meridionally but at a higher rate than warranted by the mean temperature gradient would allow study of the combined effects of meridional saline variation and smoothing.

Because salinity measurements are more expensive to make and more difficult to obtain than temperature observations, it may be desirable to estimate salinity from a known temperature-salinity (T-S) correlation (Stommel, 1947). Emery (1975) has shown that the accuracy of dynamic height calculations made from such derived salinities can, at least in some cases, be comparable to the accuracy of determinations made from observed salinities. In these cases, the salinity field in general can be accurately inferred from expendable bathythermograph observations alone, as Rienecker *et al.* (1985) have attempted.

The validity of such salinity inferences depends completely on the strength of the T-S correlation, or what Stommel (1947) called "range of uncertainty", i.e., the "tightness" of a particular T-S curve. This uncertainty in differential salinity can be related to:

$$\sqrt{(1 - r_{ts}^2) \times (\Delta S)^2}, \quad (17)$$

where ΔS is determined from the T-S curve, r_{ts} is the coefficient of determination for temperature and salinity, and $(1 - r_{ts}^2)$ is the fraction of salinity variance that cannot be explained by temperature variance. Clearly the uncertainty increases as the strength of the correlation (and magnitude of r_{ts}^2) decreases. Therefore, it may be reasonable to expect the method of salinity inference from T-S relationship to be most accurate in regions of highest T-S correlations, and least accurate in regions where the T-S correlation is weak. Blumberg *et al.* (1984) concluded that development of T-S curves for the CCS would not be cost effective for modeling efforts due to combinations of relatively poor T-S correlations inherent in near surface waters (less than 200 m), and lack of significant numbers of temperature observations in deeper areas where the idea might otherwise work.

Preliminary investigations have been made to determine seasonal values of the T-S correlation (i.e., coefficients of determination) at 10, 100, 200 and 500 m. Even at 500 m, areas where temperature variance has as much as a 50 percent linear relationship with salinity are rare (Figure 62), and those areas are not constant from month to month. This result strongly supports the statements of Blumberg *et al.* (1984). A modeler might be served as well by using salinity climatology as by attempting to prescribe the salinity field based on its relationship with temperature. An

observationalist should probably take full CTD casts to determine the salinity in the CCS. Calculations could be performed to confirm these statements.

The geographic distribution of salinity in the CCS may be sufficiently linear, at least regionally, to allow worthwhile use of linear regression coefficients on latitude, longitude and/or depth. Sums required by least squares techniques to compute statistically significant coefficients of such a regression equation are easily obtainable through techniques used in this study. Model runs using the resulting salinity parameterization would be instructive, as would the shorthand description of the salinity field represented by the parameterization itself. If results of any of these model runs differ significantly from corresponding constant salinity runs, decisions concerning the best method to include salinity could be made.

D. SOUND SPEED CALCULATIONS

Salinity is a variable in the equation for sound speed in seawater but is generally estimated by a climatological mean when tactical acoustic range predictions are computed. The considerable database now available in the CCS should allow a numerical evaluation of the validity of such a parameterization.

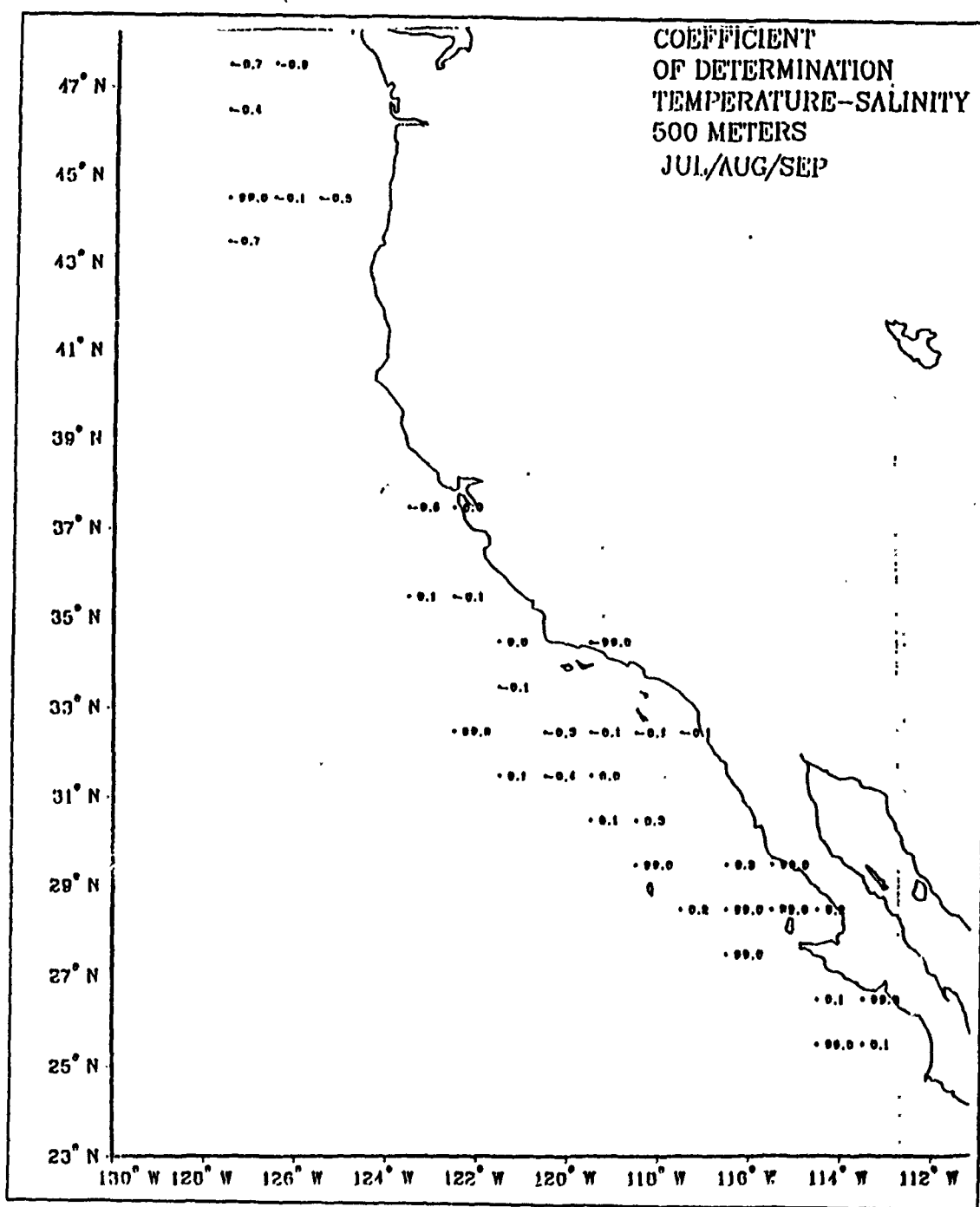


Figure 62. Coefficient of Determination (T-S), Summer, 500 m: r^2 (the algebraic sign is obtained from covariance, and "99" indicates a bad data processing point).

APPENDIX A. NUMBER OF OBSERVATIONS

This appendix provides plots of the number of observations associated with each data block (for those data blocks having at least ten observations) for the months January, April, July, and October and the depths 10 and 500 m.

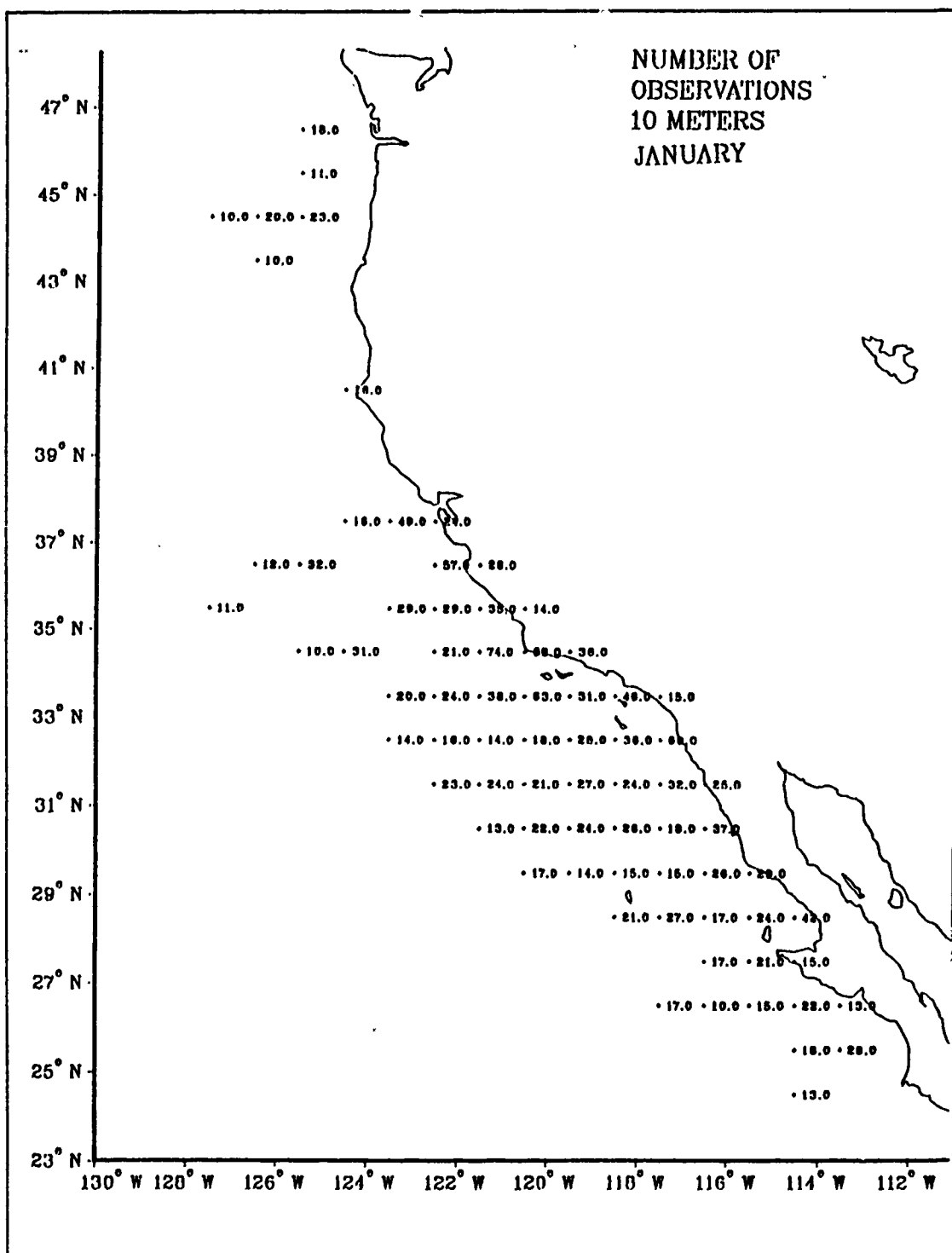


Figure 63. Number of Observations at 10 m, January.

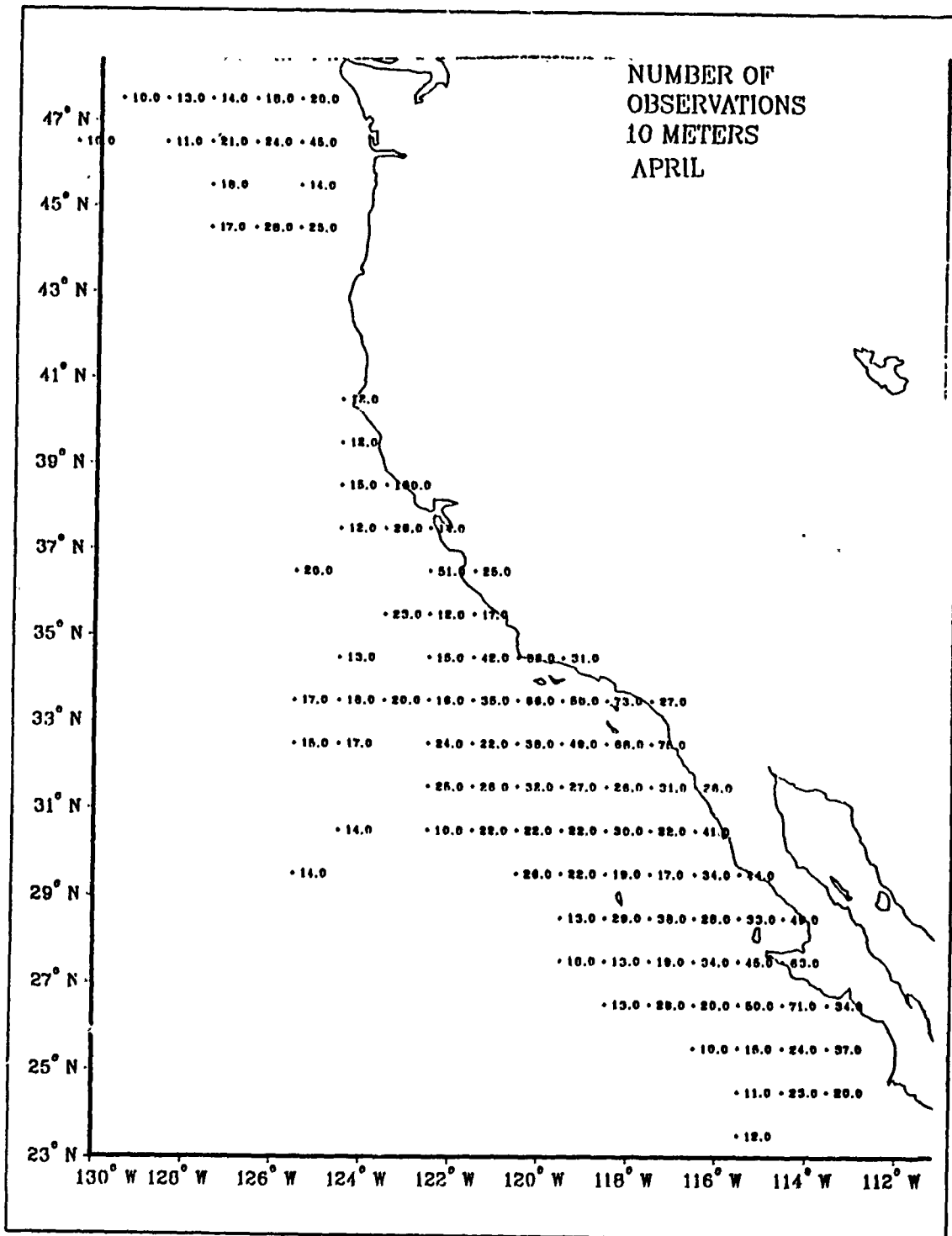


Figure 64. Number of Observations at 10 m, April.

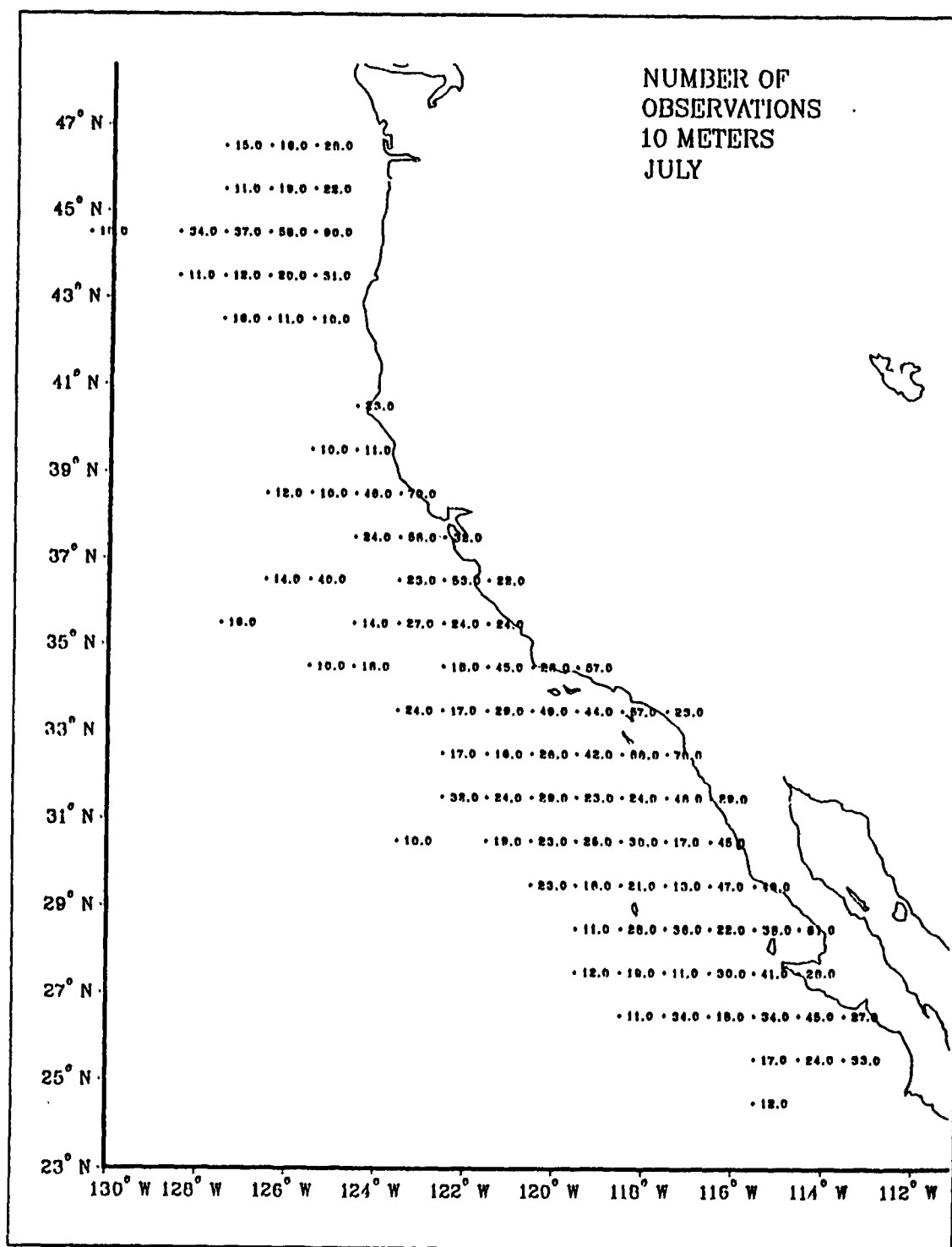


Figure 65. Number of Observations at 10 m, July.

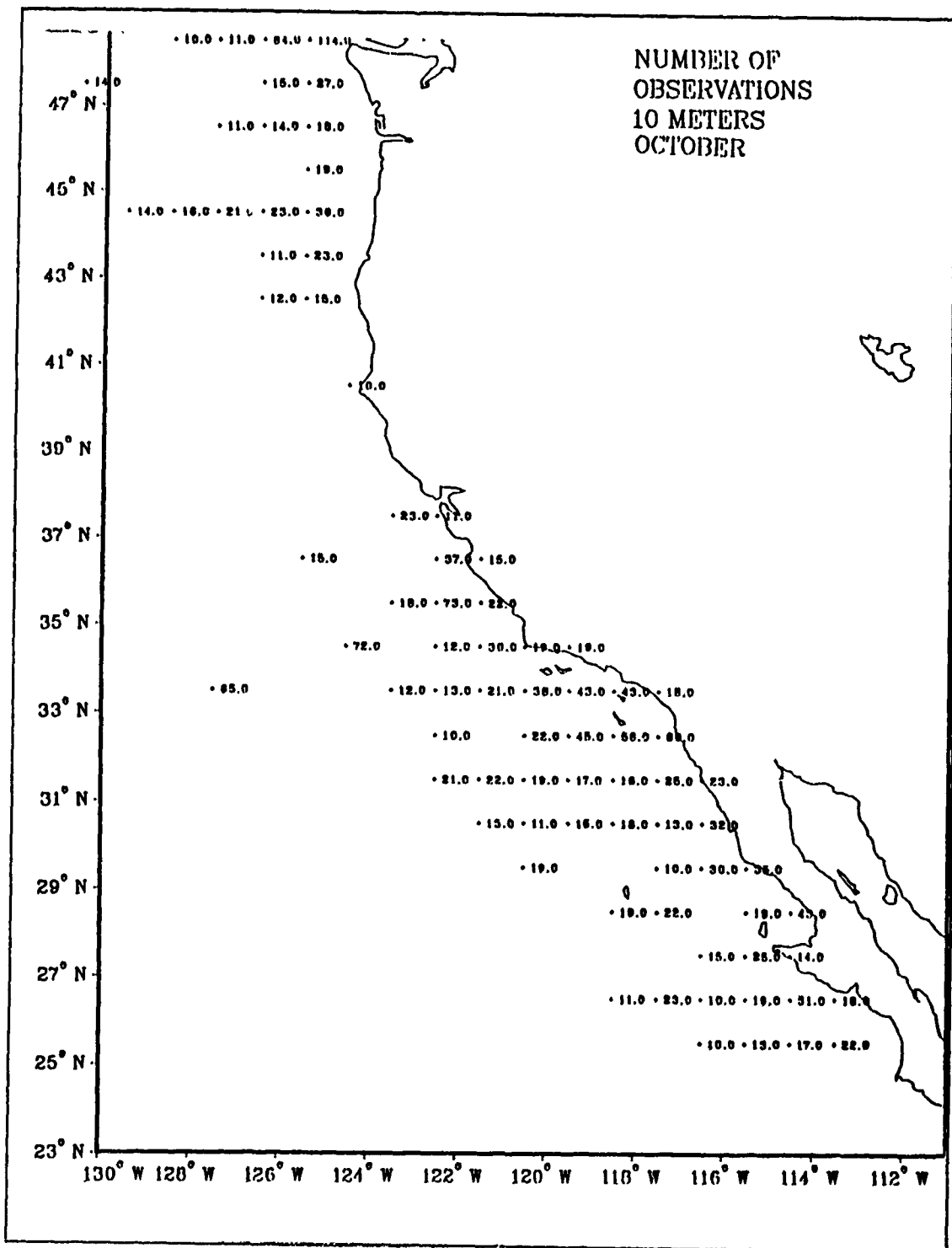


Figure 66. Number of Observations at 10 m, October.

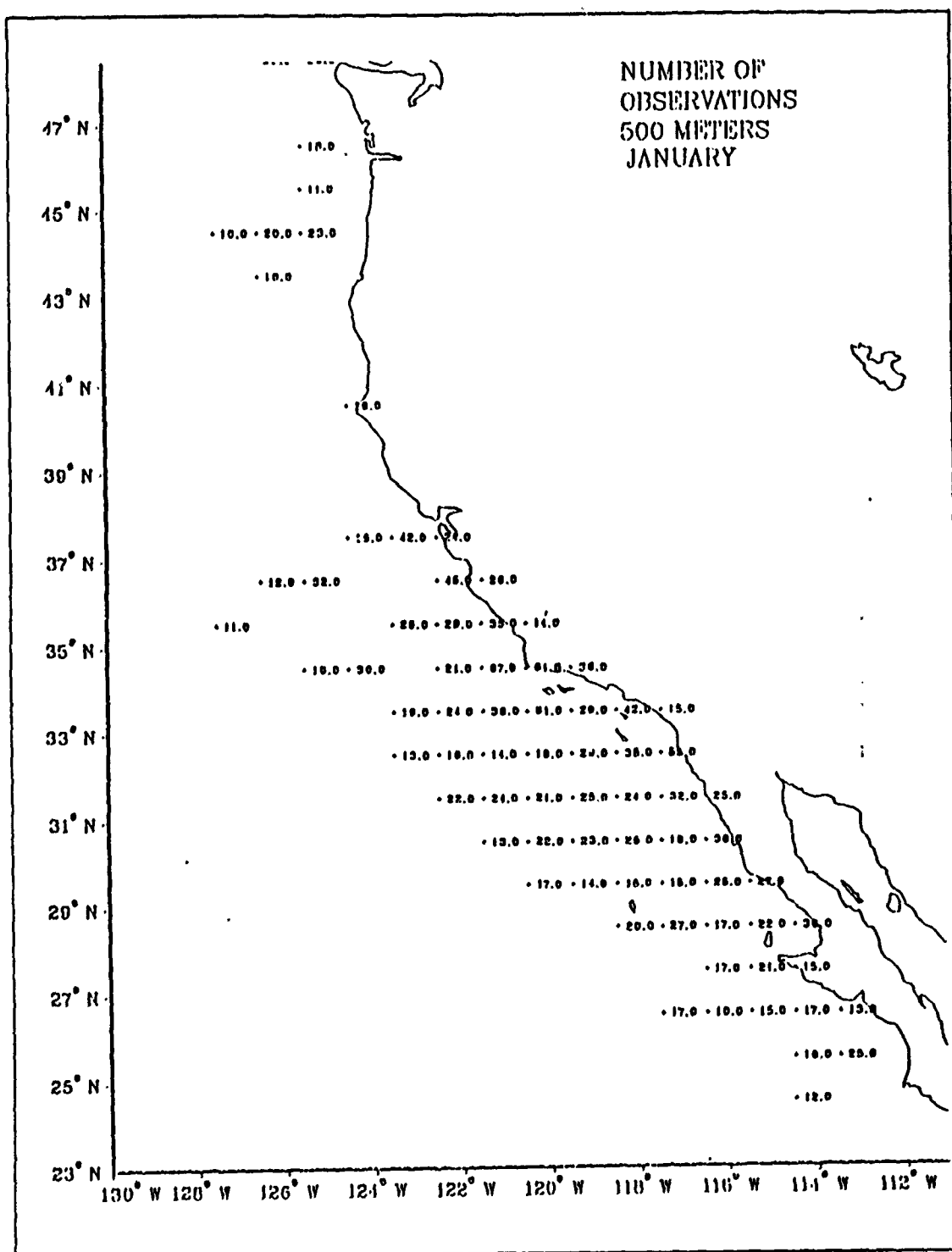


Figure 67. Number of Observations at 500 m, January.

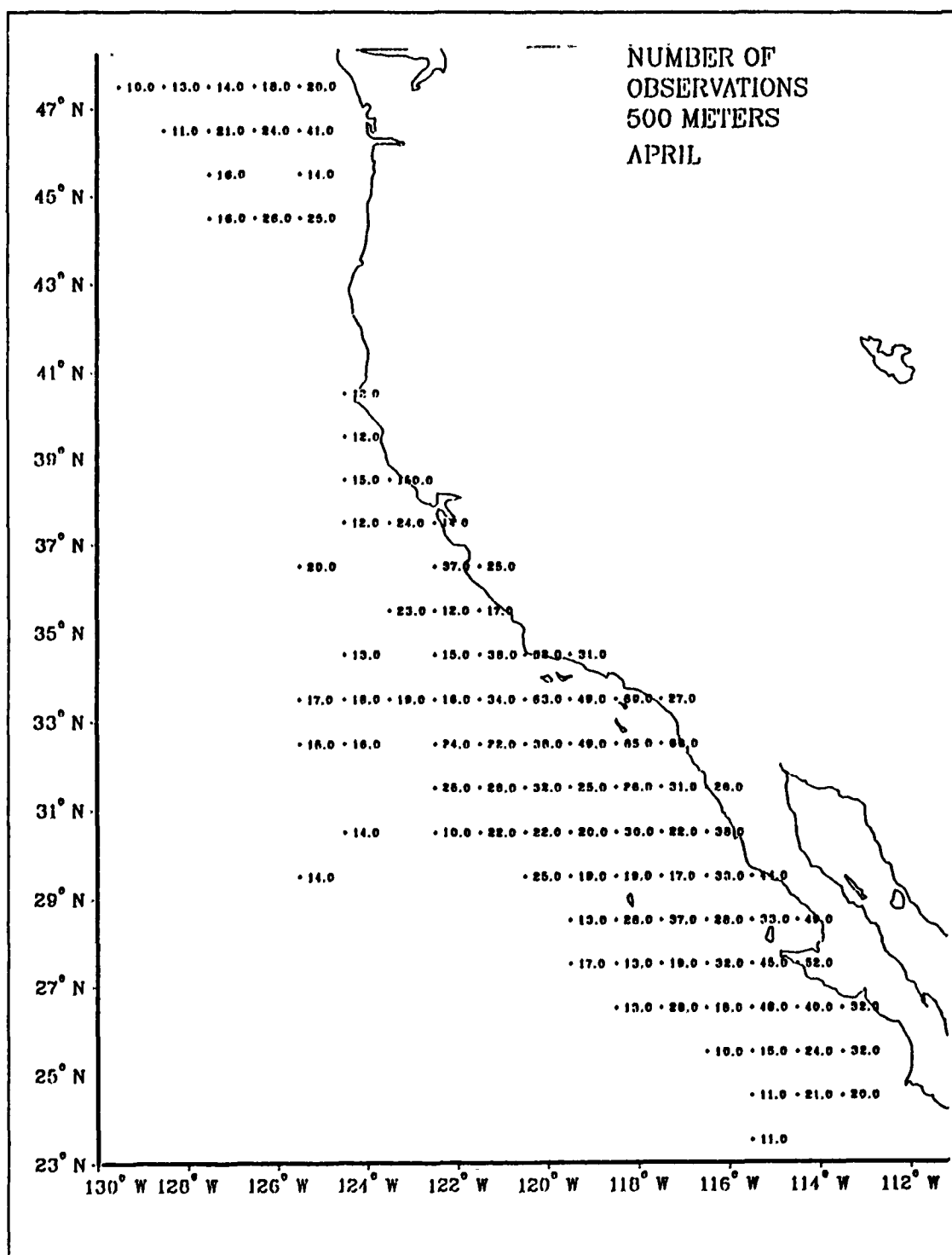


Figure 68. Number of Observations at 500 m, April.

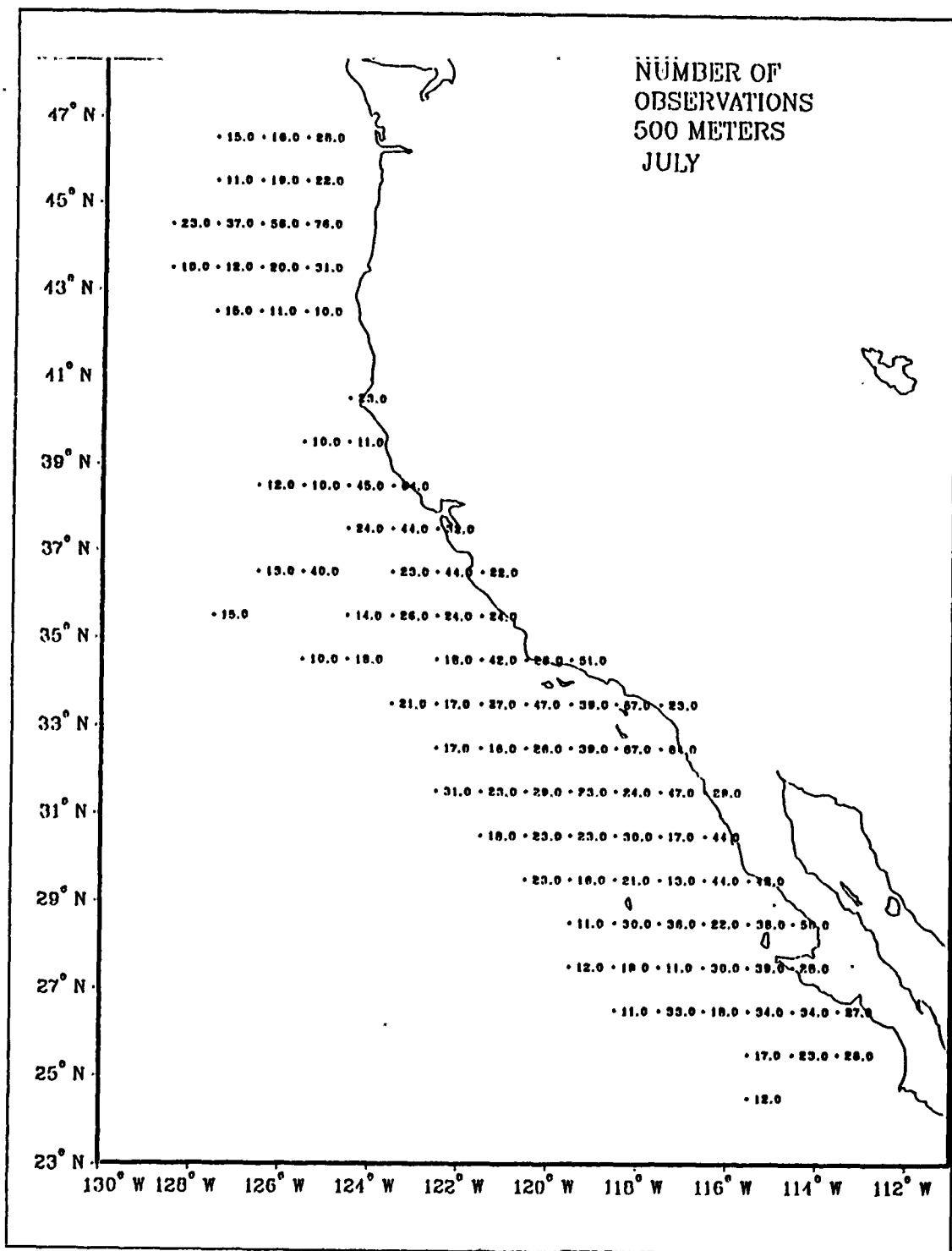


Figure 69. Number of Observations at 500 m, July.

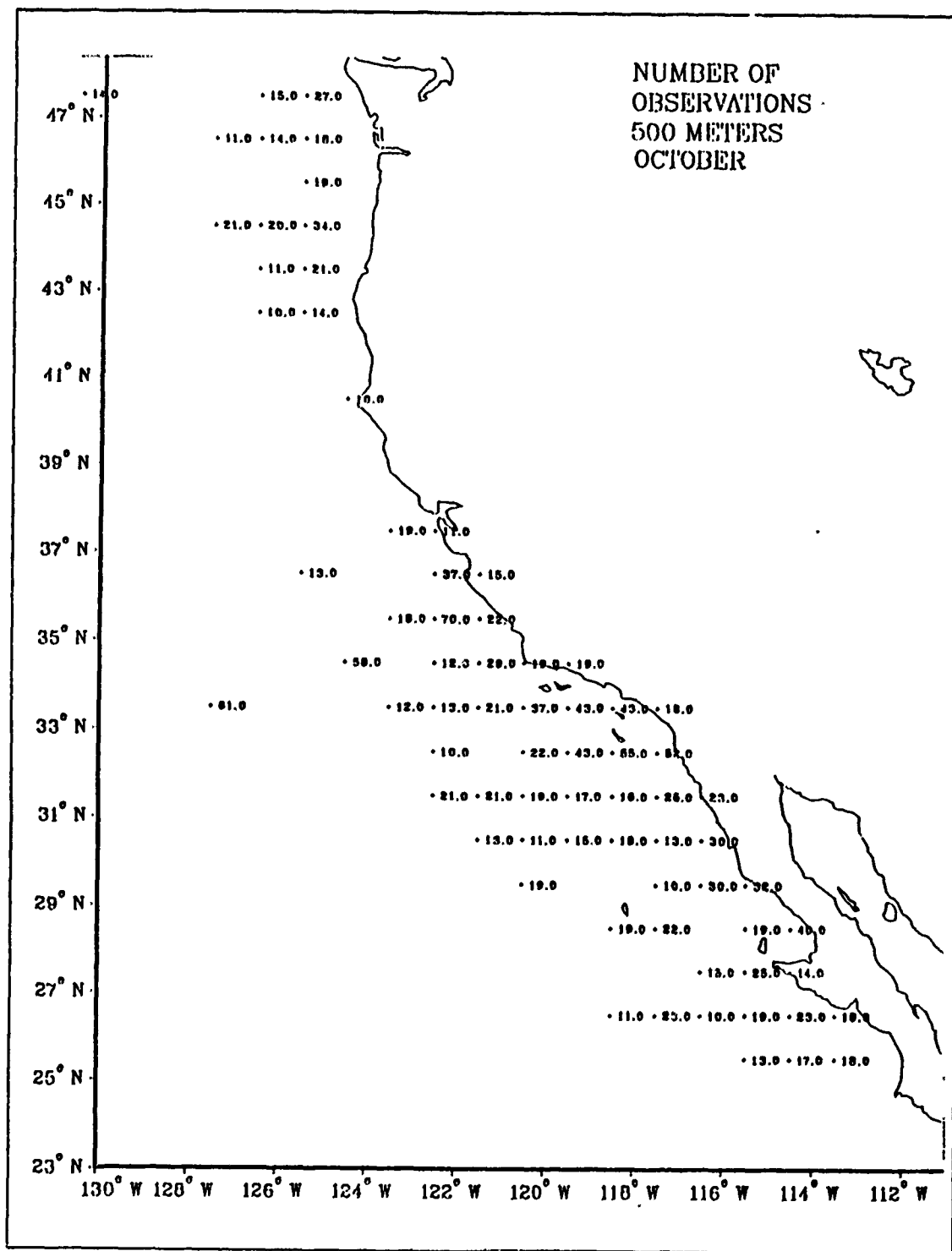


Figure 70. Number of Observations at 500 m, October.

APPENDIX B. SMALL SCALE EFFECTS OF SALINITY ON DYNAMIC HEIGHT

In addition to introducing the general large-scale biases to the estimated geostrophic flow field discussed in section IVE, the $\Phi_{35\sigma_\theta}$ estimator may misrepresent some smaller scale features. The December mean Φ map shows a strong closed cyclonic circulation near 30° N , 121° W . The December mean $\Phi_{35\sigma_\theta}$ field also shows a strong cyclonic feature at that point, indicating a thermal front as the probable cause of the enhanced flow. However, the difference map for the period also places a cyclonic circulation at that location, showing the front to be haline as well as thermal.

In April a closed cyclone again appears on the Φ' map, this time near 32° N , 123° W . Here the $\Phi_{35\sigma_\theta}$ map shows only weak cyclonic turning in basically onshore flow. The corresponding Φ map indicates strong horizontal cyclonic shear in the region. In this case, changes in salinity over a relatively small distance induce considerable shear in the mean field. This feature would be missed entirely by an estimate based on temperature variation alone.

In May a similar cyclonic anomaly appears on the Φ' map near 36° N , 127° W . The Φ field shows a strong ridge at $37^\circ 30' \text{ N}$ and a strong trough at 36° N , while the $\Phi_{35\sigma_\theta}$ map shows a trough at 37.5° N and a ridge at 36.5° N . Admittedly the scale of this mean feature is near the resolvable limit, and some critical mean values of Φ have been determined from relatively few casts. However, if the feature is correctly represented, it demonstrates the importance of salinity as a modifier of the effects of temperature. It is interesting that Φ (200/500) and $\Phi_{35\sigma_\theta}$ (200/500) contours, by contrast, are in phase in this area. Analysis of the May salinity distribution over the area of interest shows sharp salinity gradients at the surface and less pronounced gradients at depth. Consequently, the inferred flow fields are consistent.

LIST OF REFERENCES

- Batteen, M.L., R. L. Haney, T. A. Tielking, and P. G. Renaud, 1989. A numerical study of wind forcing of eddies and jets in the California Current system. *J. Mar. Res.*, in press.
- Bernstein, R. L., L. Breaker, and R. Whritner, 1977. California Current eddy formation: ship, air, and satellite results. *Science*, 195, 353-359.
- Blumberg, A. F., L. H. Kantha, H. J. Herring, and G. L. Mellor, 1984. California shelf physical oceanography circulation model. *Dynalysis of Princeton Report No. 88*, vol. 1, 164 pp.
- Cooper, N. S., 1988. The effect of salinity on tropical ocean models. *J. Phys. Oceanogr.*, 18, 697-707.
- Dantzler, H. L., Jr., 1977. Potential energy maxima in the tropical and subtropical North Atlantic. *J. Phys. Oceanogr.*, 7, 512-519.
- Emery, W. J., 1975. Dynamic height from temperature profiles. *J. Phys. Oceanogr.*, 5, 369-375.
- Emery, W. J., and J. S. Dewar, 1982. Mean temperature-salinity, salinity-depth and temperature-depth curves for the north Atlantic and the north Pacific. *Prog. Oceanogr.*, 11, 219-305.
- Flament P., L. Armi, and L. Washburn, 1985. The evolving structure of an upwelling filament. *J. Geophys. Res.*, 90, 11,765- 11,778.
- Fofonoff, N., 1962. Dynamics of ocean currents. *The Sea, Vol. 1*, M. N. Hill, ed., 323-395.
- Greenwalt, C. R., and M. E. Shultz, 1962. Principles of error theory and cartographic applications. *ACIC Technical Report No. 96*, appendix C, 60 pp.
- Hickey, B. M., 1979. The California Current System-hypotheses and facts. *Prog. Oceanogr.*, 8, 191-279.
- Huyer, A., 1983. Coastal upwelling in the California Current System. *Prog. Oceanogr.*, 12, 259-284.
- Huyer, A., and P. M. Kosro, 1987. Mesoscale surveys over the shelf and slope in the upwelling region near Point Arena, California. *J. Geophys. Res.*, 92, 1655-1681.
- Kosro, P. M., and A. Huyer, 1986. CTD and velocity surveys of seaward jets off Northern California, July 1981 and 1982. *J. Geophys. Res.*, 91, 7680-7690.

- Levitus, S., 1982. Climatological Atlas of the World Ocean. U.S. Dep. Commer., NOAA Prof. Pap. 13, 173 pp.
- Lewis, E. L., and R. G. Perkin, 1981. The Practical Salinity Scale 1978: conversion of existing data. *Deep-Sea Res.*, 28, 307-328.
- Lillibridge, J. L. III, 1989. Computing the seawater expansion coefficients directly from the 1980 equation of state, *J. Atmos. Oceanic Technol.*, 6, 59-66.
- Lynn, R. J., K. A. Bliss, and L. E. Eber, 1982. Vertical and horizontal distributions of seasonal mean temperature, salinity, sigma-t, stability, dynamic height, oxygen, and oxygen saturation in the California Current, 1950-1978. *Calif. Coop. Oceanic Fish. Invest. Atlas 30.*, 513 pp.
- Lynn, R. J., and J. J. Simpson, 1987. The California Current System: the seasonal variability of its physical characteristics. *J. Geophys. Res.*, 92, 12,947-12,966.
- Lynn, R. J., and J. J. Simpson, 1989. The influence of bathymetry upon the flow of the Undercurrent off southern California, *J. Geophys. Res.*, submitted.
- Mooers, C. N. K., and A. R. Robinson, 1984. Turbulent jets and eddies in the California Current and inferred cross-shore transports. *Science*, 223, 51-53.
- Pickard G. L., and W. J. Emery, 1982. *Descriptive Physical Oceanography*, Fourth Edition Pergamon Press, 249 pp.
- Reid, J. L., Jr, 1988. Physical oceanography, 1947-1987, *Calif. Coop. Oceanic Fish. Invest. Rep.*, 29, 42-65.
- Rienecker, M. M., C. N. K. Mooers, D. E. Hagan, and A. R. Robinson, 1985. A cool anomaly off northern California: An investigation using IR imagery and in situ data. *J. Geophys. Res.*, 90, 4807-4818.
- Rienecker, M. M., C. N. K. Mooers, and R. L. Smith, 1988. Mesoscale variability in current meter measurements in the California Current System off Northern California. *J. Geophys. Res.*, 93, 6711-6734.
- Stommel, H., 1947. Note on the use of the T-S correlation for dynamic height anomaly computations. *J. Mar. Res.*, 6, 85-92.
- Sverdrup, H. U., 1933. Vereinfachtes verfahren zur berechnung der druckund massenverteilung im meere, *Geofysiske Publikasjoner*, 10, 9 pp.
- Sverdrup, H. U., M. W. Johnson, and R.H. Fleming, 1942. *The Oceans*, Prentice-Hall, Inc., 1087 pp.
- UNESCO, 1981. Background papers and supporting data on the international equation of state of seawater 1980. *Tech. Pap. Mar. Sci.*, 38, 192 pp.
- UNESCO, 1987. International Oceanographic Tables, Vol. 4, *Tech. Pap. Mar. Sci.*, 40, 195 pp.

- Walpole, R. E., and R. H. Myers, 1985. *Probability and Statistics for Engineers and Scientists*, Macmillan Publishing Co., 639 pp.
- Wooster, W. S., and J. L. Reid, Jr., 1963. Eastern boundary currents. *The Sea, Vol. 2*, M. N. Hill, ed., 253-280.
- Wyllie, J. G., 1966. Geostrophic flow of the California Current at the surface and at 200 meters, *Calif. Coop. Oceanic Fish. Invest. Atlas 4*, 288 pp.

INITIAL DISTRIBUTION LIST

		No. Copies
1.	Defense Technical Information Center Cameron Station Alexandria, VA 22304-6145	2
2.	Library, Code 0142 Naval Postgraduate School Monterey, CA 93943-5002	2
3.	Chairman (Code 63Rd) Department of Meteorology Naval Postgraduate School Monterey, CA 93943-5000	1
4.	Chairman (Code 68Co) Department of Oceanography Naval Postgraduate School Monterey, CA 93943-5000	1
5.	Professor C. A. Collins (Code 68Co) Department of Oceanography Naval Postgraduate School Monterey, CA 93943-5000	1
6.	Professor Mary Batteen (Code 68Bv) Department of Oceanography Naval Postgraduate School Monterey, CA 93943-5000	2
7.	Director Naval Oceanography Division Naval Observatory 34th and Massachusetts Avenue NW Washington, DC 20390	1
8.	Commander Naval Oceanography Command Naval Oceanography Command Stennis Space Center, MS 39529-5000	1
9.	Commanding Officer Fleet Numerical Oceanography Center Monterey, CA 93943	1
10.	Commanding Officer Naval Oceanographic Office Stennis Space Center, MS 39522-5001	1

- | | | |
|-----|--|---|
| 11. | Commanding Officer
Naval Ocean Research and Development Activity
Stennis Space Center, MS 39522-5001 | 1 |
| 12. | Commanding Officer
Naval Environmental Prediction Research Facility
Monterey, CA 93943-5006 | 1 |
| 13. | Chairman, Oceanography Department
U. S. Naval Academy
Annapolis, MD 21402 | 1 |
| 14. | Chief of Naval Research
800 North Quincy Street
Arlington, VA 22217 | 1 |
| 15. | Office of Naval Research (Code 420)
Naval Ocean Research and Development Activity
800 North Quincy Street
Arlington, VA 22217 | 1 |
| 16. | Professor Robert Haney (Code 6311y)
Department of Meteorology
Naval Postgraduate School
Monterey, CA 93943-5000 | 1 |
| 17. | CDR Craig S. Nelson
Department of Oceanography
Naval Postgraduate School
Monterey, CA 93943-5000 | 2 |
| 18. | LCDR Chris Gunderson
USS Independence
FPO San Francisco, CA 96618-2760 | 2 |
| 19. | Office of Naval Research
Code 1122CS
800 North Quincy Street
Arlington, VA 22217
Attn: Dr. Tom Kinder | 1 |
| 20. | Office of Naval Research
Code 1122PO
800 North Quincy Street
Arlington, VA 22217
Attn: Dr. David Evans | 1 |
| 21. | Professor Timothy P. Stanton (Code 68St)
Department of Oceanography
Naval Postgraduate School
Monterey, CA 93943-5000 | 1 |

22. Dr. H. James Herring
Dynalysis of Princeton
219 Wall Street
Princeton, NJ 08540-1512
23. Mr. Sigurd Larson
U.S. Department of the Interior
Minerals Management Service
Pacific Outer Continental Shelf Region
1340 West Sixth Street, Mail Stop 300
Los Angeles, CA 90017-1297
24. Director of Research Administration
Code 012
Naval Postgraduate School
Monterey, California 92343
25. Mr. Robert Saul
Department of Oceanography
Naval Postgraduate School
Monterey, California 92343